Holographic and Composite Models of the Axion

A DISSERTATION
SUBMITTED TO THE FACULTY OF THE GRADUATE SCHOOL
OF THE UNIVERSITY OF MINNESOTA
BY

Minh Duc Nguyen

IN PARTIAL FULFILLMENT OF THE REQUIREMENTS
FOR THE DEGREE OF
DOCTOR OF PHILOSOPHY

Tony Gherghetta, Advisor

July 2021

Acknowledgements

It would not have been possible to finish this doctoral thesis without the help and support of the kind people around me. The list is long, and to only some of whom it is possible to give mention here.

My deep gratitude goes to my advisor, Prof. Tony Gherghetta, for his wholehearted guidance through my graduate education. His enthusiasm kept me engaged with my journey. His generous support and refreshing humour helped make my time at the University of Minnesota enjoyable. It has been an honor to learn from his insight and wisdom. My thanks extends to my undergraduate advisor, Prof. Tonnis ter Veldhuis, who showed me the joy of studying theoretical physics.

Above all, I'm greatly indebted to my grandparents, who instilled in me an early interest in science and the education necessary to pursue it. Next come mom and dad, for your encouragement when I needed them the most. This thesis would have not been possible without my partner, Wendy, who patiently saw this journey with me through the end. I thank my uncle and family, for their support that helped me focus on my research.

I wish to express my sincere thanks to Dr. Peter Cox, who collaborated with me on the projects that this thesis is partly based on. I'm also thankful for my friends at the University of Minnesota. I have greatly benefited from interactions with the William Fine Theoretical Physics faculty, postdocs and students. Special thanks to Prof. Aaron Wynveen, along with other professors for whom I have had a chance to assist. The staff at the Physics and Astronomy Department have been wonderful in supporting graduate students like myself.

Finally, I would like to thank the Ph.D. committee, Prof. Roger Rusack, Prof. Yongzhong Qian and Prof. Aleksey Cherman, for overseeing my dissertation process.

Dedication

In memory of *Bà*, 1945 - 2019.

Abstract

The axion, first proposed to solve the absence of a neutron electric dipole moment, is also an excellent dark matter candidate. If the axion is composite, it must be bound by a novel strong interaction. Some strongly-coupled models, mathematically intractable until now, are recently discovered to be calculable through a mapping onto 5-dimensional gravity. We propose a series of composite and extra dimensional axion models. A basic 5-dimensional model first incorporates the known forces while keeping the axion consistent with gravitational corrections. More sophisticated extensions address other problems in particle physics unrelated to the axion, providing nontrivial predictions that can be tested experimentally. We further propose a composite model that incorporates both the Higgs boson and the axion. By enlarging the color gauge group, we provide a consistent procedure to raise the axion masses as high as TeV collider energy scales, further motivating experimental searches for axion-like particles.

Contents

List of Tables

List of Figures

Chapter 1

Introduction

The Standard Model of particle physics has provided our most successful description of Nature to date. The theory categorizes the fundamental constituents of matter into quarks and leptons, and their interactions into the electromagnetic, weak, and strong nuclear forces. Including general relativity and the Standard Cosmological Model, the theory is capable of predicting observable phenomena ranging from the subnuclear structure of quarks and gluons, to the expansion of the Universe.

The development of the Standard Model first started with the formulation of quantum electrodynamics (QED). QED successfully described the interaction of radiation and matter as an Abelian quantum gauge theory. The theory was called "the jewel of Physics" [1] thanks to the capability of extremely accurate predictions of observable quantities, such as the Lamb shift of the hydrogen energy levels [2], or the electron anomalous magnetic moment. This feature originates from the perturbative characteristic of the theory, in which observable quantities can be calculated using a perturbation expansion of calculable Feynman diagrams. Abelian gauge theory was then extended to general non-abelian groups by Yang and Mills [3], which paved the way for the further description of the weak interaction with an SU(2) group [4], and the strong interaction with an SU(3) group.

The current theoretical structure of the Standard Model was conceptualized beginning in the 1960s, with the three fundamental interactions underlying the three generations of leptons and quarks [5]. Finally, the Higgs boson was introduced to resolve the problem of massive vector bosons, consequently providing a dynamical mass generating mechanism to

fundamental fermions [6, 7]. These aspects of the Standard Model are confirmed through its ability to produce accurate predictions, inherent of its predecessor QED, and through extensive experiments: the discoveries of the bottom quark in 1977 [8], the top quark in 1995 [9], the tau neutrino in 2000 [10], and the Higgs boson in 2012 [11], which perhaps is the most famous triumph of the Standard Model.

Nonetheless, it is clear that the Standard Model is an effective description of a more complete theory that describes physics at higher energies. The Standard Model only unifies electromagnetism and the weak interaction, and it is widely believed that at some *grand unification scale* (GUT), the strong nuclear force can also be included. The Standard Model, as a quantum field theory, also neglects the classical description of general relativity. In principle, the Standard Model remains valid up to the (reduced) *Planck scale* $M_{\rm Pl} = 2.435 \times 10^{18}$ GeV, where quantum gravity becomes important. Nonetheless, there surely must be novelties waiting to be explored in the 16 orders-of-magnitude *Great Desert* between the current TeV experimental scale and the Planck scale.

The first clue of new physics comes directly from this discrepancy between the weak scale and the Planck scale in the form of the *gauge hierarchy problem*. Although some may consider the problem not a drawback of the Standard Model, but rather the susceptibility of elementary scalar particles to quantum corrections. Specifically, the leading Higgs mass-squared correction from a Yukawa coupling y_f to a fermion is

$$\delta m_H^2 = -\frac{|y_f|^2}{8\pi^2}\Lambda_{\rm UV}^2 \,, \tag{1.1}$$

where the largest correction is due to the top quark with $y_f \sim 1$, and $\Lambda_{\rm UV}$ is an ultraviolet cutoff. Given that the observed mass is a combination of the bare mass and the quantum correction in Eq. (1.1), these two contributions must be *fine-tuned* to a high level of accuracy to produce the observed Higgs mass at 125 GeV, provided $\Lambda_{\rm UV}$ is identified with a physical mass scale in a UV complete theory.

There exist multiple solutions to the Higgs mass hierarchy problem. One could use the dimensional regularization scheme instead and renormalize the UV divergence in Eq. (1.1).

However, if the UV theory is finite, the Higgs mass will receive a new correction from any UV particle, which will then lead to a severe tuning. As the name suggests, the gauge hierarchy problem really is the question of why the weak scale is so much lower than the gravity scale (or why gravity is so much weaker than the other forces). One can alleviate the problem by interpreting $\Lambda_{\rm UV}$ not as the gravity scale, but the scale of new physics. At this scale, particles from theories beyond the Standard Model (BSM) could be observable experimentally. These new states could be supersymmetric (SUSY) partners of the Standard Model[1], the Kaluza-Klein (KK) modes from hidden extra dimensions (see Chapter 3), or dark mesons from novel strong dynamics that admits the Higgs boson as a composite bound state (see Chapter 5). A naturally small correction requires these new states to be at around $10 - 100$ TeV. Even at this scale there is a *little hierarchy* which needs to be explained, but it is still orders of magnitude better than the Standard Model. Thus, if the gauge hierarchy problem is taken seriously, the LHC would be our best bet to detect new physics from current collider searches.

The gauge hierarchy problem, that has driven particle physics so far, is an example of a *fine-tuning problem*. In a natural theory, dimensionless parameters should be of order one, or equivalently, quantities of the same origin should have the same order of magnitude. A mathematical formulation of this principle can be derived from Bayesian statistics using concepts such as parameter space and distribution [14, 15]. These formulations, however, are only well defined in the high energy, or ultra-violet (UV) region of the theory, which is inaccessible at low energy, or the infra-red (IR). In a theory with an unnaturally small parameter, if a symmetry in the UV theory could be recovered when the parameter is put to zero, then the fine-tuning problem can be addressed [16]. This is often referred to as the *naturalness principle*, a stronger form of the fine-tuning principle. The gauge hierarchy problem, for instance, violates this principle since there is no symmetry obtained when the Higgs mass is taken to zero. The most common solution to naturalness problems is thus enhancing the UV theory with a protective symmetry. An alternative is to accept the fine-tuning as evidence of a multiverse, based on the *anthropic principle* [17]. Nonetheless,

[1] See [12] for a comprehensive SUSY review. For a historical exposition, see [13].

with the current lack of verified experimental anomalies or observations of new physics, the naturalness principle has proven to be a very robust theoretical approach driving recent particle physics developments. As such, naturalness with some unexplained mild tuning is a central theme of this thesis, as we explore how composite and extra dimensional frameworks can be utilized to explain some of the Standard Model's current problems.

Fermion mass hierarchy

Another hierarchy problem of the Standard Model in the weak sector is the *fermion mass hierarchy*. Mathematically, fermions from the same generation in the Standard Model are treated identically. However, the observed masses, in all fermion generations, exhibit a severe hierarchy (see Table 1.1).

	m (GeV)	Ratio
u	0.0011723(5)	1
c	0.589(73)	550
t	163.004(970)	75000
d	0.0025476(100)	1
s	0.0507(32)	20
b	2.6993(12)	870
e	0.000477021(9)	1
μ	0.102698(2)	207
τ	1.74276(3)	3484

Table 1.1: Fermion masses in the Standard Model at the scale $Q = 173.1$ GeV in the $\bar{\text{MS}}$ renormalization scheme, and the ratio compared to the first generation. Fermion families are separated by horizontal lines.

In the Standard Model, fermion masses are generated through Yukawa couplings to the Higgs field. These Yukawa couplings are dimensionless parameters of the theory, and thus fail to offer an *a priori* explanation of the observed hierarchy. The hierarchy is present even at higher energies where the renormalization running is incorporated. In a Higgs doublet model, for instance, the Yukawa couplings at 10^9 GeV are reduced by roughly a factor of

two, thus offering no alleviation to the hierarchy[2].

Note that there is another mass hierarchy between the neutrinos, which are not included in Table 1.1, and the charged fermion families in the Standard Model. While the first-generation quark and charged lepton masses are approximately at the MeV scale, the neutrino masses are expected to be less than 10^{-3} eV [18]. In the Standard Model, the neutrinos are assumed to be massless. Thus current neutrino oscillation measurements, which imply that at least two of the neutrinos are massive, already require extensions beyond the SM. The simplest such extension is the inclusion of right-handed neutrinos ν_R, which allows for the *seesaw mechanism*. The right-handed neutrinos, being *sterile*, can have a Majorana mass term in addition to the usual Dirac mass term similar to those in the SM

$$\Delta\mathcal{L} = m_D \bar{\nu}_L \nu_R + m_M \nu_R \nu_R + \text{h.c.} \tag{1.2}$$

where $m_D \sim y_f v$ is the Dirac term, arising from the usual Yukawa couplings when the Higgs obtains a vev v, and m_M is the novel Majorana mass term.

If only the Dirac mass is present, then the associated neutrino-Higgs coupling must be highly suppressed of order $\sim 10^{-12}$ (in contrast with the top quark Yukawa coupling of order one). This clearly begs for an explanation. For instance, this situation can be mitigated if the Majorana mass m_M is present and very large. In this case, the physical neutrino eigenstates can be extremely light

$$m_N \propto \frac{m_D^2}{m_M} \,. \tag{1.3}$$

The expected neutrino masses can be naturally explained given a Majorana mass of order 10^{10} GeV without any tuning of the neutrino Yukawa couplings. For its simplicity, the seesaw mechanism is widely believed to be the solution to the minuscule neutrino masses. This is an example of how addressing tuning problems can guide us to simpler theories.

The fermion mass hierarchy and the neutrino will be revisited in Section 4.5, where we

[2]This fact is revisited in Chapter 4, where we use a warped extra dimension model to explain the fermion mass hierarchy.

construct a warped extra dimensional model that includes the axion. In this framework, a natural explanation for the fermion mass hierarchy can also be obtained. Instead of being near the GUT scale, the Majorana mass scale could be at a lower infra-red scale M_{IR}, where one could detect the presence of sterile neutrinos or hidden extra dimensions. Furthermore, warped extra dimensions can allow the possibility that neutrinos are Dirac particles. Next, we consider the strong CP problem, another tuning problem of the Standard Model.

CP Violation in the SM and the Strong CP problem

First we will review the CP symmetry in the Standard Model. QED, the first piece of the SM, which merged special relativity and quantum mechanics, required the existence of antiparticles. For each particle, there must exist an antiparticle with identical mass and spin but opposite charge. The observation of the *positron* - the antiparticle of the electron in 1933 confirmed the theory [19]. However, this poses a cosmological problem. In QED, particles and antiparticles are treated identically. However, astronomical and cosmological observations show that the Universe is made up solely of matter. This matter-antimatter asymmetry, also known as the *baryon asymmetry*, may result from a discrepancy in the interaction between elementary particles and anti-particles.

A quantum field theory may possess several internal discrete symmetries: charge conjugation (C), parity transformation (P), and time reversal (T). A CP transformation thus converts a particle into its antiparticle, and vice versa. In a consistent quantum field theory[3] the CPT symmetry must be present. However, while CPT must be an exact symmetry, P and CP may be violated. In fact, in 1956, the weak decays were shown to violate parity [20]. This was due to the mixing angles between the generations of quarks, that appear in the CKM matrix [21]. Similarly the mixing angles between the generations of leptons, that appear in the PMNS matrix [22, 23], allow for CP violation angles that are order one. However, these sources of CP violation within the Standard Model are insufficient to explain the observed matter-antimatter asymmetry on a cosmological scale. A new unknown source

[3] To be more exact, any Lorentz invariant local quantum field theory with a Hermitian Hamiltonian.

must be present.

One might hope to find another CP violation source within the strong interactions. However, unlike the weak force, the strong nuclear force exhibits almost exactly no CP violation. In the 1970s, it was discovered that Quantum Chromodynamics, the quantum gauge theory of the strong nuclear force, does indeed admit a parameter, called the *theta angle*, that allows for CP violation within the theory. However unlike the CP violation angle in the CKM matrix, this theta angle must be quite small, up to order 10^{-10}, to be consistent with current experimental bounds on CP violation within the strong interactions, specifically from the neutron electric dipole moment [24, 25, 26]. This is the *strong CP problem*. Among the solutions of the strong CP problem, the Peccei-Quinn mechanism with an axion is the most elegant solution, and is the main subject of this thesis.

Dark Matter

Matter-antimatter asymmetry aside, there is a much more severe experimental problem: the existence of dark matter and dark energy. Multiple cosmological probes varying in size (from dwarf galaxies [27], the Milky Way [28], to galaxy clusters [29]) have confirmed that the baryonic matter contributes roughly 19% of the mass density, and only 5% of the total Universe mass-energy density[4]. The prototype of this missing mass, generally referred to as *cold dark matter*, is a *weakly interacting massive particle* (WIMP): non-relativisitic, heavy compared to SM particles, and interacts via the weak force with SM particles. The WIMP scenario has been preferred since it frequently arises in BSM scenarios, such as the neutralinos in SUSY, KK modes in extra dimensional models, and resonances in composite Higgs models. Nonetheless, since the search for the WIMP has proven to be fruitless so far, it behooves us to explore new possibilities.

The axion and axion-like particles, thus has emerged recently as one of the prime candidates for dark matter. The typical axion is ultra-light and weakly interacting, and thus has wave-like characteristics on large scales (often named *fuzzy* or *wave* DM). The long wave-

[4]There exist modified gravity models to explain DM, but generally fail to work across different scales.

length axions, including the QCD axion, thus can serve as cold dark matter that populate the Universe after the Big Bang. Furthermore, the axion that solves the strong CP problem may not necessarily be light, but could be heavy in some variant scenarios. In Chapter 5, we explore how to construct a family of heavy axions in the context of composite Higgs models, and study the dark matter candidates predicted by these models.

Organization

The previous problems are not the only theoretical drawbacks of the Standard Model. Some other problems include the proton decay problem, stability of the electro-weak scale, why there are three generations of fermions, the origin of the cosmological constant (or dark energy), and how to incorporate a quantum theory of gravity. Eventually a complete UV description should be able to explain all of these problems.

The central theme of this thesis has a more modest goal to consider the axion and the strong CP problem. A particularly interesting framework that can simultaneously address multiple problems of the Standard Model is that of warped extra dimensions, where multiple hierarchies can be naturally explained. Furthermore, warped extra dimensions are dual to classes of four-dimensional (4D) composite models via the remarkable AdS/CFT correspondence [30]. While the exact mapping is not yet known, studying the axion from both sides of the duality thus provides insights on axion models that can give new predictions and guide experimental searches.

In Chapter 2, we review in more depth the strong CP problem and the axion solution. In Chapter 3, we review the framework of warped extra dimensions. These two chapters serve as the background material for subsequent chapters. Chapter 4 presents a five-dimensional (5D) axion model that is free of the *axion quality problem*. This chapter also extends the model to incorporate Standard Model fermions, and shows that the warped extra dimensional framework can offer a natural solution to the fermion mass hierarchy. Chapter 5 presents composite axion models. One of the models will have the feature that the axion is heavy and detectable in collider experiments. Finally, in Chapter 6 readers can find a summary of

the major results of this thesis and comments on future directions.

This thesis is based on the work published in [31, 32, 33] and work that is currently in preparation [34] at the University of Minnesota.

Chapter 2

Strong CP Problem and the Axion

The axion is a hypothetical particle originally introduced in [35, 36, 37, 38] to solve the strong CP problem of Quantum Chromodynamics (QCD). It arises as a Nambu-Goldstone boson (NGB) from an anomalous U(1) Peccei-Quinn (PQ) global symmetry, that is spontaneously broken at some high energy scale $F_{\rm PQ} \simeq 10^9 - 10^{12}$ GeV. The global symmetry is explicitly broken by non-perturbative QCD dynamics, which generates an axion potential. At this potential minimum, the axion precisely cancels the $\bar{\theta}$ term, and therefore provides a dynamical reason of why there is no CP violation in QCD.

If it exists, the axion is predicted to have an extremely small mass and weak coupling to the Standard Model particles. As such, the axion has emerged as one of the prime candidates for dark matter. The existence of the axion can simultaneously solve both the strong CP and dark matter problem of the Standard Model. Thus, after the discovery of the Higgs boson, the axion is the next sought-after particle, and is actively studied both theoretically and experimentally.

Nonetheless, the axion solution, while arguably the most elegant, is not the only solution of the strong CP problem. There exist other solutions, such as the massless up quark [39], and spontaneous P/CP violation models (such as the Nelson-Barr model [40, 41]). Furthermore, the axion solution, by itself, is not free of theoretical problems. The most severe one is the *axion quality problem*, in which the strong CP solution is spoiled by quantum gravity corrections. In a larger context, extensions to the popular axion solution are thus required, although there is a risk of complicating the model and diminishing the elegance

of the original mechanism. As the axion has gained renewed interest, these problems have also been under extensive theoretical studies.

Depending on the context, the term axion may also refer to *axion-like particles* (ALP), that have no relation to the strong CP problem. A spin-zero particle with properties resembling those of the axion appears in a multitude of different theoretical contexts. These particles could be pseudoscalars like the QCD axion, or scalars like the dilaton or moduli in string theory. These particles also appear in composite Higgs models as siblings of the Higgs boson [42], in extra dimensional models, in string theories [43], or in theories with hidden sectors. While the study of ALPs is a very rich subject, in this thesis we are only interested in the QCD axion in the traditional sense, as a solution to the dark matter and strong CP problems of the Standard Model.

QCD is a vast subject, and this review no doubt will omit several steps that may be deemed fundamental depending on the reader background. A more complete overview can be found in Chapter 9 of [44]. In Section 2.1, we briefly introduce QCD in a historical context and highlight ideas that are important for our purposes. In Section 2.2, we introduce the chiral Lagrangian and the U(1) problem, which is closely related to the strong CP problem, reviewed in Section 2.3. Some solutions to the strong CP problem are introduced in Section 2.4. Aspects of the axion solution including the *axion quality problem*, one of the theoretical hurdles of axion models, are presented in Section 2.4.1.

2.1 Brief Introduction to QCD

Quantum Chromodynamics (QCD) is a quantum gauge field theory that describes the interaction between quarks and gluons, through a non-abelian gauge invariance $SU(3)_c$. Unlike the electro-weak sector, QCD exhibits *confinement*, in which the quarks are not directly observable, but are hadronized into bound states such as mesons and baryons. Furthermore, QCD is non-perturbative, meaning that (at low energies) there is no reliable perturbative expansion to calculate physical quantities. The problem of proving the mass gap existence from confinement is still an open problem in physics, and is one of the Millennium Prize Problems [45].

With the invention of bubble chambers in the 1950s, particle physicists discovered a large number of hadronic particles. In the following years, these particles were classified by charge and isospin by Wigner and Heisenberg, and subsequently by strangeness [46, 47]. The *eightfold way*[1] was introduced by Gell-Mann and Ne'eman in 1961 [48, 49], serving as the "Periodic Table of Nuclear Physics". In 1963, Gell-Mann and Zweig proposed the existence of three flavors of quarks and their interaction with gluons, that can be used to explain the observed hadronic spectrum [50].

Due to the Pauli exclusion principle, it soon became clear that quarks should possess additional quantum numbers. The $SU(3)_c$ gauge group of color was then introduced by Greenberg [51], and Han and Nambu [52]. Nambu and Han also noted on the existence of the modern gluons in the adjoint representation. The searches for free quarks proved unfruitful in subsequent years. For a while, quarks were considered mathematical objects and not real particles. In hindsight, these searches were bound to fail because of confinement. The existence of quarks were later confirmed in deep-inelastic experiments [53, 54], that proved quarks were not just mere mathematical devices for calculation. This was done through the contribution of Feynman [55] with the *parton* model, and Bjorken scaling [56].

Modern QCD as the theory of color was developed by Gell-Mann, Fritzsch and Leutwyler

[1] An allusion to the Noble Eightfold Path in Buddhism.

[57] employing the Yang-Mill theory [3] with a deceptively simple Lagrangian.

$$\mathcal{L}_{\text{QCD}} = -\frac{1}{4}F^a_{\mu\nu}F^{a\mu\nu} + \bar{\psi}_i(i\gamma^\mu D_\mu - m)_{ij}\psi_j\,, \tag{2.1}$$

where A^a_μ is the gluon field with $a = 1 \ldots N_c^2 - 1$ (8 for $N_c = 3$), $D^a_\mu = \partial_\mu - igA^a_\mu$ is the covariant derivative with g the dimensionless strong gauge coupling and $F^a_{\mu\nu} = \partial_\mu A^a_\nu - \partial_\nu A^a_\mu + gf^{abc}A^b_\mu A^c_\nu$ is the field strength tensor. The ψ_i are Dirac fields with flavor index i. It is a miracle, both in mathematical and realistic sense, that this Lagrangian can give rise to such a rich multitude of phenomena.

Of course mathematically, it is uncertain how such a confinement mechanism works. The main hurdle is that QCD is non-perturbative at low energies; the coupling constant $\alpha_S = g^2/4\pi$ is greater than unity, thus dashing any hope of a perturbative expansion that has been so successful in QED and the electroweak theory. However, just like in other field theories, the coupling constant is not a constant at all. The Lagrangian in (2.1) with the Standard Model fermion content allows us to write down the renomalization group equation (RGE)

$$\beta(\alpha_S) = \mu^2\frac{d\alpha_S}{d\mu^2} = -(b_0\alpha_S^2 + \ldots)\,, \tag{2.2}$$

where $b_0 = (33 - 2n_f)/12\pi$ is the 1-loop β-function coefficient, and the "..." represents higher-loop orders. The negative sign in Eq. (2.2) is the basis behind the discovery of *asymptotic freedom* by Gross, Wilczek [58] and Politzer [59]. Asymptotic freedom means that for processes involving large momentum transfers (hard collisions), the strong coupling becomes weak, thus perturbative QCD (pQCD) calculations can be employed along with the parton model for experimental predictions. In hard interactions, final state partons and hadrons mostly appear in collimated *jets*. The first observation of gluons as a jet event was discovered in 1979 at PETRA of DESY in Germany [60]. Though limited in scope, pQCD calculations have provided the most precise tests to date.

If one truncates the β-function in (2.2) at some higher order terms (in practice, greater than four) and solves for α_S, one finds that α_S becomes infinite at some scale $\bar{\mu} \equiv \Lambda_{\text{QCD}} \sim 0.2$

GeV. This is the confinement scale of QCD, at which hadronization occurs. Below the confinement scale, pQCD is no longer valid, and other effective approaches have to be deployed. One genius of physicists during this era is the "workaround" theories developed to understand the hadron structures. As one might put it, the evolution of QCD is the struggle of physicists to "break free from Feynman diagrams". In hindsight, these works define the physics theme for the next century. To list a few, these include

* Chiral Lagrangian (Section 2.2), which reasonably predicts the hadronic spectrum and the U(1) problem.
* Study of the QCD anomaly and the strong CP problem gave rise to the discovery of the topological aspects of QCD such as topological defects: instantons, skyrmions, domain walls, and strings, which then find their full potential in supersymmetric theories.
* Initial string theories to model the "stringy" one-dimensional interaction within hadrons.
* Large N simplification, in which large classes of Feynman diagrams are suppressed by higher orders of $1/N$. These subsequently led to the study of conformal field theories.
* Last but not least, completing the circle, the AdS/CFT correspondence relates some string theories with lower-dimension conformal field theories.

Standing on the shoulder of the QCD fore-fathers, we will utilize the AdS/CFT correspondence as a central framework in this thesis.

2.2 Chiral Lagrangian and the U(1) Problem

At low energy where the quarks are confined within hadrons, effective field theories can be employed to study QCD. The up and down quarks are much lighter than the confinement scale $\Lambda_{\rm QCD}$, and thus can be considered massless for practical purposes. This approximation may extend to include the strange quark, whose mass is slightly below $\Lambda_{\rm QCD}$. Other quarks (charm, bottom and top) are considered *heavy quarks* and require a different treatment.

For simplicity, let us consider two light flavors $\psi = (u, \quad d)$. Each Dirac fermion can be decomposed into Weyl components $\psi_i = (\chi_\alpha, \quad \xi^{\dot\alpha})$ where $\alpha, \dot\alpha$ are SU(2) spinor indices. Thus in this limit, the theory possesses a chiral symmetry $\mathrm{U}(2)_L \times \mathrm{U}(2)_R$. Specifically

$$\chi_\alpha \to L_\alpha^{\ \beta} \chi_\beta \,, \qquad \xi^{\dot\alpha} \to (R^*)^{\dot\alpha}_{\ \dot\beta} \xi^{\dot\beta} \,, \tag{2.3}$$

where $L(R)$ are $\mathrm{U}(2)_{L(R)}$ transformations. If the strange quark is also considered, the flavour group is instead SU(3) with a $\mathrm{U}(3)_L \times \mathrm{U}(3)_R$ global symmetry. This extension is straightforward to implement, but for simplicity we will restrict to two flavours. The global symmetry $\mathrm{U}(2)_L \times \mathrm{U}(2)_R$ can be decomposed further into

$$\mathrm{U}(2)_L \times \mathrm{U}(2)_R = \mathrm{SU}(2)_V \times \mathrm{U}(1)_V \times \mathrm{SU}(2)_A \times \mathrm{U}(1)_A \,. \tag{2.4}$$

The global symmetry $\mathrm{SU}(2)_V$ (setting $R = L$) is realized in Nature as the isospin symmetry, and $\mathrm{U}(1)_V$ is baryon number. The axial symmetry $\mathrm{SU}(2)_A$, on the other hand, must be spontaneously broken. Let us for now assume that $\mathrm{U}(1)_A$ is also broken, thus there are four Nambu-Goldstone bosons (NGBs). However, since there is no fundamental scalar field that could acquire a VEV, we must instead utilize a composite field made from the quarks. The simplest candidate is $(\chi\xi)_\alpha^{\ \dot\beta}$ where

$$\langle 0 | \chi_\alpha \xi^{\ \dot\beta} | 0 \rangle \approx -\Lambda_{\rm QCD}^3 \delta_\alpha^{\ \dot\beta} \,. \tag{2.5}$$

This is the *fermion condensate*. The RHS is determined by the confinement scale, the only

scale available, as we have not introduced any bare quark masses. Note that because of the flavor symmetry, an expansion of the LHS vanishes to all perturbative orders. Thus, Eq. (2.5) is non-perturbative.

Now, the spontaneous symmetry breaking pattern is

$$\mathrm{U}(2)_L \times \mathrm{U}(2)_R \to \mathrm{SU}(2)_V \times \mathrm{U}(1)_V \,. \tag{2.6}$$

Thus, we would expect four NGBs in the spectrum. These are the three pions and the η' meson. We can model these fields using the sigma model by considering

$$U(x) = \exp\left(\frac{i}{\sqrt{2}F_\pi} T^a \Pi^a(x)\right) , \tag{2.7}$$

where a runs from 0 to 4, $T^a = (\mathbb{I}, \vec{\tau})$ where $\vec{\tau}$ are the three Pauli matrices. The Π^a component is associated with the pions with decay constant F_π, and the Π^0 component is associated with the η' meson where we have taken $F_{\eta'} \sim F_\pi$. The matrix $U(x)$ is unitary, transforming as a $(2,2)$ under the $\mathrm{SU}(2)_L \times \mathrm{SU}(2)_R$ symmetry, and can be understood as a slowly varying field on the background of the fermion condensate

$$U(x) \equiv -\frac{1}{\Lambda_{\mathrm{QCD}}^3} \langle \chi_\alpha(x) \xi^{\dot{\beta}}(x) \rangle \ . \tag{2.8}$$

To determine F_π, we write down the appropriate Lagrangian

$$\mathcal{L} = F_\pi^2 \,\mathrm{Tr}\, \partial_\mu U \partial^\mu U^\dagger = \frac{1}{2} \partial_\mu \Pi^a \partial^\mu \Pi^a + \cdots \tag{2.9}$$

where the dots contain higher dimensional terms. Next, the quark masses can be included with the leading operator

$$\Delta\mathcal{L} = a F_\pi^3 \,\mathrm{Tr}\, MU + \mathrm{h.c.}\,, \tag{2.10}$$

where a is an $\mathcal{O}(1)$ dimensionless constant and $M = \mathrm{diag}(m_u, \quad m_d)$. Note that the masses may contain phases θ_u, θ_d. We assume, for now, that these phases can be rotated away using

the $U(1)_V$ and $U(1)_A$ symmetry. Expanding the chiral Lagrangian in terms of the pion fields yields

$$aF_\pi(m_u + m_d)\pi^+\pi^- + \frac{1}{2}aF_\pi\left(\pi^0\eta'\right) + \cdots \tag{2.11}$$

where $\pi^\pm = \frac{1}{2}\left(\pi^1 \pm i\pi^2\right)$. This gives a sum rule for the η' mass

$$m_{\eta'} = 2m_{\pi^+} - m_{\pi^0}\,. \tag{2.12}$$

Thus we expect $m_{\eta'} \approx m_{\pi^+} \approx m_{\pi^0} \approx 140$ MeV, which however contradicts the experimental value that $m_{\eta'} \approx 960$ MeV! Including the s quark does not improve the situation, and a more sophisticated analysis yields [61]

$$m_{\eta'} \leq \sqrt{3}m_\pi\,. \tag{2.13}$$

This discrepancy is the U(1) problem of QCD. In deriving these results, we have assumed the $U(1)_A$ to be a "good" symmetry of the theory and is not broken by the fermion condensate. In general, the mass matrix in equation (2.10) contains phases that can only be removed via axial phase rotations. This $U(1)_A$, however, is anomalous, generating an extra term in the QCD Lagrangian

$$\Delta L = \frac{\alpha}{16\pi^2}F_{\mu\nu}\tilde{F}^{\mu\nu} \tag{2.14}$$

where α is the axial angle and $\tilde{F}^{\mu\nu} = \epsilon_{\mu\nu\rho\sigma}F^{\rho\sigma}$. The U(1) problem is resolved because of the anomaly, and the η' thus obtains further mass contributions from non trivial topological configurations called *instantons* [62, 63]. The vacua of these states are controlled by a hidden parameter in the theory: the θ angle. Thus resolving the U(1) problem requires non-perturbative physics of QCD[2].

[2]For a summary, see [64]. See [65] for a beautiful summary of the resolution to the U(1) problem.

2.3 The strong CP problem

The Lagrangian in (2.1) omits another dimension-four term that can be written down, namely

$$\Delta L = -\frac{g^2\theta}{32\pi^2} F^a_{\mu\nu}\tilde{F}^{a\mu\nu}\,. \tag{2.15}$$

This term is a total derivative

$$F\tilde{F} = \partial_\mu K^\mu \quad , \quad \text{where} \quad K^\mu = \epsilon^{\mu\nu\rho\sigma}\left(F^a_{\rho\sigma} - \frac{g}{3} f^{abc} A^b_\rho A^c_\sigma\right)\,, \tag{2.16}$$

and thus for a long time was considered to be unphysical. Using the divergence theorem, the total energy is thus proportional to K^μ evaluated at infinity. In particular, if the integral falls off faster than $1/r^3$, which is naively expected, then the divergent term will not contribute to the total energy.

The discovery of instantons, however, changed the story. In 1976, t'Hooft [62] used the following gauge-field configuration

$$A_\mu = \frac{r^2}{r^2+\rho^2} h\partial_\mu h^{-1} \quad \text{where} \quad h = \frac{x_4 \mathbb{I} + i\vec{x}\cdot\vec{\tau}}{r}\,, \tag{2.17}$$

ρ is the instanton size, $\vec{\tau}$ are the Pauli matrices and h is a gauge transformation. It was discovered that this gauge-field configuration indeed has finite energy and that

$$\int d^4x \frac{1}{32\pi^2} F^a_{\mu\nu}\tilde{F}^{a\mu\nu} = 1\,, \tag{2.18}$$

representing a topological number. Furthermore, the Hamiltonian of this gauge field contribution produces a spectrum labeled by θ, interpreted as the winding angle of the configuration

$$|\theta\rangle \propto \sum_n e^{in\theta}\,|n\rangle\,, \tag{2.19}$$

where n is an integer. Given that it is impossible to transition between different values of θ, the appearance of θ in the QCD Lagrangian denotes a state in the *theta vacua*. Thus, the θ term indeed should have a physical effect. As noted in Section 2.2, the axial $\mathrm{U}(1)_A$ symmetry is anomalous. An axial rotation also contributes to the $G\tilde{G}$ term in the Lagrangian Eq. (2.15), and thus the physical quantity is not θ but instead

$$\bar{\theta} = \theta + \theta_u + \theta_d \,, \tag{2.20}$$

In 1979, Crewther, Di Vecchia, Veneziano and Witten [66] showed that a nonzero theta term will produce a nonzero neutron electric dipole moment

$$d_n = \frac{e\bar{\theta} g_a c_+ \mu}{8\pi^2 F_\pi^2} \log \frac{\Lambda^2}{m_\pi^2} \sim 10^{16}\bar{\theta} \quad e\,\mathrm{cm}\,, \tag{2.21}$$

where $\mu = m_u m_d/(m_u + m_d)$ is the reduced quark mass, $c_+ \approx 1.7$ is a mass splitting factor between various nucleons, and $g_A \approx 1.27$ is the interaction between protons and neutrons (to leading order). The energy scale $\Lambda \sim 4\pi F_\pi$ is the UV cutoff of the pion effective theory. The current bound thus implies $\bar{\theta} \lesssim 10^{-10}$. This is the strong CP problem. Naturally, $\bar{\theta}$, as an angle, is expected to be of order one. However, an *unnaturally* small theta term is required from the fact that we have not observed CP violation in the strong interactions.

2.4 Strong CP solutions

Unlike all other naturalness problems in the SM, the strong CP problem is the only puzzle for which the solution is unlikely to be anthropic. For example, if the observed theta angle was 10^{-3} instead of the current bound at 10^{-10}, there would be no significant change in the Universe. For this reason, dynamical solutions to the strong CP problem have always been of interest. There are several active solutions, that are still under research (see [67] for a review). However in this section, we only introduce the two solutions relevant for this thesis: the massless quark solution, and the axion solution.

2.4.1 The Axion solution

In all axion models, a new field, a is present that gives an effective Lagrangian

$$\mathcal{L} = \left(\frac{a}{F_a} + \bar{\theta}\right) \frac{1}{32\pi^2} F^a_{\mu\nu} \tilde{F}^{a\mu\nu} + V(a)\,, \tag{2.22}$$

where F_a is the axion decay constant and $V(a)$ is an effective axion potential term, often taken to be quartic. Note that the term which shows up in the potential is now $a/F_a + \bar{\theta}$ instead of $\bar{\theta}$. Thus when a potential for a is generated, the minimum occurs at

$$\frac{\langle a \rangle}{F_a} + \bar{\theta} = 0\,. \tag{2.23}$$

Typically, the axion arises from a global $\mathrm{U}(1)_{PQ}$ symmetry, called the Peccei-Quinn symmetry. The axion decay constant F_a thus is related to the PQ symmetry breaking scale F_{PQ}. Various models differ in the origin of this symmetry, which determines how the axion couples to Standard Model particles. The resulting axion mass is then determined by the QCD topological susceptibility χ

$$m_a^2 F_a^2 = \chi \equiv \int d^4x\ \langle q(x) q(0) \rangle \qquad \text{where} \quad q(x) = -\frac{1}{32\pi^2} F^a_{\mu\nu} \tilde{F}^{a\mu\nu}\,. \tag{2.24}$$

This term can be evaluated [68, 69] using chiral perturbation theory yielding $\chi \approx m_\pi^2 F_\pi^2$, or through QCD lattice simulations [70] to give

$$m_a = (5.70 \pm 0.007)\,\mu\text{eV}\left(\frac{10^{12}\,\text{GeV}}{F_a}\right). \tag{2.25}$$

The axion quality problem

If the axion is fundamental, then the theory can be extrapolated up to the Planck scale. However, the effective Lagrangian in Eq. (2.22) may well contain other higher-dimension terms such as

$$\Delta L \sim \frac{\Phi^n}{M_{\text{Pl}}^{n-4}}, \tag{2.26}$$

which explicitly violates the Peccei-Quinn symmetry. This introduces a correction to the theta angle that upsets the axion solution of the strong CP problem. Thus to ensure that gravity preserves the strong CP solution, these higher-dimension terms must be suppressed up to terms of dimension $n \sim 14$. This highlights the importance of constructing a UV complete model and significant efforts have been developed.

There are several ways to solve the axion quality problem. A UV completion of the axion is the composite axion (Choi Kim [71, 72]). Similar to the pion in QCD, the axion is a bound state of new strong dynamics, and thus gravitational violation of the PQ symmetry can be suppressed. Another UV completion is that the $\text{U}(1)_{\text{PQ}}$ symmetry may be an accidental symmetry, $\text{U}(1)_{\text{PQ}}$ may come from a 5D gauge symmetry or the $\text{U}(1)_{\text{PQ}}$ symmetry arises from an anomalous symmetry in a hidden axicolor, a new strong dynamics.

Invisible Axion

Since the axion has not yet been detected, a common feature is that it must be extremely weakly interacting and light. The coupling is controlled by the decay constant F_a which indicates the scale of new physics underlying the UV completion of the model. Initially, F_a was taken to be near the electroweak scale, which however was quickly ruled out. From

Eq. (2.25), we see that by raising the scale F_a, one can obtain a weaker-coupling axion, thus evading experimental limits. This class of models with a very high F_a ($\gtrsim 10^9$ GeV), are called *invisible axion* models. Within this class we can also distinguish "hadronic axion" models, which identify F_a with the mass scale of new heavy quarks carrying $\mathrm{U}(1)_{\mathrm{PQ}}$ charges. The SM quarks and leptons, on the other hand, do not couple directly with the axion. The prototype for this class is the KSVZ model [73, 74]. Alternatively, the SM quarks and leptons may also carry PQ charges, such as in the DFSZ model [75, 76], although this model requires at least two Higgs doublets. The KSVZ and DFSZ models are the two standard models, often used for benchmark purposes.

Composite Axion

Like the pions and η', the axion could be a composite state of some new strong dynamics, called *axi-color* [71, 72]. If the strong dynamics confines at a very high scale Λ_a, then we must have $F_a \sim \Lambda_a$. This also explains the scale of F_a which is due to dimensional transmutation of the new strong group. Composite axion models can help alleviate the axion quality problem, since the $\mathrm{U}(1)_{\mathrm{PQ}}$ can now be identified as $\mathrm{U}(1)_A$ in the novel dynamics, and survive as an accidental symmetry up to higher-dimension terms.

Extra Dimensional Axion

In warped extra dimensional models, the global symmetry in the 4D dual theory corresponds to the local 5D gauge symmetry. The $\mathrm{U}(1)_{\mathrm{PQ}}$ symmetry is thus modelled as a local U(1) gauge symmetry in the bulk. The explicit symmetry breaking terms can then be naturally suppressed in these models, solving the axion quality problem. Interestingly, because of the AdS/CFT correspondence, the extra dimensional axion models naturally have a dual description as composite axion models.

Heavy Axion

In some models, the axion can obtain mass contributions from other sources, such as strong dynamics at a higher energy scale, or novel strong dynamics from dark sectors. For the

latter case, a generic Lagrangian often has the form

$$\mathcal{L} = \left(\frac{a}{F_a} + \bar{\theta}\right) \frac{1}{32\pi^2} F^a_{\mu\nu} \tilde{F}^{a\mu\nu} + \left(\frac{a}{F_a} + \bar{\theta}'\right) \frac{1}{32\pi^2} F'^a_{\mu\nu} \tilde{F}'^{a\mu\nu} \,, \tag{2.27}$$

where F', θ' belong to the new strong group. The difficulty with models containing an extra sector, is to ensure that at the axion minimum all extra sources of CP violation are cancelled

$$\langle a \rangle = -F_a \bar{\theta} = -F_a \bar{\theta}' \,, \tag{2.28}$$

which often requires the strong sector to be mirrored (with a Z_2 symmetry), or the cancellation originates from some UV theory. One such example is considered in Chapter 5.

2.4.2 The massless quark solution

A very interesting solution, though it is currently ruled out, is the massless quark solution. We review this mechanism in the QCD context since a similar mechanism will play a role when we consider composite axion models. If one of the quark masses is zero, then the $\bar{\theta}$ term is automatically unobservable, solving the strong CP problem. One can then try to explain the smallness of the up quark through other means, such as quantum corrections. The interesting aspect, is that below the confinement scale, there should be a dual description of the solution. Continuing the discussion on the U(1) problem, we have seen that the effective potential written down is incorrect since $\mathrm{U}(1)_A$ is not a good symmetry of the theory. A chiral rotation transforms $U \to e^{i\alpha} U$, and thus the Lagrangian derived in (2.10) needs to be modified by adding a new term [69]

$$\mathcal{L} = a F_\pi^3 \left(\mathrm{Tr}\, MU + \mathrm{Tr}\, MU^\dagger \right) - \frac{b}{2N} F_\pi^2 (-i \ln \det U - \theta)^2 \,. \tag{2.29}$$

This Lagrangian is thus invariant under $\mathrm{SU}(2)_L \times \mathrm{SU}(2)_R \times \mathrm{U}(1)_V$, but not $\mathrm{U}(1)_A$. A Taylor expansion of this term gives the second term in the following effective Lagrangian

$$\mathcal{L} = \frac{g^2}{32\pi^2}\left(\theta - \sqrt{2}\frac{\eta'}{F_{\eta'}}\right) F^a_{\mu\nu}\tilde{F}^{a\mu\nu} + \frac{1}{2}m^2_{\eta'}\left(\eta' - \frac{\theta F_{\eta'}}{\sqrt{2}}\right)^2 , \tag{2.30}$$

where the η' pre-factor in the first term comes from the normalization and we have assumed $\mathrm{Tr}\, T^a T^b = 1$. If one quark is massless, then its phase can be used to rotate all other quark phases, thus $\theta = \bar{\theta}$. In this case, the anomalous $\mathrm{U}(1)_A$ can play the role of $\mathrm{U}(1)_{\mathrm{PQ}}$. At the minimum of the potential, the mass term disappears since $\langle \eta' \rangle = \theta F_{\eta'}/\sqrt{2}$, parallel to the axion solution in Eq. (2.23). Thus, η' becomes a true Nambu-Goldstone boson, and plays the role of an axion that solves the strong CP problem. This is the dual description of the massless quark solution at low energy [77]. In Section 5.1, we consider a variant of this description with massless non-QCD quarks in the UV. Besides $\mathrm{SU}(3)_c$, if these massless quarks contain other quantum numbers from a new strong gauge group, they will be confined in bound states at a high energy scale and evade detection.

Chapter 3

Warped Extra Dimensions and AdS/CFT

Extra dimensional models refer to models where the number of dimensions exceeds the usual (3+1)-dimensional spacetime. The idea of extra dimensions dates back as far as the birth of modern physics. In 1914, Nordström proposed the first known 5D theory that extended the electromagnetic vector field to a fifth dimension to incorporate a scalar theory of gravity [78]. In 1920, Kaluza promoted the 4D metric tensor (of general relativity) to 5D that included the 4D metric tensor, an electromagnetic vector, and a scalar field (now known as the *radion*, or *dilaton*). The theory was given a quantum interpretation by Klein in 1926 [79, 80] preceding the then-recent discoveries of Schrodinger and Heisenberg. While the theory is incorrect as it failed to incorporate the known fermions, it remains an important prototype of extra dimensional models.

In subsequent years, extra spatial dimensions were considered a remote possibility, as there was no hope to detect these dimensions and the accompanying KK states. This sentiment has changed in the last several decades due to recent theoretical as well as experimental developments. One such theoretical development is *string theory*. In particle physics, *string theory* refers to a mathematical framework, in which point-like particles are replaced by one-dimensional objects called strings. Similar to the study of strong nuclear interactions, string theory emerged as a leading candidate for quantum gravity since in the low-energy spectrum it contains both a massless spin-2 excitation, identified with the graviton, and

necessary unified groups that can contain the Standard Model field content. However, one notable requirement of string theories is the requirement of extra spatial dimensions. For instance, superstring theory requires 10-dimensional spacetime, M-theory requires 11 dimensions, and bosonic string theory requires 26 dimensions. The existence of these extra dimensions would be one proof for string theory.

The lack of experimental detection of extra dimensions implies that these dimensions must be microscopic in size. The idea promoted by Klein was that the extra dimension was compactified, the simplest geometry being a circle S_1 with radius R. For a scalar field living on this $M_4 \times S_1$ geometry where M_4 is the 4D Minkowski spacetime, this implies[1]

$$\Phi(x^\mu, y) = \Phi(x^\mu, y + 2\pi R)\,. \tag{3.1}$$

Compactification directly leads to the quantization of momenta of fields along the extra dimensions. As a result, fields propagating in the *bulk*, i.e. freely moving along these dimensions, may be decomposed in a Kaluza-Klein (KK) expansion that consists of an infinite tower of 4D fields ϕ_n

$$\Phi(x^\mu, y) = \sum_{n\in\mathbb{Z}} \phi_n(x^\mu) e^{iny/R}\,. \tag{3.2}$$

The spectrum of these KK modes depends on the spacetime geometry, the localization details of the bulk, and ultimately on the 5D mass parameter of the field. In a flat extra dimension, the masses of these "standing waves" is simply

$$m_n = \frac{|n|}{R}\,. \tag{3.3}$$

The zero mode, being massless, is special. Other modes are massive at the scale $1/R$. If the size of the extra dimension is too small, then we can only observe the massless mode, and perceive them part of our four-dimensional world. Only at energy scales higher than $1/R$

[1] Interestingly, around 1953 Pauli consequently studied $M_4 \times S_2$ geometry and discovered the Yang-Mills theory (1954) [81]. The theory produced three gauge bosons of SU(2), due to the isometries of the sphere S_2. Pauli decided not to publish the result, not knowing what to do with the massless vector fields [82].

do these states become accessible. The detection of these KK modes, thus can provide the experimental signature of the extra dimensions.

This feature, however, is not ideal for string theory, which has a compactification scale of order $1/M_{\rm Pl}$. Collider experiments at the time (and even today!) did not have the capability to detect such a small distance scale, especially given that the gravity interaction is much weaker than the other forces. Nonetheless, after the first superstring revolution which showed that string theory is capable of providing an anomaly-free unified theory describing all elementary particles and their interactions [83], systematic searches of extra dimensions began in the 1990s. In this period, one intriguing possibility was that extra dimensions will be detectable around the TeV scale, originating from the large extra dimension model of Arkani-Hamed, Dimopoulos and Dvali (ADD) [84, 85, 86]. In the ADD model, the Standard Model fields live on a 4D hypersurface (referred to as a *brane*). Gravity, on the other hand, is allowed to propagate in the $(4+n)$-dimensional *bulk*. Thus, the Planck scale that we measure is not the true fundamental scale, but is related to the higher dimension scale M_* via the relation

$$M_{\rm Pl}^2 = V_n M_*^{n+2}\,, \tag{3.4}$$

where $V_n = (2\pi R)^n$ is the volume of the extra dimensions. For $n = 2$, taking $M_* \sim 1$ TeV yields $R \sim 0.1$ mm, which is close to the current experimental limits from precision tests of the gravitational force law[2] [87].

Parallel with the developments of string-motivated phenomenology such as large extra dimensional models, is the discovery of the *AdS/CFT correspondence* (sometimes referred to as *gauge/gravity duality* or *Maldacena duality*) [88] . There is now overwhelming evidence that the physics of weakly-coupled supergravity in 5D anti-de Sitter (AdS) spacetime is equivalent to that of a strongly-coupled 4D superconformal gauge theory (CFT stands for conformal field theory) [89, 90]. The duality is a breakthrough in string theory and

[2]The current limit is $R < 0.037$ mm at 95% CL for $n = 2$, corresponding to $M_* \geq 1.44$ TeV. Note that $M_{\rm Pl}$ is the reduced Planck mass.

quantum gravity, as it provides the most successful realization of the *holographic principle*[3], put forward by t'Hooft [91] and Susskind [92]. The AdS/CFT correspondence provides a powerful toolkit to study strongly coupled theories, such as the strong interaction, and thus finds many useful applications from nuclear to condensed matter physics.

A phenomenological model with an AdS bulk spacetime was developed shortly after the ADD model. Randall and Sundrum put forth a different scenario where the extra dimension is strongly warped, ensuring the appropriate localization of gravity [93, 94]. The price to pay is that to explain the flatness of the visible brane (our Universe), one needs to "off-load" the curvature onto the five-dimensional background. Thus the RS model provides a phenomenological framework for studying the AdS/CFT correspondence, while not having to include the string theory details.

In summary, extra dimensions is a vast subject, and only a small class of models that are relevant for this thesis has been introduced. Some general reviews on extra dimensions can be found in [95, 96], with phenomenological aspects in [97]. Readers interested in flat extra dimensions can consult [98] for a comprehensive review. The development of string and D-branes/p-branes that gave rise to the brane construction are reviewed in [99, 100]. An independent idea from the localization on topological defects was formed by Rubakov and Shaposhnikov [101], and later developments on localizing non-abelian gauge fields are included in [102, 103]. Holography and AdS/CFT correspondence reviews can be found in [104, 105].

In this thesis, we are directly interested in the extensions of the warped extra dimension model to construct a 5D model of the axion. In Section 3.1, we introduce the basic setup of a warped extra dimension model. Section 3.2 reviews the mathematics of localizing particles in the bulk, a new feature of the RS model not present in ADD. Finally, in Section 3.3, we review the AdS/CFT picture using the constructed 5D setup. These sections are directly relevant for Chapter 4, where the axion is incorporated.

[3] According to holographic principle, string theory admits lower-dimensional descriptions. An example of such a principle is black hole thermodynamics, where the maximal entropy scales with the area of the black hole.

3.1 Warped Extra Dimensions

Following the RS model, let us assume the simplest compactification over a circle S^1 with radius R, and let y be the coordinate along this dimension. A modern feature of compactification that differs from those of the KK theory is the ability to include chiral fermions. This can be achieved through an orbifold, in this case $S_1/\mathbb{Z}_2$

$$(x^\mu, y) \leftrightarrow (x^\mu, -y)\,. \tag{3.5}$$

The resulting segment thus has domain $[0, \pi R]$. For convenience, we will work with the conformal variable $z = e^{ky}/k$, where k is the curvature mass scale of the warping, and $z \in [z_{UV}, z_{IR}]$. The 5D spacetime coordinate is thus $x^M = (x^\mu, z)$. Let us assume that the 5D theory has a cosmological constant Λ_5 in the bulk, and $\Lambda_{UV/IR}$ are cosmological constants on the two UV/IR boundaries. The 5D action is then

$$S_5 = -\int d^4x \int_{z_{UV}}^{z_{IR}} dz\sqrt{-g}\left[\left(\frac{1}{2}M_5^3\mathcal{R}_5 + \Lambda_5\right) + \sqrt{-g_{UV}}\delta(z - z_{UV})\Lambda_{UV} + \sqrt{-g_{IR}}\delta(z - z_{IR})\Lambda_{IR}\right]\,, \tag{3.6}$$

where M_5 is the 5D Planck scale, $g_{IR/UV}$ are the respective induced metric determinants, and $\mathcal{R}_5$ is the 5D Ricci scalar. Solving the Einstein equations yields the metric[4]

$$ds^2 = A^2(z)(\eta_{\mu\nu}dx^\mu dx^\nu + dz^2) \equiv g_{MN}dx^M dx^N\,, \tag{3.7}$$

where $A(z) = 1/(kz)$ is the warp factor controlling how the 4D scale changes in the extra dimension. Specifically, IR energy scales are red-shifted by a factor $1/kz_{IR}$ with respect to those in the UV. Note that when $A(z)$ is a constant, one recovers the flat extra dimension of the ADD model.

[4] We take $\eta_{\mu\nu} = \mathrm{diag}(-+++)$

Consistency of the warped solution requires

$$k^2 = -\frac{\Lambda_5}{6M_5^3}\,, \tag{3.8}$$

and that

$$\Lambda_{UV} = -\Lambda_{IR} = -\Lambda_5/k\,. \tag{3.9}$$

This relation implies that Λ_5 is strictly negative, and thus the bulk is a slice of anti-de Sitter spacetime. By considering the graviton zero mode in the bulk and matching the low energy effective theory, Randall and Sundrum obtained the relation (up to first order, truncating exponentially small corrections)

$$M_{\rm p}^2 = n_{\rm throat}\frac{M_5^3}{2k} \tag{3.10}$$

where $n_{\rm throat}$ is the number of throats present in the theory. In this thesis we will only consider the axion throat thus taking $n_{\rm throat} = 1$ and neglect the Higgs branch. Thus throughout this thesis we will assume $M_5 \sim k \sim M_{\rm P}$, such that there is no dimensionful parameter appearing in the fundamental Lagrangian. The IR boundary scale is thus $M_{IR} = M_{\rm Pl}/(kz_{IR}) \equiv M_{\rm Pl}e^{-k\pi R}$, which could be at the TeV scale given a redshift of order 35.

For the RS model to explain the gauge hierarchy, the 5D construction needs to be stabilized. A natural mechanism was proposed involving an extra modulus field, known as the Goldberger-Wise mechanism[5] [106, 107]. The modulus potential is generated by a bulk scalar field with a brane interaction potential. The minimum of this potential then yields the compactification scale, thus dynamically solving the hierarchy problem.

[5]More elaborate mechanisms are required in ADD models.

3.2 Bulk Fields in a Slice of AdS

In the RS model, the Standard Model content was localized on the IR brane. It was eventually realized that for the gauge hierarchy problem, only the Higgs needed to be localized. Shortly after the RS model, bulk gauge fields were introduced [108], and bulk fermions followed soon after [109, 110, 111, 112, 113]. In this section, we briefly cover the bulk structure of fundamental particles. Again, we will not try to cover this development in detail, but only focus on important aspects relevant for this thesis. More details can be found in existing reviews [114, 115].

The equations of motion for the bulk fields are obtained by varying the corresponding action. Generically for a bulk field ϕ one can write

$$\delta S_5 = \int d^5x\, \delta\phi\, (\mathcal{D}\phi) + \int d^4x\, \delta\phi\, (\mathcal{B}\phi)|_{z^*}\,, \tag{3.11}$$

where $z^* = z_{UV/IR}$. The first term thus gives rise to the equation of motion $\mathcal{D}\phi = 0$, while the second term leads to the boundary conditions. Note that these conditions may only need to satisfy either $\delta\phi|_{z^*}$ or $\mathcal{B}\phi|_{z^*} = 0$, depending on the model. As is standard, we require the fields to also vanish at infinity in 4D spacetime.

3.2.1 Scalars

We consider the simplest scalar field in the bulk

$$S_\Phi = \int d^5x\sqrt{-g}\left(g^{MN}\partial_M\Phi\partial_N\Phi - \frac{1}{2}m_\Phi^2\Phi^2\right) - \int d^4x\sqrt{-g_4}U(\Phi)\,, \tag{3.12}$$

where for generality, a brane potential $U(\Phi)$ has been included. The KK mode decomposes as

$$\Phi(x^\mu, z) = \sqrt{k}\sum_n \phi^{(n)}(x) f_\phi(z)\,, \tag{3.13}$$

where $\phi^{(n)}(x)$ satisfy $\partial^2\phi^{(n)} = m_n^2\phi^{(n)}$. The mode equation is

$$\partial_z\left(\frac{1}{z^3}\partial_z f_\phi\right) - m_\Phi^2 A^5 f_\phi = m_n^2 f_\phi\,. \tag{3.14}$$

For the zero mode $n = 0$, the general solution has a simple form

$$f_\phi(z) = k^{3/2}\left(\lambda\,(kz)^{4-\Delta} + \sigma\,(kz)^{\Delta}\right)\,, \tag{3.15}$$

where $m_\Phi^2 = \Delta(\Delta-4)k^2$ or that $\Delta = 2 \pm \sqrt{4 + m_\Phi^2/k^2}$. Depending on the value of Δ, we see that the zero mode can localized anywhere in the bulk. With respect to the 5D flat metric, the zero mode profile (for the Δ term in Eq. (3.15)) is

$$\tilde{f}_\phi \propto (kz)^{\Delta-1}\,. \tag{3.16}$$

Thus in this case, for $\Delta < 1 (\Delta > 1)$ the zero mode is localized toward the UV (IR) brane, while for $\Delta = 1$ the zero mode is flat. Note that the zero mode is not guaranteed to exist, depending on the boundary conditions of the model. If boundary potentials $U_{UV/IR}$ are present, the zero mode only exists if

$$\partial_z f_\phi \mp \frac{A}{2}\left.\frac{dU}{df}\right|_{z^*} = 0\,. \tag{3.17}$$

The boundary conditions will also have to be specified such as the back-reaction on the branes is negligible. For a scalar field, this requires

$$|(\partial_z f)^2 - m_\Phi^2 f^2| \ll 12k^2M_5^2\,. \tag{3.18}$$

The presence of the UV brane potential breaks the conformal symmetry explicitly, while the IR brane potential breaks it spontaneously. The conformal symmetry implies a continuous spectrum. Thus the KK mode spectrum is a direct consequence of this symmetry breaking, similar to the pion spectrum which resulted from the chiral symmetry breaking in QCD.

More details will be included in Section 3.3. For the massive modes $m_n \neq 0$

$$f^{(n)}(z) = z^2 N_\phi \left[J_{\Delta \pm 2}\left(m_n z\right) + b\, Y_{\Delta \pm 2}\left(m_n z\right) \right] , \tag{3.19}$$

where N_ϕ and b are normalization constants. In the limit $z_{IR} \gg z_{UV}$, one can approximate the mass spectrum as

$$m_n \approx \left(n + \frac{\Delta}{2} - \frac{1}{4} \right) \frac{\pi}{z_{IR}} . \tag{3.20}$$

It can be directly checked that unlike the zero mode, the massive modes are localized near the IR brane.

3.2.2 Fermions

One initial hurdle of extra-dimensional models is how to model chiral fermions. The 4D irreducible spinor representation is the two-component Weyl spinor. In 5D, γ_5 must be included as part of the Dirac algebra, thus the smallest spinor representation is the four-component Dirac spinor. This problem was circumvented through introducing orbifolds, that impose a discrete symmetry in the bulk and allow a massless spectrum to be obtained. Consider a bulk Dirac spinor Ψ with action

$$S_f = -2 \int d^5x \, \sqrt{-g} \left[\frac{1}{2} \left(\bar{\Psi} \Gamma^M \mathcal{D}_M \Psi - (\mathcal{D}_M \bar{\Psi}) \Gamma^M \Psi \right) + M_\Psi \bar{\Psi} \Psi \right] , \tag{3.21}$$

where $\Gamma^M = e^M_A \gamma^A = A(z)^{-1} (\gamma^\mu, \gamma^5)$ are the 5D gamma matrices, and the mass coefficient $c_f = M_\Psi / k$ determines the localization of the chiral zero modes. Through a Z_2 orbifold, the bulk Lagrangian respects the $\mathbb{Z}_2$ parity

$$\gamma_5 \Psi(x^\mu, -y) = \pm \Psi(x^\mu, y) , \tag{3.22}$$

that determines the chiral components. One can decompose

$$\Psi = \Psi_L + \Psi_R \,, \tag{3.23}$$

where $\Psi_{L/R}$ correspond to the two eigenstates in Eq. (3.22) and further decompose each component into corresponding KK modes

$$\Psi(x^\mu, y)_{L/R} = \sqrt{k} \sum_n \psi^{(n)}_{L/R}(x^\mu) f^{(n)}_{L/R}(y) \,. \tag{3.24}$$

The KK modes then satisfy the mode equation[6]

$$\left(\partial_z \pm \frac{c_f}{z}\right) f^{(n)}_{L/R} = \mp m_n f^{(n)}_{L/R} \,. \tag{3.25}$$

subject to the boundary condition

$$(\delta\bar{\Psi}_R \Psi_L)_{z^*} = (\delta\bar{\Psi}_L \Psi_R)_{z^*} = 0 \,. \tag{3.26}$$

The zero modes have simple forms

$$f_{L/R}(z) = \mathcal{N}_f (kz)^{2\mp c_f} \,, \tag{3.27}$$

where the normalization is fixed by the kinetic term

$$\mathcal{N}_f = \sqrt{\frac{(1/2 \mp c_f)k}{(kz_{IR})^{1\mp 2c_f} - (kz_{UV})^{1\mp 2c_f}}} \,. \tag{3.28}$$

These states have definite helicity, and thus can be identified with the 4D Weyl fields. Specifically, the $-(+)$ sign in Eq. (3.28) is identified with the left (right)-handed fermions with parameters $c_L(c_R)$. The boundary condition Eq. (3.26) allows for only one possibility, either $\Psi_L|_{z^*} = 0$ or $\Psi_R|_{z^*} = 0$, and thus we can either have a left or right-handed massless mode.

[6] See [115] for a detailed derivation

Similar to the scalar zero mode, the fermion zero mode profile can also localized either towards the UV-boundary ($c_L(-c_R) > 1/2$) or towards the IR-boundary ($c_L(-c_R) < 1/2$). If the Higgs-boson is localized on the IR-boundary, one can exponentially suppress the Yukawa couplings by adjusting the localization of the zero modes. The slice of AdS_5, thus provides a natural framework to explain the fermion mass hierarchy in the Standard Model (see Chapter 4) via suitable choices of the order-one bulk mass parameters c_f.

For completeness, the massive fermion modes have a general solution

$$f^{(n)}_{L/R}(z) = N_\psi (kz)^{5/2} \left[J_{c_f \pm 1/2}(m_n z) + b\, Y_{c_f \pm 1/2}(m_n z) \right] . \tag{3.29}$$

In this case, the KK masses are approximately given by

$$m_n \simeq \left(n + \frac{|c_f \pm 1/2|}{2} - \frac{1}{4} \right) \frac{\pi}{z_{IR}} . \tag{3.30}$$

Since all fermions in the SM are built upon Weyl fermions, we will not be interested in these massive modes.

3.2.3 Gauge Bosons

We have seen that a common feature of the scalars and fermions is that while the massless modes can be localized anywhere depending on the bulk masses, the massive modes are always localized toward the IR brane. This is not true for gauge field zero modes. Let us consider a bulk gauge field A_M

$$S_{\text{gauge}} = \int d^5x \sqrt{-g} \left[-\frac{1}{4} g^{MP} g^{NQ} F_{MN} F_{PQ} + \frac{1}{2} b^2 k^2 g^{MN} A_M A_N \right] , \tag{3.31}$$

where $F_{MN} = \partial_M A_N - \partial_N A_M$. The 5D vector field A_M thus has dimension 3/2. The KK expansion is then

$$A_\alpha(x^\mu, z) = \sqrt{k} \sum_n A^{(n)}_\alpha(x^\mu) f^{(n)}_A(z) . \tag{3.32}$$

The equation of motion for the KK modes is

$$(m_n)^2 f_A^{(n)}(z) = -z\partial_z \left(\frac{1}{z}\partial_z f_A^{(n)}(z)\right) + \frac{b^2}{z^2} f_A^{(n)} \,. \tag{3.33}$$

The modes obey the normalization condition

$$\int \frac{dz}{z} f_A^{(m)} f_A^{(n)} = \delta^{mn} \,, \tag{3.34}$$

If the gauge symmetry is preserved in the bulk, then the mass term is necessarily zero ($b = 0$). In this case, the massless mode is given by

$$f_A^{(0)} = c_0^{(0)} + c_1^{(0)}(kz)^2 \,. \tag{3.35}$$

Thus there is no solution when Dirichlet boundary conditions are imposed. Neumann boundary conditions, on the other hand, lead to a constant mode and there is no freedom to change the localization of this mode.

In the massive case, the general mode function is then

$$f_A^{(n)} = \frac{z}{N_A^{(n)}} \left(J_\nu\left(m_n z\right) + \beta_A^{(n)} Y_\nu\left(m_n z\right)\right) \,, \tag{3.36}$$

where $\nu = \sqrt{1+b^2}$ and N_A is fixed by the normalization condition. The spectrum is approximately

$$m_n \simeq \left(n + \frac{|\nu|}{2} - \frac{1}{4}\right) \frac{\pi}{z_{IR}} \,. \tag{3.37}$$

So the massive modes are again localized near the IR brane.

3.3 AdS/CFT and Partial Compositeness

The AdS/CFT correspondence provides a connection between warped extra-dimensional models and 4D strongly-coupled theories. The following is a "dictionary" that relates the 4D and 5D theories. Specifically, the extra-dimensional coordinate z plays the role of the renormalization scale μ of the CFT. A UV cutoff scale thus explicitly breaks conformal invariance, while the IR boundary corresponds to spontaneous breaking of conformal symmetry at the IR scale. The KK states thus correspond to resonances of the strongly-coupled CFT.

Local 5D gauge symmetries correspond to global symmetries in the CFT. The UV boundary symmetry corresponds to gauging a subgroup of the bulk symmetry, while breaking gauge symmetries by IR boundary conditions corresponds to the spontaneous breaking $\mathcal{G}_5 \to \mathcal{H}_{IR}$ at the IR scale M_{IR}. The parameters of the 4D and 5D descriptions obey the following relation

$$g_5^2 k \sim \frac{16\pi^2}{N_c^r}\,, \tag{3.38}$$

where N_c is the number of colors in the CFT and $r = 1, 2$ depends on whether the CFT field is in the fundamental or adjoint representation of the gauge group. Thus the weak coupling limit in AdS_5 corresponds to the large-N expansion in the CFT.

To give an example, let us consider a bulk Higgs model with

$$\mathcal{G}_5 = \mathrm{SO}(5) \qquad \mathcal{H}_{IR} = \mathrm{SO}(4)\ . \tag{3.39}$$

The Higgs doublet arises from the coset SO(5)/SO(4) (this is the simplest composite Higgs model). Identifying the Higgs as the fifth component A_5 of a bulk gauge field A_M, this state acquires a mass of order M_{IR} when suitable IR boundary conditions are chosen. The Higgs thus emerges as a composite pseudo-Nambu-Goldstone boson arising from the spontaneous breaking $\mathcal{G}_5 \to \mathcal{H}_{IR}$.

The holographic interpretation for bulk fermions is more interesting. The 4D massless

mode described in section Section 3.2.2 corresponds to an external fermion with linear coupling to a CFT operator, $\mathcal{O}_i$

$$\Delta\mathcal{L} = \lambda_i \bar{\psi}_i \mathcal{O}_i + \text{h.c.}\,. \tag{3.40}$$

The dimension of the operator is thus $\dim \mathcal{O}_i = |c_f + 1/2| - 1$. By varying c_f, we can obtain different dimensions of the operator $\mathcal{O}_i$. For $c_f > 1/2$, the operator is relevant, corresponding to the fermion profile localized near the IR-brane. In this case, the coupling parameter becomes strong, and the fermion behaves as a composite CFT state. On the other hand, $c_f < 1/2$ implies that the operator is irrelevant, corresponding to the fermion profile localized near the UV brane, and the fermion behaves as an external elementary state. This is the idea behind *partial compositeness* realized in the context of warped dimensions. The AdS/CFT correspondence, thus provides us a novel toolkit to tackle problems in a composite theory. In Chapter 4, we will construct a holographic realization of the DFSZ axion, and apply the warped extra dimension framework to solve the axion quality problem in QCD. One can also apply the AdS/CFT correspondence to other contexts, such as constructing an axion composite sector (e.g. axicolor). Towards this purpose, we study composite axion models in more depth in Chapter 5.

Chapter 4

A Quality 5D Axion Model

In this chapter, we introduce a holographic construction of the DFSZ axion. Building upon this construction, we then provide a holographic solution of the axion quality problem in a slice of AdS_5 (see Section 3.1 and Section 3.2). Specifically, using the AdS/CFT correspondence (see Section 3.3), we model the $U(1)_{PQ}$ global symmetry of some underlying strong dynamics as a 5D $U(1)_{PQ}$ gauge symmetry that is spontaneously broken in the bulk. A massive, complex scalar field charged under the gauge symmetry corresponds to a PQ-charged operator $\mathcal{O}$ of dimension Δ. Both the explicit and spontaneous breaking of the global $U(1)_{PQ}$ symmetry are modelled by a vacuum expectation value for the bulk scalar field, with the former sourced by UV boundary terms that explicitly violate the $U(1)_{PQ}$ global symmetry.

The axion is then identified with the pseudoscalar fluctuations around this background, with a profile that depends on the arbitrary dimension Δ. Varying Δ allows the axion to be localised towards the IR brane where it is naturally sequestered from explicit gravitational violations of the Peccei-Quinn symmetry on the UV brane. A lower limit of at least $\Delta \gtrsim 10$ can then be derived to sufficiently suppress UV sources of explicit breaking for an axion decay constant $F_a \gtrsim 10^9$ GeV. This 5D model gives a simple, geometric interpretation of the axion quality problem and is dual to 4D solutions that invoke composite axions with an accidental $U(1)_{PQ}$ symmetry.

Our axion solution builds on previous work that considered axions propagating in an extra dimension. Axions in a flat extra dimension were first studied in [116]. An axion that

arises from a higher-dimensional gauge field in a warped dimension was discussed in [117]. Our solution is related but has the important difference that the symmetry is spontaneously broken by a bulk scalar vacuum expectation value (corresponding to an operator of finite dimension), as opposed to IR brane boundary conditions (corresponding to an operator of infinite dimension). Furthermore, the holographic dual of our 5D setup closely resembles 4D composite axion models. Other realisations of axions in a two-throat warped geometry were given in [118], and more recently a holographic model based on a top down construction was given in [119]. The equations of motion we derive for the pseudoscalar sector generalise similar results first obtained in the context of AdS/QCD for the QCD pseudoscalar sector [120]. For pions in QCD, the global chiral symmetry is spontaneously broken by a dimension three operator corresponding to a bilinear fermion condensate with explicit breaking by the quark masses on the UV boundary. Our result generalises the QCD pseudoscalar solution to arbitrary operator dimension Δ; furthermore, we explicitly show that the Nambu-Goldstone mode remains massless, even in the presence of a UV brane, when there is no explicit violation of the global symmetry.

The outline of this chapter is as follows. In Section 4.1 we present the 5D model in a slice of AdS_5 and derive the equations of motion and boundary conditions. In Section 4.2 we present the massless axion solutions which correspond to the spontaneous breaking of a PQ-charged operator with arbitrary dimension Δ. The massive axion solutions are given in Section 4.3, where an explicit source of PQ violation is added on the UV brane. Two realistic composite axion models are presented in Section 4.4 corresponding to placing QCD either on the UV brane or in the bulk. As expected, for QCD on the UV brane it is difficult to sequester the gravitational violation, while for QCD in the bulk the axion quality problem can be addressed. In Section 4.5 we incorporate the SM charged lepton by considering two choices for the Higgs fields. UV boundary Higgs are first considered in Section 4.5.2 where the axion-fermion couplings are shown to be flavour diagonal. Next, in Section 4.5.4, we consider the bulk Higgs case and derive the flavour-dependent, off-diagonal axion-fermion couplings for both a massless and massive axion in Section 4.5.5. A summary of the results is given in Section 4.6.

4.1 Basic 5D Setup

To model a global $\mathrm{U}(1)_{\mathrm{PQ}}$ symmetry of some underlying strong dynamics, we will consider a scalar field, Φ, charged under a $\mathrm{U}(1)_{\mathrm{PQ}}$ gauge symmetry in a slice of AdS_5 with the metric in (3.7). In the bulk we introduce a complex scalar field $\Phi = \eta\, e^{ia}$ and a U(1) gauge field $V_M = (V_\mu, V_z)$. The relevant 5D action is given by

$$\begin{aligned} S = 2\int_{z_{UV}}^{z_{IR}} d^5x\,\sqrt{-g}\,\Bigg(&-\frac{1}{4g_5^2}F^{MN}F_{MN} - \frac{1}{2}\big(D^M\Phi^\dagger\big)\big(D_M\Phi\big) - \frac{1}{2}m_\Phi^2\Phi^\dagger\Phi \\ &-\frac{1}{2g_5^2\xi}\left(g^{\mu\nu}\partial_\mu V_\nu + \xi A^{-3}\partial_z\left(AV_z\right) - \xi g_5^2\eta^2 a\right)^2\Bigg) \\ -\int d^4x\,\sqrt{-g_4}\,U(\Phi)\,, \end{aligned} \tag{4.1}$$

where g_5 is the 5D gauge coupling and $D_M = \partial_M - iV_M$. The $U(\Phi)$ are boundary potentials on the UV and IR branes whose form will be specified later. We work in R_ξ gauge with gauge parameter ξ, where the vector and scalar modes decouple.

4.1.1 Background Solution

Assuming the backreaction of the scalar Φ on the metric is negligible (Eq. (3.18)), the equation of motion for the z-dependent scalar vacuum expectation value $\eta(z)$ from Section 3.2.1 is

$$\partial_z\left(A^3\partial_z\eta\right) - m_\Phi^2 A^5\eta = 0\,, \tag{4.2}$$

with the boundary condition,

$$\partial_z\eta \mp \frac{A}{2}\frac{dU}{d\eta}\bigg|_{z_{UV},\,z_{IR}} = 0\,, \tag{4.3}$$

where the upper (lower) signs correspond to z_{UV} (z_{IR}). The equation of motion (4.2) has the general solution

$$\eta(z) = k^{3/2}\left(\lambda\,(kz)^{4-\Delta} + \sigma\,(kz)^{\Delta}\right)\,, \tag{4.4}$$

where $\Delta > 2$ is related to the bulk scalar mass according to $m_\Phi^2 = \Delta(\Delta-4)\,k^2$ [89]. The dimensionless coefficients λ and σ are fixed by the boundary conditions in Eq. (4.3), and the boundary potentials are assumed to have the following form

$$U_{UV}(\Phi) = (-\ell_{UV} k^{5/2}\Phi + \text{h.c.}) + b_{UV} k\,\Phi^\dagger\Phi\,, \tag{4.5}$$

$$U_{IR}(\Phi) = \frac{\lambda_{IR}}{k^2}\left(\Phi^\dagger\Phi - k^3 v_{IR}^2\right)^2\,, \tag{4.6}$$

where $\ell_{UV}, b_{UV}, \lambda_{IR}$ and v_{IR} are real dimensionless coefficients. Note that the linear term in (4.5) explicitly breaks the $\mathrm{U}(1)_{\mathrm{PQ}}$ symmetry on the UV brane. Solving the boundary conditions and taking the limit $z_{IR} \gg z_{UV}$ with $\Delta > 4$ one obtains

$$\lambda = \frac{\ell_{UV}}{\Delta - 4 + b_{UV}}(kz_{UV})^{\Delta-4}\,, \tag{4.7}$$

$$\sigma = \sqrt{v_{IR}^2 - \frac{\Delta}{2\lambda_{IR}}}\,(kz_{IR})^{-\Delta} \equiv \sigma_0\,(kz_{IR})^{-\Delta}\,. \tag{4.8}$$

Notice that σ is suppressed by $(kz_{IR})^{-\Delta}$, while λ is $\mathcal{O}(1)$. When ℓ_{UV}=0 sub-leading terms need to be kept and one finds in this case that λ is also suppressed:

$$\lambda = \frac{\Delta - b_{UV}}{\Delta - 4 + b_{UV}}(kz_{UV})^{2\Delta-4}\sigma\,. \tag{4.9}$$

If $b_{UV} = 0$ then λ in (4.9) is fixed in terms Δ and σ; a nonzero value of b_{UV} allows λ to be independently varied.

As summarized in Section 3.3, using the AdS/CFT correspondence, we can interpret the above 5D setup in terms of a dual strongly interacting 4D conformal field theory (CFT). The presence of the UV and IR branes correspond to explicit and spontaneous breaking of the conformal symmetry respectively, with the latter giving rise to a mass-gaped theory.

The scalar Φ is identified with a PQ-charged operator $\mathcal{O}$, with dimension Δ, in the dual strongly coupled sector. Furthermore, σ is identified with a condensate $\langle\mathcal{O}\rangle$, and ℓ_{UV} with turning on a source for $\mathcal{O}$. This source explicitly breaks $\mathrm{U}(1)_{\mathrm{PQ}}$, and for $\Delta > 4$ corresponds to breaking the global symmetry by a Planck-suppressed operator.

4.1.2 Pseudoscalar Sector

We are interested in the pseudoscalar spectrum, and in particular the lightest mode which will be identified with the axion. Varying the action (4.1) with respect to V_z and a one obtains the following equations of motion

$$A\,\Box V_z + g_5^2 A^3 \eta^2 \left(\partial_z a - V_z\right) + \xi A \partial_z \left(A^{-1}\partial_z\left(AV_z\right) - g_5^2 A^2 \eta^2 a\right) = 0\,, \tag{4.10}$$

$$A^3\eta^2\,\Box a + \partial_z\left(A^3\eta^2\left(\partial_z a - V_z\right)\right) + \xi A^2\eta^2\left(\partial_z\left(AV_z\right) - g_5^2 A^3\eta^2 a\right) = 0\,, \tag{4.11}$$

where $\Box \equiv \eta^{\mu\nu}\partial_\mu\partial_\nu$ and $\eta^{\mu\nu} = \mathrm{diag}(-,+,+,+)$. We solve the equations of motion by performing the KK expansion,

$$a(x^\mu, z) = \sum_{n=0}^{\infty} f_a^{(n)}(z) a^{(n)}(x^\mu)\,, \tag{4.12}$$

$$V_z(x^\mu, z) = \sum_{n=0}^{\infty} f_{V_z}^{(n)}(z) a^{(n)}(x^\mu)\,, \tag{4.13}$$

where $a^{(n)}(x^\mu)$ satisfies $\Box a^{(n)} = m_n^2 a^{(n)}$. Note that a and V_z are expanded in terms of the same set of 4D modes. The boundary conditions are

$$\pm\frac{2}{g_5^2}\left(A\eta^{\mu\nu}\partial_\mu V_\nu + \xi\left(\partial_z\left(AV_z\right) - g_5^2 A^3\eta^2 a\right)\right)\delta V_z\Big|_{z_{UV},z_{IR}} = 0\,, \tag{4.14}$$

$$\left(\pm 2A^3\eta^2\left(\partial_z a - V_z\right) - A^4\frac{\delta U}{\delta a}\right)\delta a\Big|_{z_{UV},z_{IR}} = 0\,, \tag{4.15}$$

$$\pm\frac{2}{g_5^2}A\left(\partial_z V_\mu - \partial_\mu V_z\right)\delta V^\mu\Big|_{z_{UV},z_{IR}} = 0\,, \tag{4.16}$$

where we have included the boundary condition obtained from varying the action with respect to V_μ. It is important to note that the 5D gauge symmetry imposes further restrictions

on the boundary conditions that can be used to satisfy the above conditions [121]. In order to have a well-defined 5D gauge transformation, one cannot impose Dirichlet conditions for V_z and either of V_μ or a on the same boundary. Doing so would constrain the form of gauge transformations in the bulk.

To satisfy eqs. (4.14) - (4.16) we impose the following boundary conditions on the fields

$$V_\mu\Big|_{z_{UV}} = 0\,, \qquad \partial_z V_\mu\Big|_{z_{IR}} = 0\,, \tag{4.17}$$

$$\xi\left(\partial_z\left(AV_z\right) - g_5^2 A^3\eta^2 a\right)\Big|_{z_{UV}} = 0\,, \qquad V_z\Big|_{z_{IR}} = 0\,, \tag{4.18}$$

$$\pm 2A^3\eta^2\left(\partial_z a - V_z\right) - A^4\frac{\delta U}{\delta a}\Big|_{z_{UV},z_{IR}} = 0\,. \tag{4.19}$$

If a and V_z were expanded in different 4D modes, then the orthogonality of the d'Alembertian eigenvectors transforms (4.10) and (4.11) into four separate equations, whose solution does not satisfy the boundary condition (4.18). Eq. (4.17), (4.18), (4.19) restrict the 5D gauge symmetry on the boundaries, where the gauge transformation parameter $\alpha(x^\mu, z)$ must satisfy

$$\begin{aligned} \partial_\mu\alpha\Big|_{z_{UV}} = 0\,, \qquad \partial_z\alpha\Big|_{z_{IR}} = 0\,, \\ \partial_z(A\partial_z\alpha) - g_5^2 A^3\eta^2\alpha\Big|_{z_{UV}} = 0\,, \end{aligned} \tag{4.20}$$

for a general infinitesimal 5D gauge transformation

$$V_M \to V_M + \partial_M\alpha(x^\mu, z)\,, \qquad a \to a + \alpha(x^\mu, z)\,. \tag{4.21}$$

The Dirichlet condition on V_μ at $z = z_{UV}$ therefore restricts the gauge symmetry to a global symmetry on the UV brane, and ensures that there is no massless vector mode in the spectrum. In other words, the global $\mathrm{U}(1)_{\mathrm{PQ}}$ symmetry in the dual 4D CFT is not gauged. This also determines the UV boundary condition for V_z. On the other hand, we want the gauge symmetry to be preserved on the IR boundary and so impose a Neumann

condition for V_μ at $z = z_{IR}$; this also fully determines the IR boundary conditions for V_z and a. The reason for this choice is that we are interested in the spontaneous breaking of the $\mathrm{U}(1)_{\mathrm{PQ}}$ symmetry by the scalar Φ, which is dual to spontaneous breaking by an operator of dimension Δ in the 4D CFT. If we were to instead impose a Dirichlet condition for V_μ it would correspond to spontaneous breaking by the infinite dimension operator associated with the IR brane. In this case one recovers the model of [117] in the limit that the scalar field Φ is decoupled. Furthermore, since our choice of boundary conditions preserves the gauge symmetry in the IR, all explicit sources of $\mathrm{U}(1)_{\mathrm{PQ}}$ violation are confined to the UV brane.

4.2 Massless 5D Axion

In this section we first look for solutions that describe an exactly massless axion ($m_0 = 0$). We therefore require that there is no source of explicit $\mathrm{U}(1)_{\mathrm{PQ}}$ breaking in the UV by taking $\ell_{UV} = 0$. We also assume $\lambda = 0$, which follows from imposing the condition $b_{UV} = \Delta$ in (4.9). We will comment on the case $\lambda \neq 0$ in section Section 4.2.2.

First, it is useful to define the new fields

$$\chi = \partial_z a - V_z \,, \tag{4.22}$$

$$\zeta = \frac{1}{A}\left(\partial_z\left(AV_z\right) - g_5^2 A^3 \eta^2 a\right) \,. \tag{4.23}$$

Notice that χ is gauge invariant. In terms of these new fields the equations of motion, (4.10) and (4.11), reduce to a coupled first order system for the massless modes in the KK expansion

$$\begin{aligned} g_5^2 A^3 \eta^2 f_\chi^{(0)} + \xi A \partial_z f_\zeta^{(0)} &= 0 \,, \\ \partial_z\left(A^3 \eta^2 f_\chi^{(0)}\right) + \xi A^3 \eta^2 f_\zeta^{(0)} &= 0 \,. \end{aligned} \tag{4.24}$$

This has the general solution (for $\lambda = 0$):

$$\begin{aligned} f_\chi^{(0)}(z) &= -(kz)^{2-\Delta}\left(c_1\, I_{\frac{1}{\Delta}-1}\left(g_5\sqrt{k}\tfrac{\sigma}{\Delta}(kz)^\Delta\right) + c_2\, I_{1-\frac{1}{\Delta}}\left(g_5\sqrt{k}\tfrac{\sigma}{\Delta}(kz)^\Delta\right)\right) \,, \\ f_\zeta^{(0)}(z) &= \frac{g_5}{\xi} k^{3/2}\sigma\,(kz)\left(c_1\, I_{\frac{1}{\Delta}}\left(g_5\sqrt{k}\tfrac{\sigma}{\Delta}(kz)^\Delta\right) + c_2\, I_{-\frac{1}{\Delta}}\left(g_5\sqrt{k}\tfrac{\sigma}{\Delta}(kz)^\Delta\right)\right) \,, \end{aligned} \tag{4.25}$$

where $I_\alpha(x)$ is the modified Bessel function of the first kind, and $c_{1,2}$ are dimensionless constants. The boundary conditions in eqs. (4.18) and (4.19) require that at least one of the $f_\chi^{(0)}$ or $f_\zeta^{(0)}$ vanish on each boundary. This is enough to enforce $c_1 = c_2 = 0$ such that $f_\chi^{(0)}$ and $f_\zeta^{(0)}$ vanish everywhere. Despite this, the solution is non-trivial when expressed back in

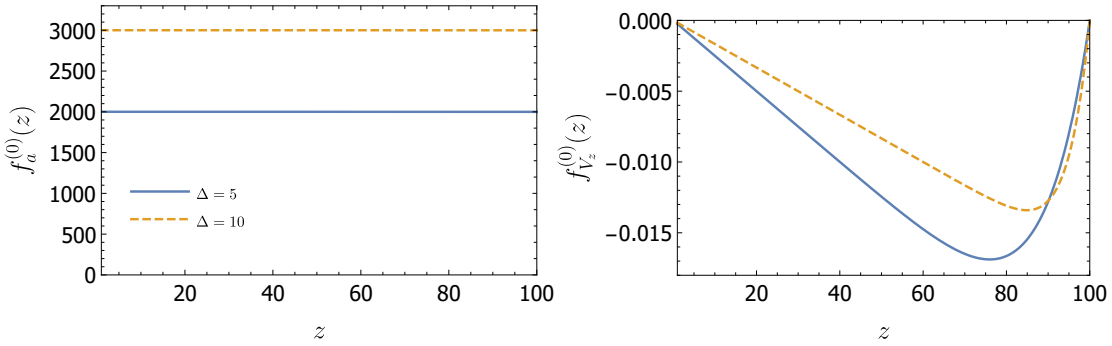

Figure 4.1: Normalised massless zero mode profiles (4.26) with $k = 1$, $kz_{UV} = 1$, $kz_{IR} = 100$, $g_5\sqrt{k} = 1$, and $\sigma_0 = 0.1$.

terms of V_z and a; solving eqs. (4.22) and (4.23) we obtain the profiles

$$\begin{aligned} f_{V_z}^{(0)}(z) &= g_5\sqrt{k}\sigma(kz)^{\Delta}\left(c_3\, I_{\frac{1}{\Delta}-1}\left(g_5\sqrt{k}\tfrac{\sigma}{\Delta}(kz)^{\Delta}\right) + c_4\, I_{1-\frac{1}{\Delta}}\left(g_5\sqrt{k}\tfrac{\sigma}{\Delta}(kz)^{\Delta}\right)\right), \\ f_a^{(0)}(z) &= z\left(c_3\, I_{\frac{1}{\Delta}}\left(g_5\sqrt{k}\tfrac{\sigma}{\Delta}(kz)^{\Delta}\right) + c_4\, I_{-\frac{1}{\Delta}}\left(g_5\sqrt{k}\tfrac{\sigma}{\Delta}(kz)^{\Delta}\right)\right), \end{aligned} \tag{4.26}$$

where c_3, c_4 are dimensionless constants. Imposing the remaining IR boundary condition, $V_z(z_{IR}) = 0$, gives

$$c_3 = -\frac{I_{1-\frac{1}{\Delta}}\left(g_5\sqrt{k}\tfrac{\sigma}{\Delta}(kz_{IR})^{\Delta}\right)}{I_{\frac{1}{\Delta}-1}\left(g_5\sqrt{k}\tfrac{\sigma}{\Delta}(kz_{IR})^{\Delta}\right)}c_4\,. \tag{4.27}$$

The last integration constant is fixed by canonically normalising the profiles, with the relevant part of the 5D action given by

$$S \supset 2\int_{z_{UV}}^{z_{IR}} d^5x\, \left(\frac{1}{2g_5^2}AV_z\Box V_z + \frac{1}{2}A^3\eta^2 a\Box a\right). \tag{4.28}$$

The resulting profiles for $f_a^{(0)}$ and $f_{V_z}^{(0)}$ are shown in Figure 4.1.

Further insight can be gained by looking at the approximate profiles obtained by expanding the Bessel functions in Eq. (4.26) for small argument. For large z_{IR}, this will be a very good approximation away from the IR brane since $\sigma = \sigma_0(kz_{IR})^{-\Delta}$. It remains a good approximation in the IR provided that $\sigma_0 < 1$; we will always assume this is the case

since it also ensures that the backreaction of the scalar can be neglected. The approximate profiles are

$$f_a^{(0)}(z) \simeq \frac{z_{IR}}{\sigma_0}\sqrt{\Delta-1}\left\{1+\frac{g_5^2 k\sigma_0^2}{4\Delta(\Delta-1)}\left[\frac{(\Delta-1)^2}{2\Delta-1}+\frac{z^2}{z_{IR}^2}\left(\left(\frac{z}{z_{IR}}\right)^{2(\Delta-1)}-\Delta\right)\right]\right\},$$
$$f_{V_z}^{(0)}(z) \simeq \frac{-1}{2\sigma_0\sqrt{\Delta-1}}\frac{z}{z_{IR}}\left(g_5^2 k\sigma_0^2\left(1-\left(\frac{z}{z_{IR}}\right)^{2(\Delta-1)}\right)\right), \tag{4.29}$$

where in the normalisation constant we have also taken $z_{IR} \gg z_{UV}$. Notice that the leading term in the $f_a^{(0)}$ profile is constant, while the solution for $f_{V_z}^{(0)}$ is approximately given by $f_{V_z}^{(0)} \propto A^{-1}$ in the UV.

4.2.1 Global U(1)$_{\rm PQ}$ Symmetry

The global U(1)$_{\rm PQ}$ symmetry that acts as a shift symmetry for the axion is realised as a subset of the 5D gauge transformations. Specifically, consider the subset of gauge transformations where the gauge parameter depends only on z and takes the same form as $f_a^{(0)}(z)$:

$$\alpha(x^\mu, z) = \alpha_0\, f_a^{(0)}(z)\,, \tag{4.30}$$

where α_0 is an arbitrary constant. One can easily check that this form also satisfies the boundary conditions in Eq. (4.20). Since $f_{V_z}^{(0)}(z) = \partial_z f_a^{(0)}(z)$, these gauge transformations act as a shift symmetry on the 4D axion mode; specifically,

$$a^{(0)}(x^\mu) \to a^{(0)}(x^\mu) + \alpha_0\,. \tag{4.31}$$

This is just the action of the global U(1)$_{\rm PQ}$ symmetry in the 4D effective theory.

4.2.2 Comment on $\lambda \neq 0$

So far, we have restricted ourselves to the assumption that $\lambda = 0$. A naïve application of the standard AdS/CFT dictionary might suggest that this is a necessary condition to

obtain a massless mode, since a non-zero λ is usually identified with turning on a source for the corresponding operator in the dual CFT. However, when $\ell_{UV} = 0$ the UV boundary condition in Eq. (4.3) relates λ and σ in (4.9); λ is then associated with a source for the operator $\mathcal{O}^\dagger\mathcal{O}$ [122] and so does not explicitly break $\mathrm{U}(1)_{\mathrm{PQ}}$. The scaling with z_{UV} in (4.9) also shows that λ should be identified with a source for an operator of dimension 2Δ. The situation changes once $\ell_{UV} \neq 0$, as can be seen from Eq. (4.7). This now describes a CFT with a non-zero source for the operator $\mathcal{O}$, which explicitly breaks $\mathrm{U}(1)_{\mathrm{PQ}}$. We will consider this case in section Section 4.3.

From the point of view of the 5D theory, there is no explicit breaking of the $\mathrm{U}(1)_{\mathrm{PQ}}$ global symmetry when $\ell_{UV} = 0$, even for non-zero λ. In fact, one can quite easily see that there is still a massless mode in the spectrum, since $\chi = \zeta = 0$ is a solution to Eq. (4.24) for any value of λ. The only difference is that it is no longer straightforward to solve eqs. (4.22) and (4.23) to obtain expressions for the profiles (except in the limit $g_5\sqrt{k} \to 0$).

4.3 Massive 5D Axion

Global symmetries are expected to be violated by quantum gravity. This in general presents a significant hurdle to axion solutions to the strong CP problem, since the stringent upper bound on $\bar{\theta}$ requires $\mathrm{U}(1)_{\mathrm{PQ}}$ to be an extremely good approximate global symmetry. This problem can be addressed if the global symmetry has its origin as a gauge symmetry in higher dimensions [123, 117], since this severely restricts possible sources of explicit $\mathrm{U}(1)_{\mathrm{PQ}}$ symmetry breaking. Within the current setup, the 5D gauge symmetry restricts global $\mathrm{U}(1)_{\mathrm{PQ}}$ breaking to two possible sources:

1. Terms localised on the UV brane, where the gauge symmetry is reduced to a global symmetry, $\partial_\mu \alpha(x^\mu, z_{UV}) = 0$;

2. Bulk terms that transform as a total derivative under gauge transformations, such as a Chern-Simons term.

It is important to note that although the global $\mathrm{U}(1)_{\mathrm{PQ}}$ symmetry that acts as a shift symmetry on the axion in Eq. (4.31) is explicitly broken on the UV brane, there remains a 5D gauge symmetry with a gauge parameter that satisfies $\alpha(x^\mu, z_{UV}) = 0$. Furthermore, in the case of a bulk Chern-Simons term, fermions must be added on the IR brane to cancel the localised gauge anomaly.

For now, let us focus on UV-localised sources and look for a solution that describes a massive axion in the presence of $\mathrm{U}(1)_{\mathrm{PQ}}$ breaking effects from Planck-suppressed operators. To achieve this we include a UV boundary potential for Φ that explicitly breaks the global $\mathrm{U}(1)_{\mathrm{PQ}}$ symmetry. The leading effects will come from a term linear in Φ; this can also be easily understood from the point of view of the dual CFT, where it corresponds to adding a source term for the operator $\mathcal{O}$ that spontaneously breaks $\mathrm{U}(1)_{\mathrm{PQ}}$.

It is straightforward to see that the inclusion of such a boundary term will give rise to a mass for the axion. Rewriting the linear term in Eq. (4.5) in terms of a gives

$$U_{UV}(\Phi) \supset -2\ell_{UV} k^{5/2} \eta \cos(a) = -2\ell_{UV} k^{5/2} \eta \left(1 - \frac{1}{2}a^2 + \dots\right) . \tag{4.32}$$

More precisely, the above potential modifies the boundary condition in Eq. (4.19) such that there is no longer a massless mode in the spectrum.

For massive modes and non-zero λ it is no longer straightforward to solve the equations of motion in general; however, an analytic solution can be obtained perturbatively in $g_5\sqrt{k}$. Note that since the g_5-dependent terms in the equations of motion are also proportional to $\eta^2(z)$, this expansion is expected to provide a good approximation even for relatively large values of g_5, as $\eta(z) \lesssim 1$ if the scalar backreaction can be neglected. For our purposes it is sufficient to work at leading order in g_5; the equations of motion then simplify significantly, since from Eq. (4.28) one can see that V_z must vanish at zeroth order. Eq. (4.11) can then be solved to obtain the $f_a^{(n)}$ profile,

$$f_a^{(n)}(z) = \frac{\sqrt{k}(kz)^2}{\eta(z)} \left(\frac{m_n}{k}\right)^{2-\Delta} \left(d_1 J_{\Delta-2}(m_n z) + d_2 Y_{\Delta-2}(m_n z)\right) , \tag{4.33}$$

where $d_{1,2}$ are dimensionless constants. Given that we are predominantly interested in the lightest mode, for which we expect $m_0 z_{IR} \ll 1$ (assuming $\Delta > 4$), it is useful to expand the Bessel functions for small argument to obtain the approximate axion profile,

$$\begin{aligned} f_a^{(0)}(z) \simeq \frac{\sqrt{k}(kz)^{4-\Delta}}{\eta(z)} \Bigg[& \frac{d_1}{2^\Delta \Gamma(\Delta)} \left(4(\Delta-1) - (m_0 z)^2\right) (kz)^{2(\Delta-2)} \\ & - \frac{d_2 \Gamma(\Delta-3)}{2^{4-\Delta}\pi} \left(\frac{m_0}{k}\right)^{2(2-\Delta)} \left(4(\Delta-3) + (m_0 z)^2\right) \Bigg] . \end{aligned} \tag{4.34}$$

Imposing the IR boundary condition, $\partial_z f_a^{(0)}|_{z_{IR}} = 0$, yields

$$\begin{aligned} d_2 = -d_1 \frac{\pi\, 4^{2-\Delta}}{\Gamma(\Delta)\Gamma(\Delta-3)} & (m_0 z_{IR})^{2(\Delta-2)} \\ & \times \frac{\lambda(\Delta-1)((m_0 z_{IR})^2 - 4(\Delta-2)) + \sigma_0 (m_0 z_{IR})^2 (k z_{IR})^{\Delta-4}}{\lambda (m_0 z_{IR})^2 - \sigma_0 (\Delta-3)(k z_{IR})^{\Delta-4}((m_0 z_{IR})^2 + 4(\Delta-2))} . \end{aligned} \tag{4.35}$$

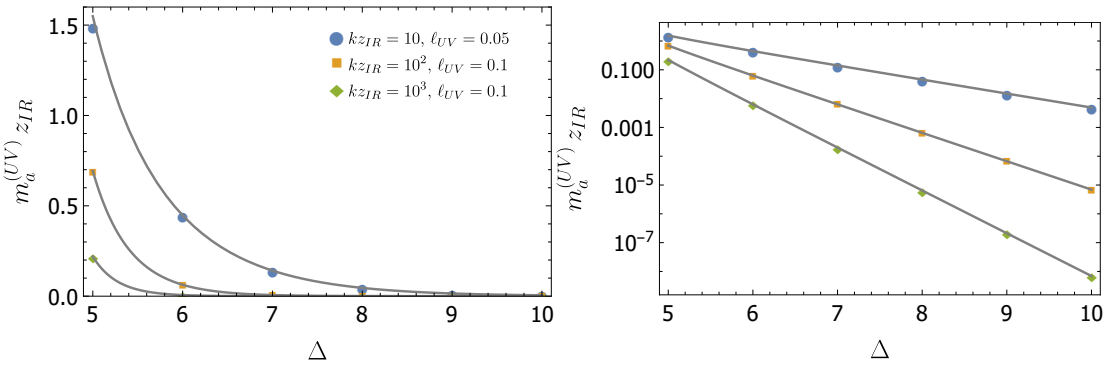

Figure 4.2: Axion mass relative to the compositeness scale (z_{IR}^{-1}), with $kz_{UV} = 1$, $\sigma_0 = 0.1$ and $b_{UV} = 0$. The curves correspond to the analytic solution for $g_5 = 0$ (4.36), while the points are obtained by numerically solving the equations of motion with $g_5\sqrt{k} = 1$.

The axion mass ($m_a^{(UV)} \equiv m_0$) is then determined by the UV boundary condition:

$$(m_a^{(UV)} z_{IR})^2 = \frac{4\ell_{UV}}{\sigma_0} \frac{\lambda(\Delta-1)(\Delta-2)(kz_{IR})^{4-\Delta}}{\ell_{UV} + 2(\Delta-2)\sigma_0 (z_{UV}/z_{IR})^{\Delta}} \,, \tag{4.36}$$

$$\simeq \frac{4\ell_{UV}}{\sigma_0} \frac{(\Delta-1)(\Delta-2)}{\Delta - 4 + b_{UV}} \left(\frac{z_{IR}}{z_{UV}}\right)^{4-\Delta} . \tag{4.37}$$

In the first line we have taken the $z_{IR} \gg z_{UV}$ limit for simplicity, but have also kept the leading ℓ_{UV}-independent term. The mass is proportional to ℓ_{UV} and vanishes in the absence of explicit breaking in the UV (so far we have not included the coupling to QCD). In the second line above we have used Eq. (4.7) and taken the limit $z_{IR} \gg z_{UV}$. The factor $(z_{IR}/z_{UV})^{4-\Delta}$ can be understood from the dual theory as being due to the RG running from the UV scale down to the confinement scale ($\sim z_{IR}^{-1}$), and is consistent with explicit breaking by an operator of dimension Δ. This results in a significant suppression of the axion mass when $z_{IR} \gg z_{UV}$ and Δ is large. This is shown in Figure 4.2, where we also compare with the mass obtained by numerically solving the equations of motion with $g_5\sqrt{k} = 1$. Notice that Eq. (4.36) continues to be a good approximation when $g_5 \sim 1$, since $\eta(z) \lesssim 0.1$.

We fix the remaining constant d_1 by canonically normalising the kinetic term in Eq. (4.28).

This requires the solution for V_z at $\mathcal{O}(g_5\sqrt{k})$, which is obtained by solving (4.10):

$$f_{V_z}^{(n)}(z) = g_5\sqrt{k}z\left(d_3 J_0\left(\frac{m_n}{\sqrt{\xi}}z\right) + d_4 Y_0\left(\frac{m_n}{\sqrt{\xi}}z\right)\right), \tag{4.38}$$

where $d_{3,4}$ are dimensionless constants. However, to satisfy the boundary conditions (4.18) and (4.19) requires $d_3 = d_4 = 0$. The leading term in V_z is then $\mathcal{O}(g_5^2 k)$, as was previously found for the massless solution in (4.29), and can be neglected to the order we are working. Substituting (4.34) into Eq. (4.28) then gives

$$d_1 = \frac{2^{\Delta-2}\Gamma(\Delta)}{\sqrt{\Delta-1}}(kz_{IR})^{1-\Delta}. \tag{4.39}$$

Putting everything together, the approximate axion profile, valid when $z_{IR} \gg z_{UV}$, is

$$f_a^{(0)}(z) \simeq z_{IR}\frac{k^{3/2}}{\eta(z)}\sqrt{\Delta-1}\left(\frac{z}{z_{IR}}\right)^{\Delta}\left[1 + \frac{2\lambda(\Delta-2)(kz_{UV})^{\Delta}(kz)^{2(2-\Delta)}}{\ell_{UV} + 2\sigma_0(\Delta-2)(z_{UV}/z_{IR})^{\Delta}}\right]. \tag{4.40}$$

The axion profile is plotted in Figure 4.3. Notice that, in contrast to the massless case, the profile becomes highly suppressed in the UV, particularly for large Δ. This feature will play an important role when constructing composite axion models in the following section. Figure 4.4 shows the profiles for both $f_a^{(0)}$ and $f_{V_z}^{(0)}$ with $g_5\sqrt{k} = 1$, obtained by numerically solving the equations of motion. The $f_a^{(0)}$ profile closely matches the perturbative solution in Figure 4.3, while $f_{V_z}^{(0)}$ remains largely unchanged from the massless case.

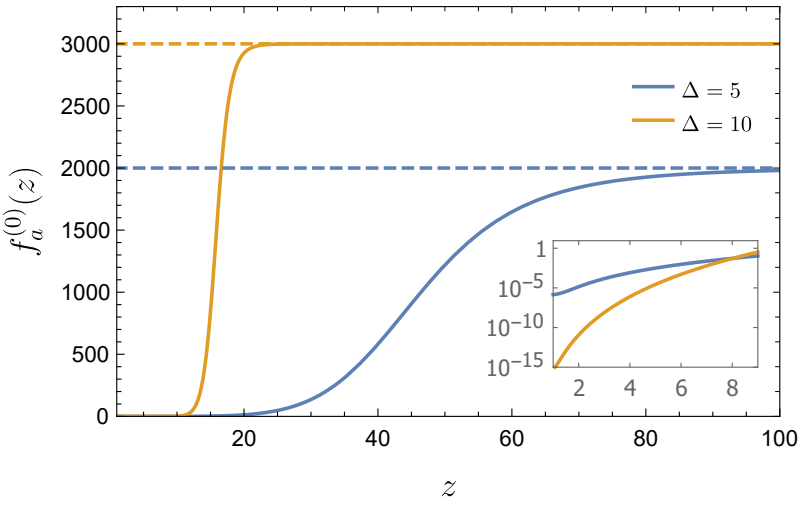

Figure 4.3: Normalised axion profile with explicit $\mathrm{U}(1)_{\mathrm{PQ}}$ breaking UV boundary term. The solid lines show the approximate profile in Eq. (4.40), while the dashed lines show the massless ($\ell_{UV} = \lambda = 0$) solution (4.26) for comparison. We fixed $k = 1$, $kz_{UV} = 1$, $kz_{IR} = 100$, $\sigma_0 = 0.1$, $\ell_{UV} = 0.1$, and $b_{UV} = 0$.

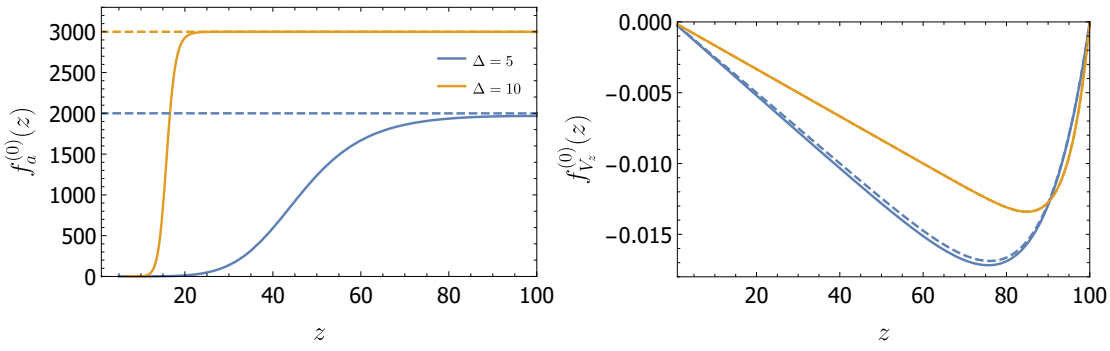

Figure 4.4: Same as Figure 4.3, except with $g_5\sqrt{k} = 1$ and the solid lines have been obtained by numerically solving the equations of motion.

4.4 Solving the The Axion Quality Problem

In this section we show how the 5D solution obtained in the previous section can be used to construct holographic descriptions of composite axion models [72, 71]. This requires introducing the usual coupling between the axion and QCD ($\mathrm{SU}(3)_c$). There are in principle two ways to do this, and each corresponds to a different class of composite axion models:

- $\mathrm{SU}(3)_c$ localised on the UV brane
- $\mathrm{SU}(3)_c$ in the bulk

In the following sections we discuss each of the above models, and in particular show that only the latter can provide a solution to the axion quality problem.

4.4.1 $\mathbf{SU}(3)_c$ on the UV Brane

Here the Standard Model fields are localised on the UV brane. One can then add either an additional Higgs doublet or additional coloured fermions to construct a DFSZ-[76, 75] or KSVZ-type [73, 74] model on the UV brane. In either case, the effective action for the axion takes the form

$$\mathcal{S}_{eff} = \int d^4x \left(\frac{1}{2} a^{(0)} \left(\Box - m_a^2 \right) a^{(0)} + \frac{N g_s^2}{32\pi^2} f_a^{(0)}(z_{UV}) a^{(0)} G\tilde{G} + \frac{E g^2}{32\pi^2} f_a^{(0)}(z_{UV}) a^{(0)} F\tilde{F} + \cdots \right), \tag{4.41}$$

where the anomaly coefficients E and N are determined by the charges of the UV localised fermions, and $g_s\,(g)$ is the QCD (QED) coupling. The axion decay constant is therefore determined by the value of the profile on the UV brane. Using Eq. (4.40) we obtain

$$F_a = \frac{1}{f_a^{(0)}(z_{UV})} = \frac{z_{IR}^{-1}}{\sqrt{\Delta - 1}} \left(\frac{z_{IR}}{z_{UV}} \right)^{\Delta} \left(\lambda (k z_{UV})^{4-\Delta} + \sigma_0 (z_{UV}/z_{IR})^{\Delta} \right) \times \left[1 + \frac{2\lambda(\Delta - 2)(k z_{UV})^{4-\Delta}}{\ell_{UV} + 2\sigma_0(\Delta - 2)(z_{UV}/z_{IR})^{\Delta}} \right]^{-1} . \tag{4.42}$$

When $\ell_{UV} = 0$ the decay constant is of order the IR scale, z_{IR}^{-1} (recall that $\lambda \propto z_{IR}^{-\Delta}$ when $\ell_{UV} = 0$, see (4.9)). However, once explicit sources of $\mathrm{U}(1)_{\mathrm{PQ}}$ breaking are included the axion profile becomes highly suppressed in the UV, as shown in Figure 4.3. The effective decay constant for couplings to UV localised fields is then significantly larger than the UV scale, z_{UV}^{-1}, as it is enhanced by the factor $(z_{IR}/z_{UV})^{\Delta-1}$. This scaling can be understood as a consequence of partial compositeness in the dual theory, where the coupling arises via mixing between the composite operator of dimension Δ and an elementary scalar with mass of order z_{UV}^{-1}.

Since all UV boundary terms see the same effective axion decay constant, there is no way to suppress non-QCD sources of $\mathrm{U}(1)_{\mathrm{PQ}}$ breaking. Hence, this model cannot solve the axion quality problem. This construction might still have an interesting application as a continuum limit of clockwork models [124], since it allows for hierarchically different axion couplings on the UV and IR branes.

4.4.2 $\mathbf{SU}(3)_c$ in the Bulk

The second class of models involves enlarging the 5D gauge symmetry to $\mathrm{SU}(3)_c \times \mathrm{U}(1)_{PQ}$. We assume that the rest of the SM fields are confined to the UV brane. The axion coupling to $G\tilde{G}$ can be generated from the Chern-Simons term,

$$-\frac{\kappa}{32\pi^2}\int_{z_{UV}}^{z_{IR}} d^5x\, \epsilon^{MNPQR} V_M G^a_{NP} G^a_{QR}\,, \tag{4.43}$$

where κ is a dimensionless constant and ϵ^{MNPQR} is the 5D Levi-Civita tensor density. Under a 5D gauge transformation, $V_M \to V_M + \partial_M \alpha$, this term is only invariant up to a total derivative, giving rise to boundary terms

$$\delta S = -\frac{\kappa}{32\pi^2}\left[\int d^4x\, \alpha(x^\mu, z)\, \epsilon^{\mu\nu\rho\sigma} G^a_{\mu\nu} G^a_{\rho\sigma}\right]_{z_{UV}}^{z_{IR}}. \tag{4.44}$$

The gauge parameter satisfies $\alpha(x^\mu, z_{UV}) = 0$ and so the $z = z_{UV}$ term above vanishes. However, in the IR there is a localised gauge anomaly that needs to be cancelled by adding

appropriately charged fermions on the IR brane (one might therefore expect that κ is quantised). In the effective action for the axion, this is equivalent to adding the term

$$\frac{\kappa}{32\pi^2}\int d^4x\, a\, G\tilde{G}\Big|_{z_{IR}} . \tag{4.45}$$

Thus, the combined action (4.43) and (4.45) is invariant under the gauge transformation. Integrating over z, and using the fact that the massless gluon profile is constant, we obtain the effective action for the axion,

$$\mathcal{S}_{eff} = \int d^4x \left(\frac{1}{2}a^{(0)}\left(\Box - m_a^2\right)a^{(0)} + \frac{g_s^2}{32\pi^2 F_a}a^{(0)}G\tilde{G}\right) , \tag{4.46}$$

where from Eqs. (4.43) and (4.45) the axion decay constant is

$$\frac{1}{F_a} = \kappa\left(f_a^{(0)}(z_{IR}) - \int_{z_{UV}}^{z_{IR}} dz\, f_{V_z}^{(0)}(z)\right) . \tag{4.47}$$

Substituting the profile in Eq. (4.40) gives

$$F_a \simeq \frac{1}{\kappa}\frac{\sigma_0}{\sqrt{\Delta-1}} z_{IR}^{-1} , \tag{4.48}$$

and the axion decay constant is of order the IR scale. We have confirmed numerically that this also remains the case when $g_5\sqrt{k}$ is $\mathcal{O}(1)$.

On the other hand, axion couplings to any additional, UV localised sources of $\mathrm{U}(1)_{\mathrm{PQ}}$ breaking are highly suppressed in this model. This is again a consequence of the fact that the $f_a^{(0)}(z)$ profile is IR localised and becomes highly suppressed in the UV when Δ is large.[1] In addition, V_z can only appear in the UV boundary action in the gauge invariant combination $F_{\mu z} = \partial_\mu V_z - \partial_z V_\mu$. This is due to the fact that V_z, unlike a, still transforms non-trivially on the UV brane under 5D gauge transformations, $V_z \to V_z + \partial_z\alpha|_{z_{UV}}$, as $\partial_z\alpha|_{z_{UV}} \neq 0$. Therefore, since V_z must be derivatively coupled, UV localised sources of explicit breaking

[1] Note that if there were additional bulk fields charged under $\mathrm{U}(1)_{\mathrm{PQ}}$ these could spoil the suppression if their 5D masses corresponded to operators of lower dimension. On the other hand, any contributions to the axion potential from additional UV-localised PQ-charged fields will be suppressed.

only generate a potential for the axion through their coupling to a, which is suppressed.

The bulk $\mathrm{SU}(3)_c \times U(1)_{PQ}$ model therefore provides a realistic, holographic description of a composite axion that can solve the axion quality problem. For large Δ the effects of explicit breaking sources in the UV can be sufficiently suppressed, while the axion decay constant that determines the QCD contribution to the axion potential is only weakly dependent on Δ. For a given decay constant, there is then a minimum critical value Δ_c needed to address the axion quality problem.

The value of Δ_c is determined by comparing the two contributions to the axion potential. In order to solve the strong CP problem the axion mass from QCD must dominate over the contribution arising from explicit UV violations of the $\mathrm{U}(1)_{\mathrm{PQ}}$ symmetry. Recall that the QCD instanton contribution to the axion mass is given by [125]

$$(m_a^{(QCD)})^2 \simeq \frac{m_u m_d}{(m_u + m_d)^2} \frac{m_\pi^2 F_\pi^2}{F_a^2} \simeq (5.7\,\mathrm{meV})^2 \left(\frac{10^9\,\mathrm{GeV}}{F_a}\right)^2 , \tag{4.49}$$

where $m_{u,d}$ are the up, down quark masses, $m_\pi \simeq 135\,\mathrm{MeV}$, and $F_\pi = 92\,\mathrm{MeV}$. Combining Eqs. (4.37) and (4.48) gives the UV contribution to the axion mass in terms of the decay constant

$$(m_a^{(UV)})^2 = \frac{4\ell_{UV}\sigma_0(\Delta-2)}{\kappa^2(\Delta-4+b_{UV})} \left(\frac{\kappa\sqrt{\Delta-1}}{\sigma_0}\right)^{\Delta} \left(\frac{F_a}{\Lambda_{UV}}\right)^{\Delta-4} F_a^2 , \tag{4.50}$$

where we have defined $\Lambda_{UV} \equiv z_{UV}^{-1}$. The two contributions to the axion mass are shown as a function of F_a in the left panel of Figure 4.5 for $\Delta = 11$. The axion potential with both of these contributions then becomes

$$V(a^{(0)}) \simeq -(m_a^{(QCD)})^2 F_a^2 \cos\left(\frac{a^{(0)}}{F_a} + \bar{\theta}\right) - (m_a^{(UV)})^2 F_a^2 \cos\left(\frac{a^{(0)}}{F_a} + \delta\right) , \tag{4.51}$$

where $\delta - \bar{\theta}$ is the relative phase between $\bar{\theta}$ and the PQ-violating operator of dimension Δ.

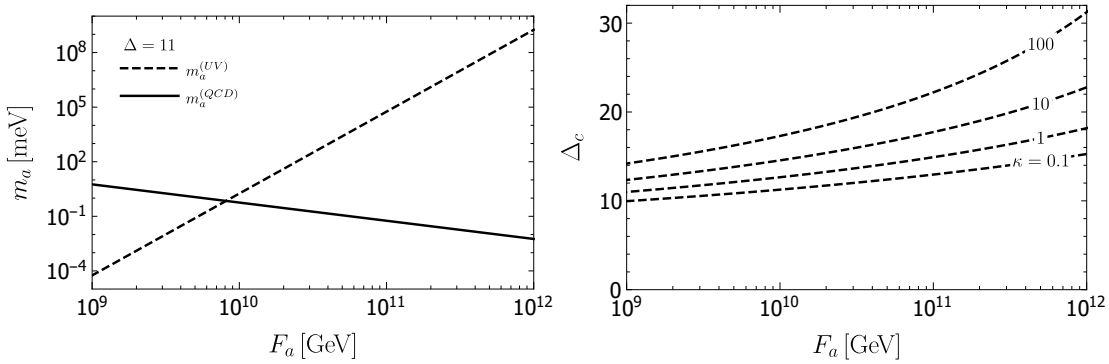

Figure 4.5: Left panel: QCD (solid) and UV (dashed) contributions to the axion mass for $\Delta = 11$ and $\kappa = 1$. Right panel: Critical operator dimension, Δ_c, needed to solve the axion quality problem. We fixed $k = M_P$, $kz_{UV} = 1$, $\sigma_0 = 0.1$, $\ell_{UV} = 0.1$, and $b_{UV} = 0$.

The minimum of the axion potential (4.51) is now displaced from the origin to the value

$$|\bar{\theta}_{eff}| \equiv \left| \left\langle \frac{a^{(0)}}{F_a} + \bar{\theta} \right\rangle \right| \simeq \frac{(m_a^{(UV)})^2 \sin(\delta - \bar{\theta})}{(m_a^{(QCD)})^2 + (m_a^{(UV)})^2 \cos(\delta - \bar{\theta})} \,. \tag{4.52}$$

Requiring that this shift be no larger than the experimental upper bound, $|\bar{\theta}_{eff}| \lesssim 10^{-10}$, leads to the condition $(m_a^{(UV)})^2 \lesssim 10^{-10}\,(m_a^{(QCD)})^2$, assuming an order one phase difference $\delta - \bar{\theta}$. This condition gives a lower bound, Δ_c, on the operator dimension, with the value needed to address the axion quality problem for a given decay constant shown in the right panel of Figure 4.5. The critical dimension is shown for several choices of κ, although it is mostly sensitive to just the ratio κ/σ_0, as can be seen from Eq. (4.50). For the range of decay constants 10^9 GeV $\lesssim F_a \lesssim 10^{12}$ GeV, consistent with obtaining the relic dark matter abundance with an order one initial misalignment angle, one requires at least $\Delta_c \gtrsim 10$.

Finally, in this class of models, the presence of $\mathrm{SU}(3)_c$ as a 5D gauge symmetry in the bulk means that in the dual theory (some of) the fundamental constituents of the composite sector must be charged under QCD. This is analogous to 4D composite axion models considered in the literature [126, 127, 128]. Note that in our holographic description the operator dimension Δ is a free parameter, since the underlying explicit 4D model is not specified. However, requiring that the 5D theory is perturbative does imply that we are considering the

composite model in the large-N_c limit (where N_c is the number of colours in the confining gauge group) via the relation $g_5^2 k \sim (4\pi)^2/N_c$ [129, 130]. Furthermore, the coupling of the axion to $G\tilde{G}$ is generated via the $\mathrm{U}(1)_{\mathrm{PQ}}$–$\mathrm{SU}(3)_c^2$ anomaly and hence $\kappa \propto N_c$.

4.5 Including the SM Charged Fermions

In this section, we extend the 5D axion model to include the axion-fermion couplings while automatically address the fermion mass hierarchy and axion quality problem, unlike the original 4D DFSZ model. The bulk fermion profiles are controlled by order one 5D fermion mass parameters. Once these parameters are chosen to explain the Standard Model fermion mass hierarchy and mixings, they give predictions for the axion couplings to fermions. For a boundary-localized Higgs sector, only flavour-diagonal couplings are generated. This follows from the orthonormality of the bulk fermion profiles. However, when the Higgs sector propagates in the bulk, there is a non-trivial wavefunction overlap between the axion and the fermion profiles that gives off-diagonal fermion couplings. The predictions for the off-diagonal couplings involving quarks and charged leptons are consistent with the current experimental limits [131, 132]. Assuming an axion decay constant $F_a \sim 10^9$ GeV, the effective scale of the axion-fermion off-diagonal couplings is of order $10^{11} - 10^{15}$ GeV.

4.5.1 Bulk Standard Model Fermions

In addition to the bulk $\mathrm{U}(1)_{\mathrm{PQ}}$ there is also the Standard Model gauge group $\mathrm{SU}(3)_c \times SU(2)_L \times U(1)_Y$. The bulk Standard Model gauge bosons have Neumann boundary conditions so that the massless zero modes are identified with the Standard Model gauge bosons (see Ref. [115]). Later, we will consider two possibilities for breaking the electroweak gauge symmetry.

The bulk Standard Model gauge group allows for the Standard Model fermions to be located in the bulk. The localization of the zero modes is then responsible for generating the fermion mass hierarchy and will also lead to flavour-dependent axion-fermion couplings. Denoting the 5D $SU(2)_L$ quark doublet field by Q and the singlet fields by U, D, the bulk

fermion action for the quark sector is given by [115, 133]

$$S_f = -2\int_{z_{UV}}^{z_{IR}} d^5x\,\sqrt{-g}\Bigg(\frac{1}{2}\left(\bar{Q}_i\Gamma^M\mathcal{D}_M Q_i - (\mathcal{D}_M\bar{Q}_i)\Gamma^M Q_i\right) + M_{Q_i}\bar{Q}_i Q_i \\ + \frac{1}{2}\left(\bar{U}_i\Gamma^M\mathcal{D}_M U_i - (\mathcal{D}_M\bar{U}_i)\Gamma^M U_i\right) + M_{U_i}\bar{U}_i U_i \\ + \frac{1}{2}\left(\bar{D}_i\Gamma^M\mathcal{D}_M D_i - (\mathcal{D}_M\bar{D}_i)\Gamma^M D_i\right) + M_{D_i}\bar{D}_i D_i\Bigg)\,, \tag{4.53}$$

where $\Gamma^M = e^M_A\gamma^A = A(z)^{-1}(\gamma^\mu,\gamma^5)$, with $\gamma^5 = ((\mathbb{1},0),(0,-\mathbb{1}))$, and the fermions carry PQ charges $X_{Q,U,D}$. The 5D masses, $M_X \equiv c_X k$, determine the localization of the chiral zero modes, to be identified with the SM fermions, and i is a flavour index. Following Section 3.2.2, we can decompose the Dirac spinor Q_i in terms of its Weyl components $Q_i = (Q_{iL}, Q_{iR})^T$, the equation of motion is

$$\gamma^\mu\partial_\mu Q_{iL(R)} \mp \partial_z Q_{iR(L)} + \frac{1}{z}(c_{Q_i} \pm 2)Q_{iR(L)} = 0\,. \tag{4.54}$$

To solve this equation, we perform the KK expansion,

$$Q_{iL(R)}(x^\mu, z) = \sum_{n=0}^{\infty} f^n_{Q_{iL(R)}}(z)Q^n_{iL(R)}(x^\mu)\,, \tag{4.55}$$

where $\not{\partial}Q^n_{iL(R)} = -m_n Q^n_{iR(L)}$, and similarly for U and D. After imposing Dirichlet conditions $Q_{iR} = U_{iL} = D_{iL} = 0$ on both boundaries, there are chiral zero modes with profiles

$$\begin{aligned} f^0_{Q_{iL}}(z) &= \mathcal{N}_{Q_i}(kz)^{2-c_{Q_i}}\,,\\ f^0_{U_{iR}}(z) &= \mathcal{N}_{U_i}(kz)^{2+c_{U_i}}\,,\\ f^0_{D_{iR}}(z) &= \mathcal{N}_{D_i}(kz)^{2+c_{D_i}}\,. \end{aligned} \tag{4.56}$$

Normalising the 4D kinetic terms fixes the constants

$$\mathcal{N}_X = \sqrt{\frac{(1\mp 2c_X)k}{2((kz_{IR})^{1\mp 2c_X} - (kz_{UV})^{1\mp 2c_X})}}\,, \tag{4.57}$$

where $-(+)$ refers to the left (right) handed profiles. Similar expressions are obtained in the lepton sector.

4.5.2 Boundary Higgs Fields

We first consider a setup with boundary-localized Higgs fields $H_{u,d}$ to construct a 5D model of the DFSZ axion [76, 75]. The Higgs doublet fields, which transform as $H_{u,d} \sim (\mathbf{2}, \mp\frac{1}{2})$ under the $SU(2)_L \times U(1)_Y$ electroweak gauge group, are localized on the UV boundary. They are also charged under the $\mathrm{U}(1)_{\mathrm{PQ}}$ symmetry with charges X_{H_u,H_d}, such that

$$X_{H_u} + X_{H_d} + 2X_\Phi = 0 \tag{4.58}$$

. The most general scalar potential on the UV boundary is thus

$$\begin{aligned} U_{UV}(\Phi, H_u, H_d) = {} & \lambda_u(|H_u|^2 - v_u^2)^2 + \lambda_d(|H_d|^2 - v_d^2)^2 + b_{UV}k|\Phi|^2 \\ & + (a|H_u|^2 + b|H_d|^2)|\Phi|^2 + c(H_u H_d \Phi^2 + h.c.) \\ & + d|H_u H_d|^2 + e|H_u^\dagger H_d|^2 \,, \end{aligned} \tag{4.59}$$

where $H_u H_d = \epsilon_{ij} H_u^i H_d^j$ with ϵ_{ij} the $SU(2)$ antisymmetric tensor.

To obtain the axion couplings, we first parametrise the scalar fields by

$$H_u = \frac{v_u}{\sqrt{2}} e^{i\frac{a_u(x)}{v_u}} \begin{pmatrix} 1 \\ 0 \end{pmatrix}, \qquad H_d = \frac{v_d}{\sqrt{2}} e^{i\frac{a_d(x)}{v_d}} \begin{pmatrix} 0 \\ 1 \end{pmatrix}, \qquad \Phi = \eta(z) e^{ia(x,z)} \,, \tag{4.60}$$

where we have ignored the radial components and the electromagnetically-charged NG bosons in $H_{u,d}$. The global 4D $\mathrm{U}(1)_{\mathrm{PQ}}$ symmetry is a remnant of the 5D local $\mathrm{U}(1)_{\mathrm{PQ}}$ symmetry and is realised by choosing the 5D gauge transformation parameter $\alpha(x,z) = \alpha_0 f_a^0(z)$, such that the axion zero mode transforms as

$$a^0(x) \to a^0(x) + \alpha_0 \,. \tag{4.61}$$

In this case, the 4D PQ current can then be written as

$$J_\mu^{PQ} = X_\Phi f_a^0 (z_{UV})^{-1} \partial_\mu a^0 + X_{H_u} H_u^\dagger i \overleftrightarrow{\partial_\mu} H_u + X_{H_d} H_d^\dagger i \overleftrightarrow{\partial_\mu} H_d + \dots \,, \tag{4.62}$$

where $H_i^\dagger \overleftrightarrow{\partial_\mu} H_i = \partial_\mu (H_i^\dagger) H_i - H_i^\dagger \partial_\mu H_i$. The physical 4D axion, a_4, is then defined by using the Goldstone theorem $\langle 0 | J_\mu^{PQ} | a_4 \rangle = i F_a p_\mu$. This gives:

$$F_a a_4(x) \equiv X_\Phi f_a^0 (z_{UV})^{-1} a^0 + X_{H_u} v_u a_u + X_{H_d} v_d a_d \,, \tag{4.63}$$

where

$$\sum_i X_i^2 v_i^2 = F_a^2 \,, \tag{4.64}$$

with $i = \Phi, H_{u,d}$ and $v_\Phi = f_a^0 (z_{UV})^{-1}$. Since $v_{u,d} \ll v_\Phi$ we obtain that $F_a \simeq v_\Phi$.

Similarly, the 4D hypercharge current is given by

$$J_\mu^Y = Y_u H_u^\dagger i \overleftrightarrow{\partial_\mu} H_u + Y_d H_d^\dagger i \overleftrightarrow{\partial_\mu} H_d = \frac{1}{2} \partial_\mu (v_u a_u - v_d a_d) \,, \tag{4.65}$$

where $Y_{u,d} = \mp 1/2$ and $a_Z \propto v_u a_u - v_d a_d$ is the NG boson eaten by the Z boson. Requiring orthogonality between the PQ and hypercharge currents, i.e. $\langle 0 | J_\mu^Y | a_4 \rangle = 0$, leads to the condition

$$X_{H_u} v_u^2 - X_{H_d} v_d^2 = 0 \,. \tag{4.66}$$

Combined with the relation $X_{H_u} + X_{H_d} + 2 X_\Phi = 0$, this fixes the PQ charges of the scalars up to an overall normalization:

$$X_\Phi = 1, \qquad X_{H_u} = -2 \cos^2 \beta, \qquad X_{H_d} = -2 \sin^2 \beta \,, \tag{4.67}$$

where $\sin \beta = v_u / v$, $\cos \beta = v_d / v$, with the electroweak VEV $v = 246\,\text{GeV}$.

In addition to the physical axion defined in (4.63) there is also a heavy axion $A(x)$ that

obtains its mass from the $H_u H_d \Phi^2 + h.c.$ term in the boundary potential (4.59). It is given by

$$A(x) \propto \frac{a_u(x)}{v_u} + \frac{a_d(x)}{v_d} + 2 f_a^0(z_{UV}) a^0(x) + \dots \tag{4.68}$$

The three physical fields a_4, a_Z and A are defined in terms of a_u, a_d and a^0. Inverting these relations determines $a_{u,d}$ as a function of the axion field $a_4(x)$. In the limit that $v_\Phi \gg v_{u,d}$ one finds the substitution relations

$$\frac{a_{u,d}}{v_{u,d}} \to X_{H_u,H_d} \frac{a_4}{F_a} \,. \tag{4.69}$$

4.5.3 Axion-Fermion Couplings with Boundary Higgs Fields

To obtain the axion-fermion couplings we first need to specify how the SM fermion masses are generated. Since the Higgs fields are UV localized, this occurs via Yukawa couplings localized on the UV brane,

$$S_{\text{Yukawa}} = -\int d^4x \sqrt{-g_{UV}} \, \frac{1}{k} \left(y^{(5)}_{u,ij} \bar{Q}_i U_j H_u + y^{(5)}_{d,ij} \bar{Q}_i D_j H_d + y^{(5)}_{e,ij} \bar{L}_i E_j H_d + \text{h.c.} \right) \Big|_{z_{UV}} , \tag{4.70}$$

where $y^{(5)}_{u,d,e}$ are dimensionless 5D Yukawa couplings. The axion couplings to fermions are then obtained by substituting (4.60) into (4.70) and using the relations (4.69).

By performing the following field redefinitions on the fermion zero modes,

$$u_i \to e^{i\gamma_5 X_{H_u} \frac{a_4}{2F_a}} u_i, \qquad d_i \to e^{i\gamma_5 X_{H_d} \frac{a_4}{2F_a}} d_i, \qquad e_i \to e^{i\gamma_5 X_{H_d} \frac{a_4}{2F_a}} e_i \,, \tag{4.71}$$

the axion field can be removed from the mass terms to give the 4D effective Lagrangian

$$\mathcal{L}_{4D} \supset -m_u^{ij} \bar{u}_{iL} u_{jR} - m_d^{ij} \bar{d}_{iL} d_{jR} - m_e^{ij} \bar{e}_{iL} e_{jR} + \text{h.c.} \,, \tag{4.72}$$

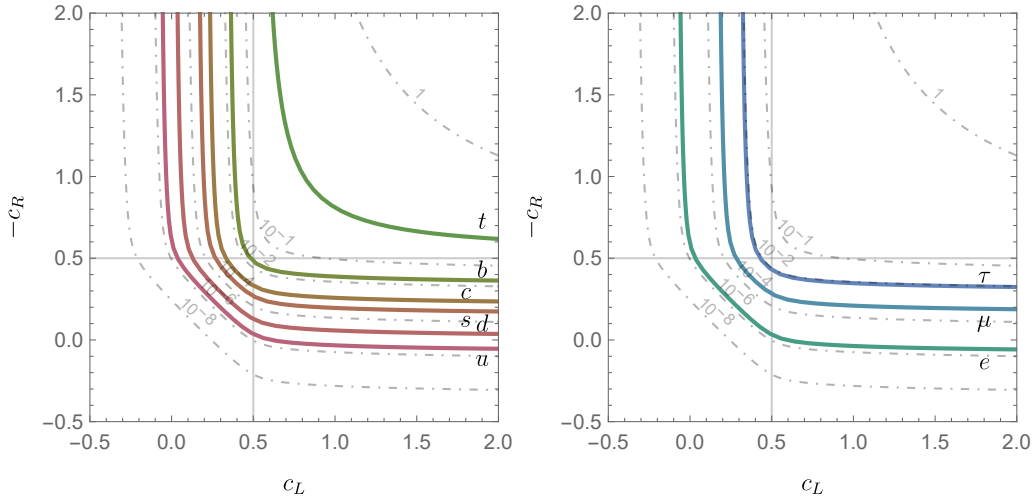

Figure 4.6: Contours of the quark (left) and charged lepton (right) masses for the UV Higgs case as a function of c_L and $-c_R$ with $\tan\beta = 3$, and $kz_{\rm IR} = 10^{10}$. The $y^{(5)}_{u,d,\ell}$ are randomly generated diagonal 5D Yukawa matrices drawn from a log-normal distribution with $\mu = 0$ and $\sigma = 0.3$. The contours correspond to the median of the generated set $(c_L, -c_R)$.

where

$$m_u^{ij} = y^{(5)}_{u,ij} \frac{v_u}{\sqrt{2}k} f^0_{Q_{iL}}(z_{UV}) f^0_{U_{jR}}(z_{UV})\,, \tag{4.73}$$

and similarly for $m^{ij}_{d,e}$. The mass matrix m^{ij}_u can be diagonalized by the singular value decomposition

$$A^{u\dagger}_L m^{ij}_u A^u_R = m_{u_i}\,, \tag{4.74}$$

where $A^u_{L,R}$ are unitary matrices and m_{u_i} is the diagonal mass matrix containing the up-type masses. For a 3×3 matrix $y^{(5)}_u$ with anarchic elements of order one, a 4D Yukawa coupling hierarchy is generated from the overlap of the bulk profiles [133]. The bulk mass parameters, c_i, are then constrained by the quark and charged lepton masses, as shown in Figure 4.6. Further details are given in Appendix A. The fermion kinetic terms are not invariant under the redefinitions (4.71) and generate derivative couplings of the axion to fermions. For the

up-type quarks, these are given by

$$
\begin{aligned}
& i \int d^4x \, \frac{X_{H_u}}{2F_a} \partial_\mu a_4 \, \left(-\bar{u}_{iL} (A_L^u A_L^{u\dagger})_{ij} \gamma^\mu u_{jL} + \bar{u}_{iR} (A_R^u A_R^{u\dagger})_{ij} \gamma^\mu u_{jR} \right) , \\
& \equiv i \int d^4x \, \left(\frac{\partial_\mu a_4}{2F_a} \, c_u^A \bar{u}_i \gamma^\mu \gamma_5 \, u_i \right) ,
\end{aligned} \tag{4.75}
$$

where $c_u^A = -X_{H_u}$. Similarly for the down-type quarks and leptons. Thus, for boundary-localized Higgs fields, the vector couplings vanish and the axial-vector couplings are flavour-diagonal. The current experimental constraints on the c^A are given in Ref. [131]. The redefinitions (4.71) also induce axion couplings to gluons and photons, as in the standard DFSZ model. A more detailed investigation of the axion-gluon/photon couplings in the bulk Higgs case will be discussed below.

4.5.4 Bulk Higgs Fields

Next, we consider the case of bulk Higgs fields, and show that this leads to flavour off-diagonal axion-fermion couplings. The Higgs fields H_u, H_d still have a UV boundary potential given by (4.59) but now they propagate in the bulk. The bulk action is

$$
\begin{aligned}
S_H = 2 \int_{z_{UV}}^{z_{IR}} d^5x \, \sqrt{-g} \, \Big(& -\big(\mathcal{D}^M H_{u,d}\big)^\dagger \big(\mathcal{D}_M H_{u,d}\big) - m_{H_{u,d}}^2 H_{u,d}^\dagger H_{u,d} \\
& - \frac{1}{2 g_Y^2 \xi_Y} \left(g^{\mu\nu} \partial_\mu B_\nu - \xi_Y g_Y^2 \left(Y_{H_u} v_u a_u + Y_{H_d} v_d a_d \right) \right)^2 \Big) \\
& - \int d^4x \, \sqrt{-g_4} \, U_{UV}(\Phi, H_u, H_d) \, ,
\end{aligned} \tag{4.76}
$$

where $\mathcal{D}_M = \partial_M - i X_{H_{u,d}} V_M + \ldots$, and ξ_Y is a $\mathrm{U}(1)_Y$ gauge-fixing parameter. Note that $a_{u,d}$ will also contribute to the $\mathrm{U}(1)_{\mathrm{PQ}}$ gauge fixing term in Eq. (4.1). The scalar fields can be parametrized as

$$
H_u = \frac{v_u}{\sqrt{2}} e^{i \frac{a_u(x,z)}{v_u}} \begin{pmatrix} 1 \\ \\ 0 \end{pmatrix} , \qquad H_d = \frac{v_d}{\sqrt{2}} e^{i \frac{a_d(x,z)}{v_d}} \begin{pmatrix} 0 \\ \\ 1 \end{pmatrix} , \qquad \Phi = \eta(z) e^{i a(x,z)} \, , \tag{4.77}
$$

where $a_{u,d}(x,z)$ are the neutral NG bosons propagating in the bulk, and the radial components and the electromagnetically-charged NG bosons in $H_{u,d}$ have again been ignored. In general, the bulk VEVs can have nontrivial z-dependence (i.e. $v_{u,d} = v_{u,d}(z)$), but for simplicity we assume they are constant. This requires adding appropriate bulk and IR boundary mass terms for $H_{u,d}$, similar to the bulk Higgs setup considered in Ref. [134]. The 4D electroweak VEV is then approximately $v^2 \approx (v_u^2 + v_d^2)/k$, assuming $z_{UV} = 1/k$ (note that the 5D fields in (4.77) have canonical mass dimension 3/2).

It is convenient to define the new fields

$$a_Y = \frac{1}{N_Y}\left(Y_{H_u} v_u a_u + Y_{H_d} v_d a_d\right) , \tag{4.78}$$

$$a_X = \frac{1}{N_X}\left(X_{H_u} v_u a_u + X_{H_d} v_d a_d\right) , \tag{4.79}$$

where $N_Y = \sqrt{Y_{H_u}^2 v_u^2 + Y_{H_d}^2 v_d^2}$ and $N_X = \sqrt{X_{H_u}^2 v_u^2 + X_{H_d}^2 v_d^2}$. The PQ charges can be chosen such that these two combinations are orthogonal:

$$Y_{H_u} X_{H_u} v_u^2 + Y_{H_d} X_{H_d} v_d^2 = 0 . \tag{4.80}$$

Combining this with the condition $X_{H_u} + X_{H_d} + 2X_\Phi = 0$ (with $X_\Phi = 1$ and $Y_{H_{u,d}} = \mp 1/2$) yields the relations

$$X_{H_u} = \frac{-2v_d^2}{v_u^2 + v_d^2} , \qquad X_{H_d} = \frac{-2v_u^2}{v_u^2 + v_d^2} , \tag{4.81}$$

and hence $N_X = 2v_u v_d/\sqrt{v_u^2 + v_d^2}$. The equations of motion for a_Y and a_X then decouple:

$$A^3 \Box a_Y + \partial_z\left(A^3 \partial_z a_Y\right) - \xi_Y A^5 g_Y^2 N_Y^2 a_Y = 0 , \tag{4.82}$$

$$\begin{aligned} &A^3 \Box a_X + \partial_z\left(A^3\left(\partial_z a_X - N_X V_z\right)\right) + \\ &\xi_{PQ} A^5 N_X\left(A^{-3}\partial_z\left(A V_z\right) - g_5^2\left(X_\Phi \eta^2 a + N_X a_X\right)\right) = 0 . \end{aligned} \tag{4.83}$$

Note that in deriving these equations we have used the fact that $v_{u,d}$ are z-independent.

The boundary conditions are

$$\left(\pm 2A^3 \partial_z a_Y - A^4 \frac{\delta U}{\delta a_Y}\right)\Big|_{z_{UV},z_{IR}} = 0\,, \tag{4.84}$$

$$\left(\pm 2A^3 \left(\partial_z a_X - N_X V_z\right) - A^4 \frac{\delta U}{\delta a_X}\right)\Big|_{z_{UV},z_{IR}} = 0\,, \tag{4.85}$$

with the relevant part of the UV boundary potential given by

$$U_{UV} \supset c v_u v_d \eta^2 \cos\left(2a - \frac{\sqrt{v_u^2+v_d^2}}{v_u v_d} a_X\right)\Big|_{z_{UV}}\,. \tag{4.86}$$

It is convenient to work in unitary gauge for $\mathrm{U}(1)_Y$ ($\xi_Y \to \infty$) since then $a_Y \to 0$. For a_X, we perform the KK expansion,

$$a_X(x^\mu, z) = \sum_{n=0}^{\infty} f_{a_X}^n(z) a^n(x^\mu)\,. \tag{4.87}$$

Note that $a^n(x^\mu)$ are the same 4D modes as in Eq. (4.12). To solve Eq. (4.83) we expand to first-order in $v_{u,d}/k^{3/2}$ (higher-order terms are negligibly small). This allows us to neglect terms proportional to a_X in the equation of motion for a and V_z. Focusing on the massless mode, we can then continue to use the solutions for f_a^0 and $f_{V_z}^0$ in (4.29). These massless profiles satisfy $A^{-3}\partial_z(A f_{V_z}^0) = g_5^2 X_\Phi \eta^2 f_a^0$. Using this relation, (4.83) reduces to

$$\partial_z\left(A^3\left(\partial_z f_{a_X}^0 - N_X f_{V_z}^0\right)\right) = 0\,, \tag{4.88}$$

for the massless mode. Imposing the IR boundary condition (4.85) enforces $\partial_z f_{a_X}^0(z) = N_X f_{V_z}^0(z)$. The UV boundary condition then becomes

$$-cA^4\eta^2\sqrt{v_u^2+v_d^2}\left(2f_a^0 - \frac{\sqrt{v_u^2+v_d^2}}{v_u v_d} f_{a_X}^0\right)\Big|_{z_{UV}} = 0\,. \tag{4.89}$$

The final solution is

$$f^0_{a_X}(z) = \frac{2v_u v_d}{\sqrt{v_u^2+v_d^2}}\left(f^0_a(z_{UV}) + \int_{z_{UV}}^{z} dz'\, f^0_{V_z}(z') + \mathcal{O}(v^2_{u,d}/k^3)\right). \tag{4.90}$$

This solution is strictly valid only for an exactly massless zero mode. However, it is expected to approximately hold even in the presence of explicit PQ breaking on the UV boundary with the replacement $f^0_a(z_{UV}) \to f^0_{a,\not{PQ}}(z_{UV})$, where the latter quantity is the boundary value of the exact massive profile.[2] The reason is that, in the limit $z_{IR} \gg z_{UV}$, the exact massive profiles $f^0_{a,\not{PQ}}$ and $f^0_{V_z,\not{PQ}}$ closely match the massless solutions everywhere except very close to the UV brane, where $f^0_{a,\not{PQ}}$ becomes highly suppressed [135]. It is therefore convenient to write

$$f^0_{a_X}(z) = \frac{2v_u v_d}{\sqrt{v_u^2+v_d^2}}\left(\widehat{f}^0_{a_X}(z) + \mathcal{O}(v^2_{u,d}/k^3)\right), \tag{4.91}$$

with

$$\widehat{f}^0_{a_X}(z) = \begin{cases} f^0_a(z)\,, & m_0 = 0\,, \\ f^0_a(z) - f^0_a(z_{UV}) + f^0_{a,\not{PQ}}(z_{UV})\,, & m_0 \neq 0\,, \end{cases} \tag{4.92}$$

where the equality should be understood as approximate when $m_0 \neq 0$. In going from (4.90) to (4.92) we have used that $f^0_{V_z} = \partial_z f^0_a$. From now on, we also approximate $f^0_{a,\not{PQ}}(z_{UV}) \approx 0$.

Finally, transforming back to $a_{u,d}$ we obtain

$$\frac{a_{u,d}}{v_{u,d}} = X_{H_{u,d}} \widehat{f}^0_{a_X}(z)\, a^0(x^\mu) + \cdots, \tag{4.93}$$

where '$\cdots$' contains the heavier modes.

[2] We have confirmed that with this replacement (4.90) holds exactly when $g_5 = 0$ and $z_{IR} \gg z_{UV}$.

4.5.5 Axion-Fermion Couplings with Bulk Higgs Fields

To obtain the axion-fermion couplings we consider the bulk Yukawa interactions

$$S_{\text{Yukawa}} = -\frac{2}{\sqrt{k}}\int_{z_{UV}}^{z_{IR}} d^5x\,\sqrt{-g}\left(y^{(5)}_{u,ij}\bar{Q}_i U_j H_u + y^{(5)}_{d,ij}\bar{Q}_i D_j H_d + y^{(5)}_{e,ij}\bar{L}_i E_j H_d + \text{h.c.}\right), \quad (4.94)$$

where $y^{(5)}_{u,d,e}$ are dimensionless 5D Yukawa couplings. Focusing for now on the quark sector, and substituting (4.77) into (4.94) gives

$$-2\int_{z_{UV}}^{z_{IR}} d^5x\,\sqrt{-g}\,\frac{1}{\sqrt{k}}\left(y^{(5)}_{u,ij}\frac{v_u}{\sqrt{2}}\bar{Q}_{u_i}U_j e^{i\frac{a_u(x,z)}{v_u}} + y^{(5)}_{d,ij}\frac{v_d}{\sqrt{2}}\bar{Q}_{d_i}D_j e^{i\frac{a_d(x,z)}{v_d}} + \text{h.c.}\right), \quad (4.95)$$

where $Q = (Q_u, Q_d)$ denote the components of the $SU(2)_L$ quark doublet. We proceed by considering just the up-type quarks. Similar expressions follow for the down-type quarks and leptons. The fermion zero-mode mass matrix for the up-type quarks is

$$m_u^{ij} = y^{(5)}_{u,ij}\frac{\sqrt{2}v_u}{\sqrt{k}}\int_{z_{UV}}^{z_{IR}}\frac{dz}{(kz)^5}\, f^0_{Q_{iL}}(z) f^0_{U_{jR}}(z)\,, \quad (4.96)$$

which is again diagonalized by $A^u_L m_u^{ij} A^{u\dagger}_R = m_{u_i}$. As in the boundary Higgs case, the bulk mass parameters, c_i, are constrained by the quark and charged lepton masses, as shown in Figure 4.7. Further details are provided in Appendix A.

The a_u dependence in (4.95) can be removed via a 5D field redefinition of the form

$$Q_{u_i}(x,z) \to e^{i\beta\frac{a_u(x,z)}{v_u}} Q_{u_i}(x,z), \quad U_i(x,z) \to e^{i(\beta-1)\frac{a_u(x,z)}{v_u}} U_i(x,z)\,, \quad (4.97)$$

where β is an arbitrary parameter. The 5D kinetic terms are not invariant under this transformation, giving rise to the terms

$$-2i\int_{z_{UV}}^{z_{IR}} d^5x\sqrt{-g}\left(\partial_M\frac{a_u}{v_u}\right)\left(\frac{1}{2}\left(\bar{Q}_{u_i}\Gamma^M Q_{u_i} - \bar{U}_i\Gamma^M U_i\right) + \left(\beta - \frac{1}{2}\right)\left(\bar{Q}_{u_i}\Gamma^M Q_{u_i} + \bar{U}_i\Gamma^M U_i\right)\right). \quad (4.98)$$

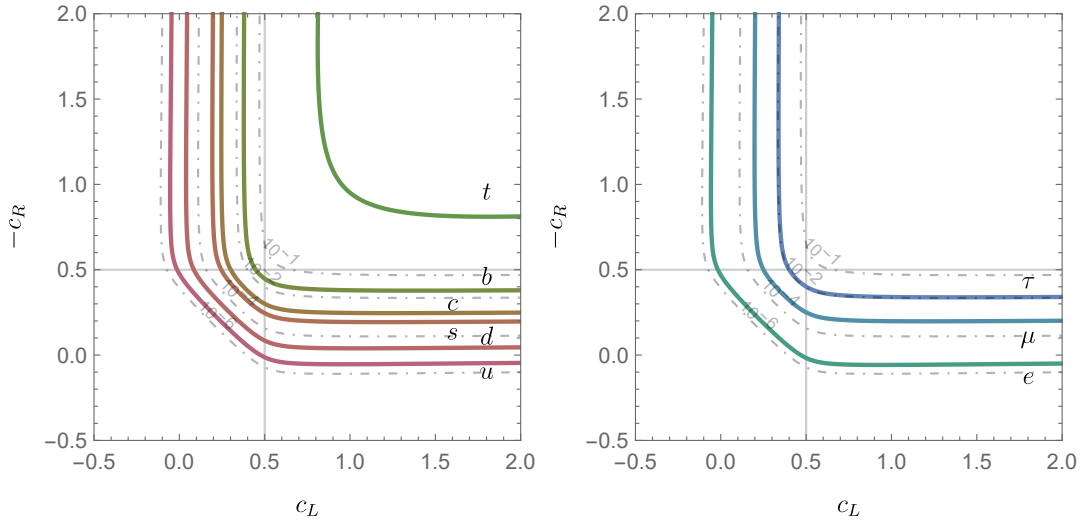

Figure 4.7: Contours of the quark (left) and charged lepton (right) masses for the bulk Higgs case using Eq. (4.96), as a function of c_L and $-c_R$ with $\tan\beta = 3$, and $kz_{\rm IR} = 10^{10}$. The $y^{(5)}_{u,d,\ell}$ are randomly generated diagonal 5D Yukawa couplings drawn from a log-normal distribution with $\mu = 0$ and $\sigma = 0.3$. The contours indicate the medians of the generated set $(c_L, -c_R)$

Restricting to the zero-modes, these terms give the axion-fermion couplings. However, care must be taken with the term on the second line, which depends on the choice of field redefinition. Notice that after integrating by parts (the boundary term vanishes) this term takes the form

$$i(2\beta-1)\int_{z_{UV}}^{z_{IR}} d^5x\,\frac{a_u}{v_u}\partial_M J_V^M\,, \qquad J_V^M = \sqrt{-g}\left(\bar{Q}_{u_i}\Gamma^M Q_{u_i} + \bar{U}_i\Gamma^M U_i\right)\,. \tag{4.99}$$

Since J_V^M is a classically conserved current, any effects from this term must be proportional to the (boundary-localized) weak anomaly. The β-dependence is then cancelled by the transformation of the path-integral measure under (4.97).

Returning to the terms in the first line of (4.98) and restricting to the zero-modes gives

$$-iX_{H_u}\int_{z_{UV}}^{z_{IR}} d^5x\,A^4(\partial_\mu a^0)\widehat{f}^0_{aX}\left(\bar{u}_{iL}(f^0_{Q_{iL}})^2\gamma^\mu u_{iL} - \bar{u}_{iR}(f^0_{U_{iR}})^2\gamma^\mu u_{iR}\right)\,, \tag{4.100}$$

where we have used (4.93) and $a^0(x)$ is identified with the axion to $\mathcal{O}(v/F_a)$. Integrating

over the profiles and rotating to the fermion mass basis we obtain the 4D effective action

$$S_{4D} \supset i \int d^4x \, \frac{\partial_\mu a^0}{2F_a} \left(\bar{u}_i \gamma^\mu \left((c_u^V)_{ij} - (c_u^A)_{ij} \gamma^5 \right) u_j \right) , \tag{4.101}$$

where

$$\begin{aligned} \frac{1}{(F_u^{V,A})_{ij}} &\equiv \frac{(c_u^{V,A})_{ij}}{F_a} \\ &= X_{H_u} \int_{z_{UV}}^{z_{IR}} \frac{dz}{(kz)^4} \, \widehat{f}^0_{a_X} \left((A_R^u)_{ik} (f^0_{U_{kR}})^2 (A_R^{u\,\dagger})_{kj} \mp (A_L^u)_{ik} (f^0_{Q_{kL}})^2 (A_L^{u\,\dagger})_{kj} \right) . \end{aligned} \tag{4.102}$$

Repeating the above steps leads to analogous expressions for the down-type quarks and charged leptons. Note that, following a similar argument to above, the flavour-diagonal vector couplings $(c^V)_{ii}$ are unphysical up to weak anomalies. Furthermore, the on-shell axion couplings are proportional to $(c^{V,A})_{ij}(m_i \mp m_j)$.

We see that with the Higgs located in the bulk both the vector, c^V, and axial-vector, c^A, couplings are non-zero and are flavour off-diagonal. These couplings depend on the mixing matrices, $A_{L,R}$, and the 5D bulk mass parameters c_i in (4.56), which are constrained by a fit to the Standard Model fermion masses and CKM/PMNS matrices, as detailed in Appendix A. In the following two subsections, we discuss the behaviour of the couplings (4.102) both for the massless axion and in the presence of explicit PQ breaking on the UV boundary.

Bulk Higgs field with Massless axion

In the absence of explicit PQ breaking on the UV brane, the axion is massless (up to QCD effects) and the profiles are given by (4.29). In this case we have that $\widehat{f}^0_{a_X}(z) = f^0_a(z)$. The $f^0_a(z)$ profile is approximately constant, up to corrections of order $g_5^2 k \sigma_0^2 / \Delta^2$, and it is convenient to parametrize it as

$$f^0_a(z) = \frac{1}{F_a} \left(1 + g^0_a(z) \right) , \tag{4.103}$$

where $g_a^0(z)$ contains the z-dependence, and we have identified the decay constant $F_a = f_a(z_{UV})^{-1} \simeq \sigma_0/(z_{IR}\sqrt{\Delta-1})$. Substituting this into (4.102) and using the fact that $A_{L,R}$ are unitary matrices leads to

$$\begin{aligned}(c_u^A)_{ij} &= X_{H_u}\left(\frac{1}{2}\delta_{ij} + \int_{z_{UV}}^{z_{IR}} \frac{dz}{(kz)^4}\, g_a^0(z)\left((A_R^u)_{ik}(f_{U_{kR}}^0)^2(A_R^{u\dagger})_{kj} + \right.\right. \\ &\qquad \left.\left.(A_L^u)_{ik}(f_{Q_{kL}}^0)^2(A_L^{u\dagger})_{kj}\right)\right), \\ (c_u^V)_{ij} &= X_{H_u}\int_{z_{UV}}^{z_{IR}} \frac{dz}{(kz)^4}\, g_a^0(z)\left((A_R^u)_{ik}(f_{U_{kR}}^0)^2(A_R^{u\dagger})_{kj} - (A_L^u)_{ik}(f_{Q_{kL}}^0)^2(A_L^{u\dagger})_{kj}\right).\end{aligned} \tag{4.104}$$

The first term in the expression for c_u^A gives the leading contribution to the diagonal couplings which are therefore similar to the boundary Higgs case. The off-diagonal couplings, on the other hand, involve overlap integrals of $g_a^0(z)$ with the fermion profiles. These integrals take a particularly simple form if the fermion profile satisfies $c_L < 1/2$ or $-c_R < 1/2$. Using the approximate axion profile in Eq. (4.29), we then obtain

$$\int \frac{dz}{(kz)^4}\, g_a^0\,(f_j^0)^2 = -\frac{\Delta(2c_j-1)(2c_j-2\Delta-3)}{8(2c_j-3)(2c_j-2\Delta-1)}\frac{g_5^2 k\sigma_0^2}{\Delta^2} + \mathcal{O}\left(\left(\frac{g_5^2 k\sigma_0^2}{\Delta^2}\right)^2\right). \tag{4.105}$$

Conversely, if $c_L > 1/2$ or $-c_R > 1/2$ the integral is suppressed by powers of kz_{IR}. From Figure 4.7, we see that for all fermions except the top quark, (4.105) is always valid for either the left- or right-handed profile. The overlap integral is plotted in Figure 4.8 using the exact massless axion profile (the dashed lines correspond to (4.105)). Notice that even when $g_5\sqrt{k}\sigma_0/\Delta \sim \mathcal{O}(1)$ the value of the overlap integral is ~ 0.1, which results in a suppression of the off-diagonal couplings relative to F_a. The off-diagonal couplings are further suppressed by the off-diagonal elements of the mixing matrices.

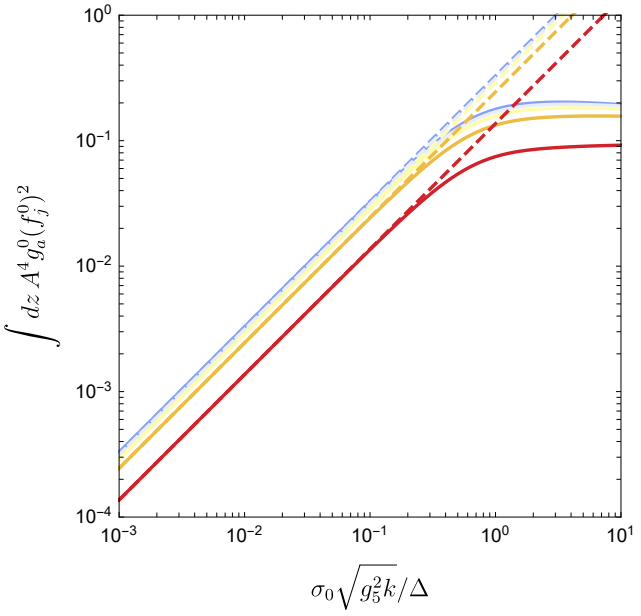

Figure 4.8: The overlap integral between the z-dependent part of the axion profile $g_a^0(z)$ and the left/right-handed quark profiles $(f_j^0)^2$ as a function of $\sigma_0\sqrt{g_5^2 k}/\Delta$, with $c_L(-c_R)$ ranging from -3 (upper) to 0 (lower) in steps of 1. The solid lines use the exact massless axion profile, while the dashed lines correspond to Eq. (4.105). We have fixed $\Delta = 10$, $g_5^2 k = 1$ and the value for kz_{IR} is adjusted to keep $F_a = 10^9\,\text{GeV}$.

Bulk Higgs field with Massive axion

In the presence of explicit PQ breaking on the UV brane $\widehat{f}^0_{a_X}(z) \approx f^0_a(z) - f^0_a(z_{UV}) = g^0_a(z)$. We then obtain the couplings

$$(c_u^{V,A})_{ij} = X_{H_u} \int_{z_{UV}}^{z_{IR}} \frac{dz}{(kz)^4}\, g^0_a(z) \left((A^u_R)_{ik} (f^0_{U_{kR}})^2 (A^{u\dagger}_R)_{kj} \mp (A^u_L)_{ik} (f^0_{Q_{kL}})^2 (A^{u\dagger}_L)_{kj} \right) . \quad (4.106)$$

Here, the diagonal couplings $(c^A_u)_{ii}$ are also suppressed, relative to F_a, by overlap integrals of $g^0_a(z)$ with the fermion profiles. The off-diagonal couplings are still expected to be smaller, due to the suppression from the off-diagonal elements of the mixing matrices. Hence, the off-diagonal couplings are approximately the same in the massive and massless cases, whereas the diagonal couplings are different.

Numerical results

The axion-fermion couplings are obtained by numerically evaluating the integral expression (4.106), as well as the corresponding expressions for the down-type quarks and charged leptons. The procedure for determining the mixing matrices $A^{u,d,\ell}_{L,R}$ is given in Appendix A.1, with the bulk mass parameters constrained by a fit to the quark and charged lepton masses (see Figure 4.7) and the CKM/PMNS mixing matrices. We also assume $z_{\rm UV} = 1/k$ and $k \sim M_P$ for all plots.

Representative values of the diagonal axial-vector couplings $c^A_{u,d,\ell}$ are shown in Figure 4.9 for the quarks and charged leptons. The axion parameters correspond to $F_a \simeq 10^9\,\text{GeV}$ and we take $\Delta = 10$ to solve the axion-quality problem. In particular, we see that the top-quark coupling c^A_{tt} is suppressed since it is mostly localized near the UV brane.

For the off-diagonal couplings, consider first the axion-quark couplings shown in the left panel of Figure 4.10 as a function of $c_{Q_3} + c_{u_3}$. The F^V_u off-diagonal matrix elements range from approximately $10^{12} - 10^{14}\,\text{GeV}$, while the F^V_d off-diagonal matrix elements are approximately $10^{11} - 10^{13}\,\text{GeV}$. The axial-vector couplings $F^A_{u,d}$ are the same order of magnitude as the $F^V_{u,d}$ and are not explicitly shown. These values are comparable to the experimental limits given in Ref. [131]. Currently, the most stringent limit is $(F^V_d)_{12} \gtrsim 6.8 \times 10^{11}\,\text{GeV}$

from $K^+ \to \pi^+ a$ decays. As shown in Figure 4.11, this bound on $(F_d^V)_{12}$ rules out values of $\sigma_0 \gtrsim 4$ for $g_5^2 k = 1$ and $\Delta = 10$. The projected future sensitivity of NA62 and KOTO to $(F_d^V)_{12}$ is $2 \times 10^{12}\,\text{GeV}$ [131], which can probe values of $\sigma_0 \gtrsim 2$.

The axion-charged lepton couplings are obtained in a similar fashion; however, the mixing matrices $A_{L,R}^{e,\nu}$ are sensitive to the mechanism for neutrino masses. For simplicity, we assume that the PMNS matrix is generated in the charged lepton sector ($U_{PMNS} = (A_L^e)^\dagger$) and leave a detailed study of the neutrino sector for future work. The charged lepton bulk mass parameters are then constrained by fitting the charged lepton masses (see Figure 4.7) and the PMNS mixing parameters. The resulting F_l^V are shown in the right panel of Figure 4.10 as a function of $c_{L_3} + c_{e_3}$, again with $F_a \simeq 10^9\,\text{GeV}$ and $\Delta = 10$. The off-diagonal F_ℓ^V matrix elements range from approximately $10^{11} - 10^{12}\,\text{GeV}$. Again, the axial-vector couplings F_ℓ^A are of the same order of magnitude as the vector couplings. The corresponding experimental limits are given in [132]. The most stringent limit is from $\mu \to e\,a$, which constrains $(F_e^V)_{12} \gtrsim 4.8 \times 10^9\,\text{GeV}$. Future sensitivity of the MEG-II-fwd and Mu3e experiments is $(F_e^V)_{12} \gtrsim 2 \times 10^{10}\,\text{GeV}$. This is still an order of magnitude smaller than the predicted values shown in Figure 4.10.

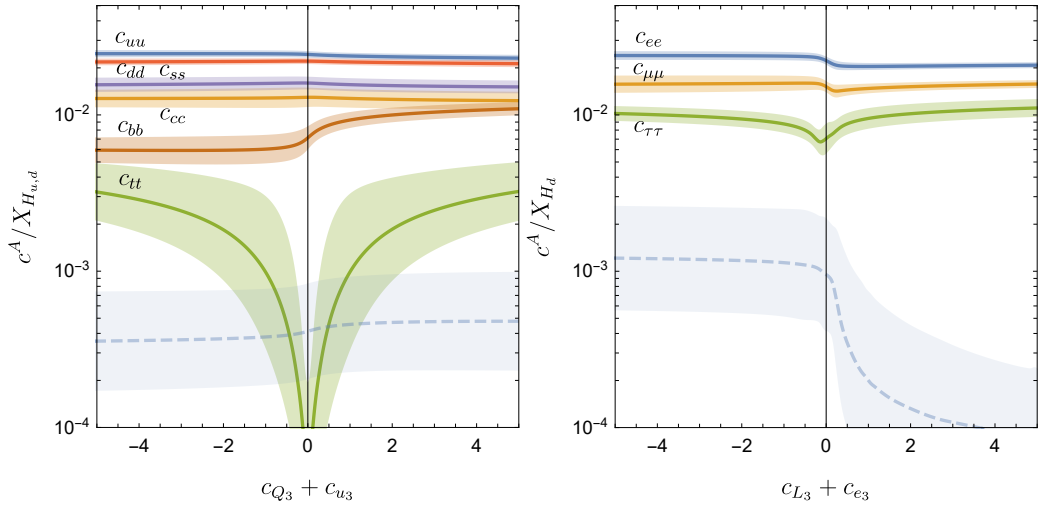

Figure 4.9: Left: absolute values of the diagonal axion-quark couplings (from top to bottom) c^A_{uu}, c^A_{cc} and c^A_{tt} in units of X_{H_u}, and c^A_{dd}, c^A_{ss} and c^A_{bb} in units of X_{H_d} as functions of $c_{Q_3} + c_{u_3}$. Right: absolute values of the diagonal axion-charged lepton couplings (from top to bottom) c^A_{ee}, $c^A_{\mu\mu}$ and $c^A_{\tau\tau}$ in units of X_{H_d} as functions of $c_{L_3} + c_{e_3}$. We fix $kz_{\rm IR} = 10^{10}, g_5^2 k = 1, \Delta = 10$ and $\sigma_0 = 3$, corresponding to $F_a \simeq 10^9\,\text{GeV}$. The curves and bands depict the mean and standard deviation of $\log_{10} F^V$ obtained from a scan over anarchic 5D Yukawa couplings. The dashed line shows (left) c^A_{uc} and (right) $c^A_{e\mu}$ for reference.

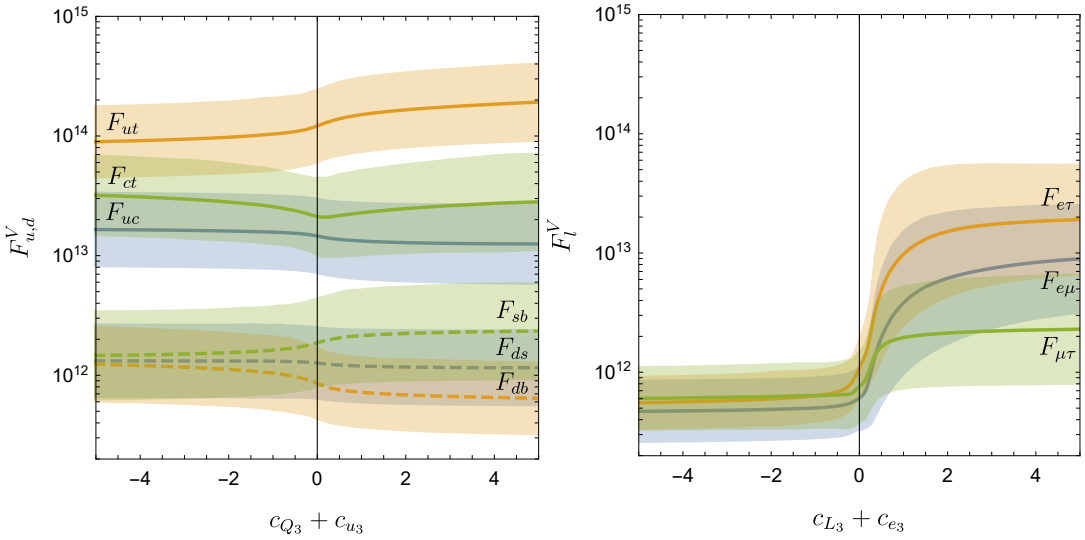

Figure 4.10: Absolute values of the off-diagonal elements of the axion-quark coupling matrix F_u^V (left, solid) and F_d^V (left, dashed) as functions of $c_{Q_3} + c_{u_3}$, and F_l^V (right) as a function of $c_{L_3} + c_{e_3}$. We fix $kz_{\rm IR} = 10^{10}$, $g_5^2 k = 1$, $\Delta = 10$ and $\sigma_0 = 3$, corresponding to $F_a \simeq 10^9$ GeV. The curves and bands depict the mean and standard deviation of $\log_{10} F^V$ obtained from a scan over anarchic 5D Yukawa couplings.

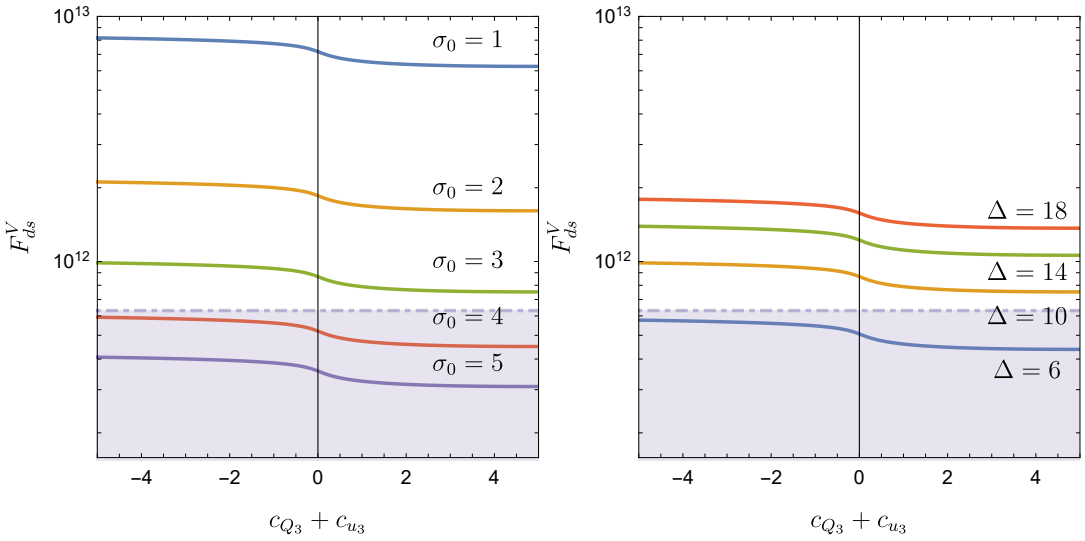

Figure 4.11: Absolute values of the axion coupling F_{ds}^V as a function of $c_{Q_3} + c_{u_3}$ for $F_a = 10^9$ GeV, $g_5^2 k = 1$ for various values of σ_0 with $\Delta = 10$ (left), and various values of Δ with $\sigma_0 = 3$ (right). The region below the dot-dashed line corresponds to the current experimental limit $F_{ds}^V \gtrsim 6.8 \times 10^{11}$ GeV [131].

4.6 5D Axion - Summary

The axion remains a favoured solution to the strong CP problem, as well as provides a candidate for the missing dark matter component of the Universe. However, the axion solution requires that the $U(1)_{PQ}$ global symmetry is preserved by quantum gravity to sufficiently high order terms in the Lagrangian. We have presented a 5D geometric solution to this axion quality problem that relies on a 5D gravitational dual description of composite axion models. The spontaneous breaking of a global $U(1)_{PQ}$ symmetry by a PQ-charged composite operator of dimension Δ is modelled by the vacuum expectation value of a bulk complex scalar field charged under a 5D $U(1)_{PQ}$ gauge symmetry. The IR brane scale is associated with the scale of spontaneous $U(1)_{PQ}$ symmetry breaking, and therefore offers an explanation as to why the axion decay constant F_a is much below the UV scale, while on the other hand explicit sources of global $U(1)_{PQ}$ violation are confined to the UV brane.

In our 5D setup, the axion quality problem is solved by localising the axion towards the IR brane and away from the explicit sources of $U(1)_{PQ}$ violation on the UV brane. The axion zero mode profile is controlled by the bulk scalar mass-squared parameter, which by the AdS/CFT dictionary is related to the operator dimension Δ. In fact, our solution for the 5D axion profile generalises previous QCD pseudoscalar solutions [120] to operators of arbitrary dimension Δ. As Δ is increased the axion becomes more IR-localised, and there is a minimum critical value Δ_c, shown in Figure 4.5, for which the UV contributions to the axion mass are sufficiently suppressed relative to the QCD instanton contribution, thereby preserving the solution to the strong CP problem. This requires that QCD is a gauge symmetry in the bulk, or equivalently that the composite sector is also charged under QCD. If QCD is instead confined to the UV brane, the axion cannot be sequestered from additional UV sources of explicit $U(1)_{PQ}$ violation while simultaneously maintaining a large coupling to QCD.

Our 5D geometric solution holographically captures a whole class of 4D composite axion models where the $U(1)_{PQ}$ symmetry is an accidental global symmetry of the underlying 4D strong dynamics. This is analogous to the SM where baryon number is an accidental global

symmetry up to dimension six operators. If a similar mechanism were to occur for the underlying 4D gauge theory responsible for a composite axion, then our analysis suggests that the $U(1)_{PQ}$ global symmetry must be preserved up to at least dimension ten for an axion decay constant $F_a \gtrsim 10^9\,\text{GeV}$. A recent attempt to construct such a 4D model is given in [128], and other constructions with larger gauge groups should also be possible. In fact, our 5D framework can be used to model and give holographic descriptions of 4D strong dynamics with larger global symmetry groups or to consider more general possibilities with SM fermions propagating in the bulk. The 5D pseudoscalar solution may also have applications for other global symmetries, such as in QCD where chiral symmetry is broken by operators of dimension three. Thus this simple, 5D geometric solution provides a new way to understand composite axion models, and in general to study accidental global symmetries of 4D strong dynamics.

The axion-fermion couplings arise from the wavefunction overlap between the axion fields and bulk fermion zero modes, and depend on the localization of the Higgs fields. When the Higgs fields are localized on the UV boundary, only flavour diagonal axion-fermion couplings are obtained due to the orthogonality of the fermion profiles. When the Higgs fields instead propagate in the bulk with a constant VEV, the wavefunction overlap between the z-dependent axion profile and the fermion zero modes produces flavour-dependent, off-diagonal axion-fermion couplings. Assuming an axion decay constant $F_a \simeq 10^9\,\text{GeV}$, the off-diagonal couplings $(F^V_{u,d,\ell})_{ij}$ range from $10^{11-15}\,\text{GeV}$, where the 5D parameters are chosen to solve the axion quality problem and obtain the Standard Model fermion masses and mixings. The off-diagonal axion-fermion couplings are most stringently constrained in the down-quark sector, where the current experimental limit on F^V_{sd} [131] restricts some 5D parameters in the model. Future planned experiments will be able to probe more of the parameter space. The couplings in the lepton sector are less constrained and remain an order of magnitude below future sensitivity.

Chapter 5

Composite Axion Models

Given the active experimental effort it behooves us to consider possible ways to vary the axion mass and couplings that can arise from UV modifications of QCD. A number of proposals were previously considered in Refs. [136, 137, 138], and more recently in Refs. [139, 140, 141, 142]. A particularly interesting possibility is that associated with enlarging the color gauge group, where new nonperturbative contributions to the axion mass are generated [143, 144]. We assume that the QCD gauge group, $\mathrm{SU}(3)_c$ is embedded into $\mathrm{SU}(N+3) \times \mathrm{SU}(N)'$ with $N \geq 3$. Although this enlarged color group can simply be broken with a new elementary Higgs sector [144], a potentially richer framework is to cause the breaking with new strong dynamics. Besides the advantage of eliminating fundamental scalar fields, this approach offers the intriguing possibility that the same strong dynamics is also responsible for a composite Higgs. In fact, the strong dynamics associated with an enlarged color group can provide all the ingredients for a composite Higgs with partial compositeness as well as a dynamical axion with new contributions to the axion mass.

While composite Higgs models have been extensively explored as an effective low energy description based on the AdS/CFT correspondence (for a review, see [145]), we will instead consider the UV completions of composite Higgs models given in Refs. [146, 147, 148]. These models contain colored fermion constituents that are needed to produce top partner bound states in order to implement the partial compositeness mechanism. An early approach that combined the axion and Higgs was considered in Ref. [149], although without an underlying four-fermion structure responsible for partial compositeness. In this chapter we will extend

the UV descriptions of composite Higgs models to incorporate the enlarged color breaking and generate dynamical axions. The new strong dynamics, referred to as *hypercolor*, will be based on the gauge groups $\mathrm{Sp}(2N_{\mathrm{HC}})$ [146, 147], where N_{HC} is a positive integer, and $\mathrm{SU}(4)_{\mathrm{HC}}$ [148]. With these gauge groups, the colored hyperfermions can transform in the fundamental representation of the hypercolor group. This restriction to the smallest representation preserves asymptotic freedom and leads to confinement of the hypercolor gauge group. The uncolored hyperfermions are chosen to be in the antisymmetric representation with an SU(5) global symmetry. Thus, there is a preference for SU(5)/SO(5) composite Higgs models [150, 148].

5.1 Hypercolor with Enlarged Color

An extended strong sector, where QCD is embedded into a larger gauge group such as SU($N+3$), can solve the strong CP problem with a heavy axion [143, 144]. Interestingly, composite Higgs models require top partners with colored constituents and these same constituents, charged under the hypercolor strong dynamics, can then play a role in breaking this enlarged color symmetry. A critical requirement in constructing such a model is that the hypercolor gauge coupling is asymptotically free and therefore hypercolor confines at low energies. This severely restricts the hyperfermion content of the model and typically favors colored constituents which are in the smallest representation of the gauge group. As will be shown in Section 5.2.5, the SU(5)/SO(5) composite Higgs model is favored because the colored constituents can transform in the fundamental representation of the UV gauge group. Thus to obtain a composite Higgs with a heavy composite axion we will consider extensions of the SU(5)/SO(5) model based on two choices of the hypercolor gauge group: the symplectic group Sp($2N_{\rm HC}$) with $N_{\rm HC}$ a positive integer, and SU(4)$_{\rm HC}$.

5.1.1 Hypercolor Gauge Groups

Sp($2N_{\rm HC}$)

We first consider the SU(5)/SO(5) composite Higgs model based on the hypercolor gauge group Sp($2N_{\rm HC}$) with a traceless, antisymmetric hyperfermion ψ^a, transforming as a fundamental under an SU(5) global symmetry with index $a = 1 \dots 5$. The Sp($2N_{\rm HC}$) gauge invariant fermion bilinear is given by

$$(\psi^a \psi^b) = \Omega_{ik}\Omega_{jl}\psi^a_{ij}\psi^b_{kl}\,, \tag{5.1}$$

where $i, j = 1 \dots 2N_{\rm HC}$ are Sp($2N_{\rm HC}$) indices, and Ω_{ij} is the symplectic metric

$$\Omega_{ij} = \begin{pmatrix} 0 & \mathbb{I}_{N_{\rm HC}} \\ -\mathbb{I}_{N_{\rm HC}} & 0 \end{pmatrix}\,, \tag{5.2}$$

with $\mathbb{I}_{N_{\rm HC}}$ the $N_{\rm HC} \times N_{\rm HC}$ identity matrix. The traceless condition can then be written as $\Omega_{ij}\psi^{ij} = 0$. Besides describing a composite Higgs, the hypercolor dynamics must also produce colored, top partner bound states that can linearly mix with the elementary top quark. In addition to generating a large top Yukawa coupling, these states are required to explicitly break the global symmetry and generate a Higgs potential. This requires adding vector-like pairs of hyperfermions, $\chi, \bar{\chi}$ charged under $\mathrm{SU}(3)_c$ as first considered in Ref. [146].

If the QCD gauge group is now extended to $\mathrm{SU}(N+3) \times \mathrm{SU}(N)'$, then the top partner hyperfermion content also needs to be enlarged to $\Psi_\chi = (\chi, \chi', \bar{\chi}, \bar{\chi}')$, where Ψ_χ are in the fundamental (pseudoreal) representation of $\mathrm{Sp}(2N_{\rm HC})$. As a result, the global symmetry group associated with Ψ_χ is $G_{\rm Sp} = \mathrm{U}(4N+6)$. The minimal anomaly-free particle content is summarized in Table Table 5.1, where the electroweak gauge group $\mathrm{SU}(2)_L \times \mathrm{U}(1)_Y$ quantum numbers have been omitted. Typically, the electroweak group weakly gauges the custodial global symmetry $\mathrm{SU}(2)_L \times \mathrm{SU}(2)_R \times \mathrm{U}(1)_X \subset \mathrm{SO}(5)$ [147].

	$\mathrm{Sp}(2N_{\rm HC})$	$\mathrm{SU}(N+3)$	$\mathrm{SU}(N)'$	$\mathrm{SU}(5)$	$\mathrm{U}(4N+6)$
ψ	$\mathbf{A_2}$	$\mathbf{1}$	$\mathbf{1}$	$\mathbf{5}$	$\mathbf{1}$
χ	$\mathbf{F}$	$\mathbf{F}$	$\mathbf{1}$	$\mathbf{1}$	$\mathbf{F}$
χ'		$\mathbf{1}$	$\mathbf{F}$		
$\bar{\chi}$		$\bar{\mathbf{F}}$	$\mathbf{1}$		
$\bar{\chi}'$		$\mathbf{1}$	$\bar{\mathbf{F}}$		

Table 5.1: The hypercolor fermion representations under the local symmetry, $\mathrm{Sp}(2N_{\rm HC}) \times \mathrm{SU}(N+3) \times \mathrm{SU}(N)'$ and global symmetry, $\mathrm{SU}(5) \times \mathrm{U}(4N+6)$.

To investigate the global symmetry breaking pattern of the strong dynamics we construct a gauged NJL model [151]. For the composite Higgs sector this can be done by introducing four-fermion interactions consisting of ψ^a, and modifying the analysis in Ref. [146] to accommodate the SU(5)/SO(5) coset. The leading interaction Lagrangian is given by

$$\mathcal{L}_{\rm int} = \frac{\kappa_\psi}{2N_{\rm HC}} (\psi^a \psi^b)(\psi_a^\dagger \psi_b^\dagger) \,. \tag{5.3}$$

Similarly to the NJL model, the vacuum structure of the $\mathrm{Sp}(2N_{\rm HC})$ strong dynamics can be

studied via the introduction of a bilinear auxiliary field

$$M^{ab} = -\frac{\kappa_\psi}{2N_{\rm HC}}(\psi^a\psi^b)\,, \tag{5.4}$$

where κ_ψ is assumed to be real and positive. Since the representation of ψ is real, M^{ab} is symmetric and can be diagonalized via the Takagi diagonalization using an SU(5) global rotation of ψ. The effective potential of M^{ab} admits a nontrivial, stationary fixed point where the singular values $m_{(i)}$ of M^{ab} satisfy the mass gap equation

$$\frac{1}{\zeta_\psi} \equiv \frac{4\pi^2}{\Lambda_{\rm UV}^2}\frac{1}{\kappa_\psi} = 1 - \frac{m_{(i)}^2}{\Lambda_{\rm UV}^2}\log\left(1+\frac{\Lambda_{\rm UV}^2}{m_{(i)}^2}\right)\,, \tag{5.5}$$

and $\Lambda_{\rm UV}$ represents a physical UV cutoff. A nontrivial stable fixed point characterized by nonzero $m_{(i)}$ only exists if the dimensionless coupling parameter ζ_ψ is greater than one. This corresponds to large κ_ψ, i.e. the four-fermion coupling is strong. The scale $\Lambda_{\rm UV}$ can thus be interpreted as the confinement scale $\Lambda_{\rm HC}$ of $\mathrm{Sp}(2N_{\rm HC})$, where these couplings are generated. Thus for generic values of ζ_ψ it is natural to expect $m_{(i)} \lesssim \Lambda_{\rm HC}$. Note that since all $m_{(i)}$ share the same gap equation and have the same value, the SU(5) global symmetry is broken down to SO(5). Thus the $\mathrm{Sp}(2N_{\rm HC})$ theory provides a suitable UV completion of the SU(5)/SO(5) composite Higgs model.

The SU(5)/SO(5) coset contains fourteen Nambu-Goldstone bosons, which under the electroweak group $\mathrm{SU}(2)_L \times \mathrm{U}(1)_Y$ decompose as [150, 148]

$$\mathbf{14} \to \mathbf{2}_{\pm\frac{1}{2}} + \mathbf{3}_0 + \mathbf{3}_{\pm1} + \mathbf{1}_0\,. \tag{5.6}$$

Besides the Higgs doublet ($\mathbf{2}_{\pm\frac{1}{2}}$) there are three electroweak triplets and a singlet. A Higgs potential arises via explicit global symmetry breaking from top quark couplings. In particular, the Higgs field receives negative mass-squared corrections from the top quark Yukawa couplings, leading to electroweak symmetry breaking. Instead the triplets in (5.6) only receive positive mass-squared loop corrections from gauge bosons, and thus their VEVs are stabilized at zero [148]. On the other hand, the singlet can receive a mass from an explicit

mass term for the ψ hyperfermions.

For the global symmetry breaking pattern of the enlarged color sector, the interaction potential for Ψ_χ is more involved, and will be discussed in Section 5.1.2. Next, we present the case of $\mathrm{SU}(4)_{\mathrm{HC}}$, which shares many similarities and provides an alternative hypercolor gauge group.

$\mathbf{SU}(4)_{\mathrm{HC}}$

The SU(5)/SO(5) composite Higgs model can also arise from the hypercolor gauge group $\mathrm{SU}(4)_{\mathrm{HC}}$ [148]. Similar to the $\mathrm{Sp}(2N_{\mathrm{HC}})$ theory, this model contains ψ in the antisymmetric representation, which is real, and Ψ_χ in the fundamental representation, which is now complex instead of pseudoreal, as in the symplectic hypercolor case. The hyperfermion content is summarized in Table Table 5.2.

	$\mathrm{SU}(4)_{\mathrm{HC}}$	$\mathrm{SU}(N+3)$	$\mathrm{SU}(N)'$	$\mathrm{SU}(5)$	$\mathrm{U}(2N+3)_L$	$\mathrm{U}(2N+3)_R$
ψ	**6**	**1**	**1**	**5**	**1**	**1**
χ	**4**	**F**	**1**	**1**	**F**	**1**
χ'	**4**	**1**	**F**			
$\bar{\chi}$	$\bar{\mathbf{4}}$	$\bar{\mathbf{F}}$	**1**	**1**	**1**	**F**
$\bar{\chi}'$	$\bar{\mathbf{4}}$	**1**	$\bar{\mathbf{F}}$			

Table 5.2: The hypercolor fermion representations transforming under the local symmetry, $\mathrm{SU}(4)_{\mathrm{HC}} \times \mathrm{SU}(N+3) \times \mathrm{SU}(N)'$ and the global symmetry, $\mathrm{SU}(5) \times \mathrm{U}(2N+3)_L \times \mathrm{U}(2N+3)_R$.

The $\mathrm{SU}(4)_{\mathrm{HC}}$ gauge group allows for an invariant fermion bilinear

$$(\psi^a \psi^b) = \epsilon^{ijkl} \psi^a_{ij} \psi^b_{kl} \,, \tag{5.7}$$

where ϵ^{ijkl} is the Levi-Civita tensor and $i, j = 1 \ldots 4$ are $\mathrm{SU}(4)_{\mathrm{HC}}$ fundamental indices. To obtain the vacuum structure, a similar four-fermion analysis can be done as in the $\mathrm{Sp}(2N_{\mathrm{HC}})$

case. Since the SU(5) global symmetry of ψ remains the same, and the invariant fermion bilinear (5.7) does not affect the global symmetry breaking dynamics, the same SU(5)/SO(5) breaking coset follows from Eqs. (5.3)-(5.5). This coset was also analyzed in Ref. [148] for $\mathrm{SU}(4)_{\mathrm{HC}}$.

However, the enlarged color sector analysis differs from the $\mathrm{Sp}(2N_{\mathrm{HC}})$ case since Ψ_χ no longer has a homogeneous representation under the hypercolor gauge group. For example, bilinears between hyperfermions $\chi(\bar{\chi})$ and $\chi'(\bar{\chi}')$ are not allowed. Furthermore, the global symmetry of Ψ_χ is now restricted to $G_{\mathrm{SU}} = \mathrm{U}(2N+3)_L \times \mathrm{U}(2N+3)_R \subset G_{\mathrm{Sp}}$. Thus, when the enlarged color symmetry is broken, the $\mathrm{SU}(4)_{\mathrm{HC}}$ case is expected to have a different vacuum structure as well as Nambu-Goldstone boson spectrum.

5.1.2 Enlarged Color Breaking with Hyperfermion Condensates

$\mathbf{SU}(N+3) \times \mathbf{SU}(N)'$ Gauged NJL Model

Similarly to the $\psi\psi$ condensate, which is responsible for breaking the global SU(5) symmetry to SO(5), the colored hyperfermion condensates will be used to break the enlarged color symmetry to $\mathrm{SU}(3)_c \times \mathrm{SU}(N)_D$. The hypercolor strong dynamics therefore provides a natural way to break the enlarged color group without the introduction of new elementary scalars in the theory.

To determine how the enlarged color symmetry is broken we will consider four fermion operators that contain the colored hyperfermions in Ψ_χ. The most compact way to write down the Lagrangian between these fields is by introducing an auxiliary field similar to M^{ab}

in Eq. (5.4). In the case of symplectic hypercolor

$$\begin{aligned}\mathcal{L}_{\rm Sp} &\supset \frac{1}{2}M_{\rm Sp}\Psi_\chi^\dagger\Psi_\chi^\dagger + \text{h.c.} \\ &\equiv \frac{1}{2}\begin{pmatrix}\chi^{\dagger F} & \chi'^{\dagger f} & \bar{\chi}_H^\dagger & \bar{\chi}_h'^\dagger\end{pmatrix}\begin{pmatrix} P_{FG} & \Phi_{Fg} & R_F{}^K & \Delta_F{}^k \\ -(\Phi^T)_{fG} & P'_{fg} & \widetilde{\Delta}_f{}^K & R'_f{}^k \\ -(R^T)^H{}_G & -(\widetilde{\Delta}^T)^H{}_g & \tilde{P}^{HK} & \widetilde{\Phi}^{Hk} \\ -(\Delta^T)^h{}_G & -(R'^T)^h{}_g & -(\widetilde{\Phi}^T)^{hK} & \widetilde{P}'^{hk}\end{pmatrix}\begin{pmatrix}\chi^{\dagger G} \\ \chi'^{\dagger g} \\ \bar{\chi}_K^\dagger \\ \bar{\chi}_k'^\dagger\end{pmatrix} + \text{h.c.}\,,\end{aligned} \tag{5.8}$$

where $P, P', \widetilde{P}, \widetilde{P}', \Phi, \widetilde{\Phi}, \Delta, \widetilde{\Delta}, R, R'$ are auxiliary fields and uppercase (lowercase) letters denote $\mathrm{SU}(N+3)$ ($\mathrm{SU}(N)'$) fundamental indices. The $P, P', \widetilde{P}$ and $\widetilde{P}'$ fields in the diagonal entries of $M_{\rm Sp}$ are antisymmetric since Ψ_χ is in the pseudoreal representation. The $P, P', \widetilde{P}, \widetilde{P}'$ and $\Phi, \widetilde{\Phi}$, auxiliary fields can be treated as mass mixing terms and can be rotated away using part of the global symmetry $G_{\rm Sp}$ of Ψ_χ. After this procedure, the rotated mass matrix is still invariant under $\mathrm{U}(2N+3)_L \times \mathrm{U}(2N+3)_R$, which incidentally is the same as $G_{\rm SU}$ in the $\mathrm{SU}(4)_{\rm HC}$ hypercolor case.

In the $\mathrm{SU}(4)_{\rm HC}$ case, the P and Φ auxiliary fields are automatically forbidden since these fields are not gauge invariant under the new hypercolor. Instead the most general auxiliary field mass matrix becomes complex symmetric

$$M_{\rm SU} = \begin{pmatrix} 0 & 0 & R & \Delta \\ 0 & 0 & \widetilde{\Delta} & R' \\ R^T & \widetilde{\Delta}^T & 0 & 0 \\ \Delta^T & R'^T & 0 & 0\end{pmatrix}. \tag{5.9}$$

So in both cases, the only fields we need to consider are $\Delta, \widetilde{\Delta}$ and R, R'. The relevant

four-fermion interaction Lagrangian is thus

$$\mathcal{L}_{\text{int}} = \frac{\kappa_R}{2N_{\text{HC}}}(\chi_F\bar{\chi}^G)\Big|_{\text{Tr}=0}(\chi^{\dagger F}\bar{\chi}^{\dagger}_G)\Big|_{\text{Tr}=0} + \frac{\kappa_{R'}}{2N_{\text{HC}}}(\chi'_f\bar{\chi}'^g)\Big|_{\text{Tr}=0}(\bar{\chi}'^{\dagger f}\bar{\chi}'^{\dagger}_g)\Big|_{\text{Tr}=0} + \frac{\kappa_\Delta}{2N_{\text{HC}}}(\chi_F\bar{\chi}'^f)(\chi^{\dagger F}\bar{\chi}'^{\dagger}_f) + \frac{\kappa_{\widetilde{\Delta}}}{2N_{\text{HC}}}(\bar{\chi}^F\chi'_f)(\bar{\chi}^{\dagger}_F\bar{\chi}'^{\dagger f})\,, \tag{5.10}$$

where similar to κ_ψ, the four-fermion couplings $\kappa_R, \kappa_{R'}, \kappa_\Delta, \kappa_{\widetilde{\Delta}}$ are assumed to be real and positive. Note that in the case of $\text{SU}(4)_{\text{HC}}$, the $2N_{\text{HC}}$ factor in (5.10) and subsequent expressions is replaced with 4. The relevant auxiliary field definitions are

$$\begin{aligned} R_F{}^G &= -\frac{\kappa_R}{2N_{\text{HC}}}(\chi_F\bar{\chi}^G)\Big|_{\text{Tr}=0}\,, & R'^{\,g}_f &= -\frac{\kappa_{R'}}{2N_{\text{HC}}}(\chi'_f\bar{\chi}'^g)\Big|_{\text{Tr}=0}\,, \\ \Delta_F{}^f &= -\frac{\kappa_\Delta}{2N_{\text{HC}}}(\chi_F\bar{\chi}'^f)\,, & \widetilde{\Delta}^F{}_f &= -\frac{\kappa_{\widetilde{\Delta}}}{2N_{\text{HC}}}(\bar{\chi}^F\chi'_f)\,. \end{aligned} \tag{5.11}$$

The full interaction Lagrangian can now be written as a Yukawa model:

$$\begin{aligned} \mathcal{L}_{\text{int}} = &-\Big(R^T(\chi\bar{\chi}) + R'^T(\chi'\bar{\chi}') + \Delta^\dagger(\chi\bar{\chi}') + \widetilde{\Delta}^\dagger(\bar{\chi}\chi') + \text{h.c.}\Big) \\ &- \frac{2N_{\text{HC}}}{\kappa_R}\,\text{Tr}\,(R^2) - \frac{2N_{\text{HC}}}{\kappa_{R'}}\,\text{Tr}\,(R'^2) - \frac{2N_{\text{HC}}}{\kappa_\Delta}\,\text{Tr}\,(\Delta\Delta^\dagger) - \frac{2N_{\text{HC}}}{\kappa_{\widetilde{\Delta}}}\,\text{Tr}\,(\widetilde{\Delta}\widetilde{\Delta}^\dagger)\,. \end{aligned} \tag{5.12}$$

Note that the traces $\chi_F\bar{\chi}^F$ and $\chi'_f\bar{\chi}'^f$ have not been included in Eqs. (5.10)-(5.12). These fields are singlets under $\text{SU}(N+3)$ and $\text{SU}(N)'$, and thus will be omitted from the Ψ_χ effective potential because they do not break any gauge symmetries. Nonetheless, these traces can still acquire VEVs through non-perturbative effects or can have arbitrary bare mass terms $m_\chi\chi_F\bar{\chi}^F$ and $m_{\chi'}\chi'_f\bar{\chi}'^f$, that break the axial symmetry $\text{U}(1)^A_\chi$ and $\text{U}(1)^A_{\chi'}$ of $\text{SU}(N+3)$ and $\text{SU}(N)'$ respectively (see Appendix Appendix C). If these mass terms are set to zero, then these symmetries are still anomalous due to the enlarged color instanton contributions at the scale Λ_{HC}. We denote the Nambu-Goldstone bosons associated with the breaking of these symmetries σ and σ', respectively. In our model, we will assume that $m_{\chi,\chi'}$ are nonzero, but small compared to Λ_{HC}. For simplicity, we also assume that $m_{\chi,\chi'}$ are real, so that the topological aspects of the hypercolor and the enlarged color sectors are entirely

separated. The σ and σ' masses obtain contributions, either from these explicit breaking mass terms, or from hypercolor or enlarged color instantons. Therefore, it is reasonable to assume that these singlets will be as heavy as the $\Lambda_{\rm HC}$ scale.

Effective Potential for the Auxiliary Fields

The next step is to obtain the effective potential by integrating out the fermions. First we derive the gap equation for the auxiliary field, Δ. To a good approximation (see appendix Appendix B)

$$\begin{aligned} V_{\rm eff} \approx & \frac{2N_{\rm HC}}{\kappa_\Delta}\,{\rm Tr}\,(\Delta\Delta^\dagger) \\ & -\frac{N_{\rm HC}}{8\pi^2}\,{\rm Tr}\,\left(\Lambda_{\rm UV}^2\Delta\Delta^\dagger-(\Delta\Delta^\dagger)^2\log\left(1+\frac{\Lambda_{\rm UV}^2}{\Delta\Delta^\dagger}\right)+\Lambda_{\rm UV}^4\log\left(1+\frac{\Delta\Delta^\dagger}{\Lambda_{\rm UV}^2}\right)\right) \\ & -\frac{N_{\rm HC}}{16\pi^2}\,{\rm Tr}\,\left(\left(-\frac{2\Lambda_{\rm UV}^2}{\Lambda_{\rm UV}^2+\Delta\Delta^\dagger}+\log\left(1+\frac{\Lambda_{\rm UV}^2}{\Delta\Delta^\dagger}\right)\right)\Delta R'\widetilde{\Delta}R+{\rm h.c.}\right)\,, \end{aligned} \tag{5.13}$$

where the first two terms are the standard Coleman-Weinberg potential for Δ. The last term is novel, arising from loops that contain Δ as well as other fields R, R'. In this approximation, other auxiliary fields have been kept only to first order. Using the global symmetry ${\rm SU}(N+3)_\chi\times{\rm SU}(N+3)_{\bar\chi}\times{\rm SU}(N)_{\chi'}\times{\rm SU}(N)_{\bar\chi'}\subset G_{\rm SU}$, one can simultaneously decompose either the pair Δ, $\widetilde{\Delta}$ or the pair R, R', but not both pairs of fields. Without loss of generality, we choose to apply the singular value decomposition on Δ, $\widetilde{\Delta}$, which gives

$$\Delta = U_\chi\Delta_D V_{\bar\chi'}^\dagger, \qquad \widetilde{\Delta} = U_{\bar\chi}\widetilde{\Delta}_{\widetilde{D}}V_{\chi'}^\dagger\,. \tag{5.14}$$

The non-negative singular values are correspondingly Δ_n and $\widetilde{\Delta}_n$ $(n = 1 \dots N)$

$$\Delta_D = \begin{pmatrix} \operatorname{diag}(\Delta_1, \dots, \Delta_N) \\ \hline \mathbf{0}_{3\times N} \end{pmatrix}, \qquad \widetilde{\Delta}_D = \begin{pmatrix} \operatorname{diag}\left(\widetilde{\Delta}_1, \dots, \widetilde{\Delta}_N\right) \\ \hline \mathbf{0}_{3\times N} \end{pmatrix} \tag{5.15}$$

For the eigenvalues, Δ_n, the mass gap equation is now coupled with other fields

$$\frac{1}{\zeta_\Delta} \equiv \frac{4\pi^2}{\kappa_\Delta \Lambda_{\mathrm{UV}}^2} = 1 - \frac{2\phi_n^\Delta}{\Delta_n^2(\Lambda_{\mathrm{UV}}^2 + \Delta_n^2)} - \frac{\Delta_n^2}{\Lambda_{\mathrm{UV}}^2}\left(1 - \frac{\phi_n^\Delta}{\Delta_n^4}\right)\log\left(1 + \frac{\Lambda_{\mathrm{UV}}^2}{\Delta_n^2}\right), \tag{5.16}$$

where ϕ^Δ controls the amount of mixing with other fields. By setting $\phi^\Delta = 0$ one recovers the original gap equation in (5.5). The gap equations for $\Delta, \widetilde{\Delta}, R$ and R' only differ by the definition of ϕ

$$\begin{aligned} (\phi^\Delta)_n &= \Delta_n \widetilde{\Delta}_n \sum_{m=1}^{N} R^{\dagger n}{}_m R'^{\dagger m}{}_n\,, & (\phi^{\widetilde{\Delta}})_n &= \Delta_n \widetilde{\Delta}_n \sum_{m=1}^{N} R'^{\dagger n}{}_m R^{\dagger m}{}_n\,, \\ (\phi^R)_n{}^m &= R_n{}^m \Delta_m R'_m{}^n \widetilde{\Delta}_n\,, & (\phi^{R'})_n{}^m &= R'_n{}^m \widetilde{\Delta}_m R_m{}^n \Delta_n\,. \end{aligned} \tag{5.17}$$

The $R_F{}^G$ components where $F, G > N$ have not been included, since the mixing term ϕ^R for these components is zero, i.e. these components do not mix with other fields, thus satisfy the original gap equation.

For simplicity we assume $\kappa_\Delta = \kappa_{\widetilde{\Delta}}$ and $\kappa_R = \kappa_{R'}$, such that there are only two parameters controlling the symmetry breaking pattern. In this case, one can numerically solve the system of equations in (5.16) by further assuming that $R_n{}^m$ have the same value for $n \neq m$.

When ζ_Δ and ζ_R are less than one, both Δ and R stabilize at zero. Thus in this regime, the enlarged color symmetry is unbroken. In the regime where $\zeta_\Delta > 1$ and $\zeta_R < 1$, the numerical result (see Figure 5.1) indicates that the mixing term ϕ^Δ has little effect on the mass gap equation for Δ. Thus for all $n = 1 \dots N$, the eigenvalues Δ_n share the same

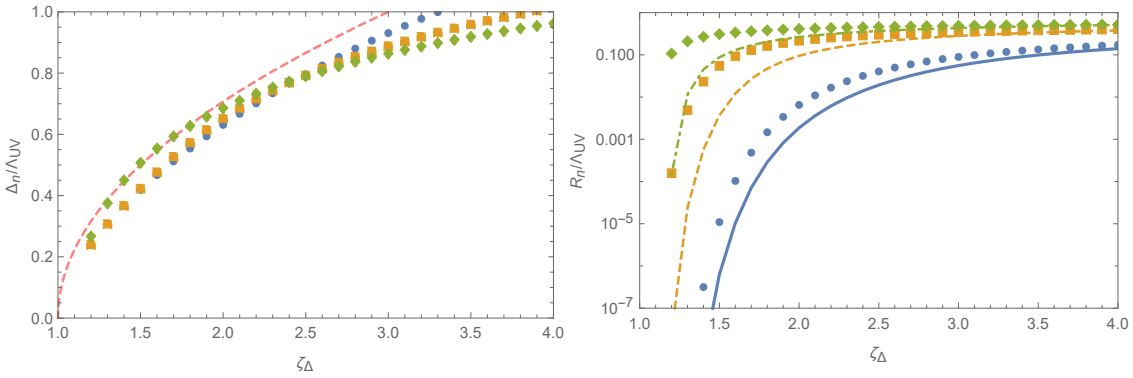

(a) (b)

Figure 5.1: Numerical values for (a) Δ_n and (b) ${R_n}^m$ as functions of ζ_Δ in the regime $\zeta_\Delta > 1, \zeta_R < 1$. The dots, squares and diamonds correspond to $\zeta_R = 0.2, 0.5$, and 0.8, respectively. In (a), the dashed curve represents the analytic approximation for Δ_n without mixing terms given in Eq. (5.18). In (b), the solid, dashed and dot-dashed curves represent the analytic approximation for ${R_n}^m$ given in Eq. (5.19). This approximation works better for small ζ_R (lower curves).

analytic expression, derived from the original gap equation,

$$\frac{\Delta_n}{\Lambda_{\rm UV}} \approx \sqrt{\frac{\zeta_\Delta - 1}{2}}\,. \tag{5.18}$$

Without the mixing term, ${R_n}^m$ should stabilize at zero given that $\zeta_R < 1$. With the new ϕ^R term, ${R_n}^m$ is now allowed to be nonzero, though turned out to be exponentially suppressed. The analytic approximation for R derived from (5.16) is

$${R_n}^m \approx \Lambda_{\rm UV} \exp\left(-\frac{\Lambda_{\rm UV}^2}{2\zeta_R \Delta_n \widetilde{\Delta}_m}\right). \tag{5.19}$$

Thus in this parameter subspace, Δ is the relevant VEV. Since Δ is a bifundamental under $\mathrm{SU}(N+3)\times\mathrm{SU}(N)'$, the enlarged color is broken to the diagonal subgroup $\mathrm{SU}(N)_D \times \mathrm{SU}(3)_c$. When $\zeta_R > 1$ and $\zeta_\Delta < 1$, it is straightforward to see that the field Δ and R now have reverse roles. The auxiliary field $R(R')$, which is an adjoint under $\mathrm{SU}(N+3)(\mathrm{SU}(N)')$, is now the relevant VEV, and thus breaking the symmetry to $\mathrm{SO}(N+3)\times\mathrm{SO}(N)$. The phase diagram summarizing this result is shown in Figure Figure 5.2.

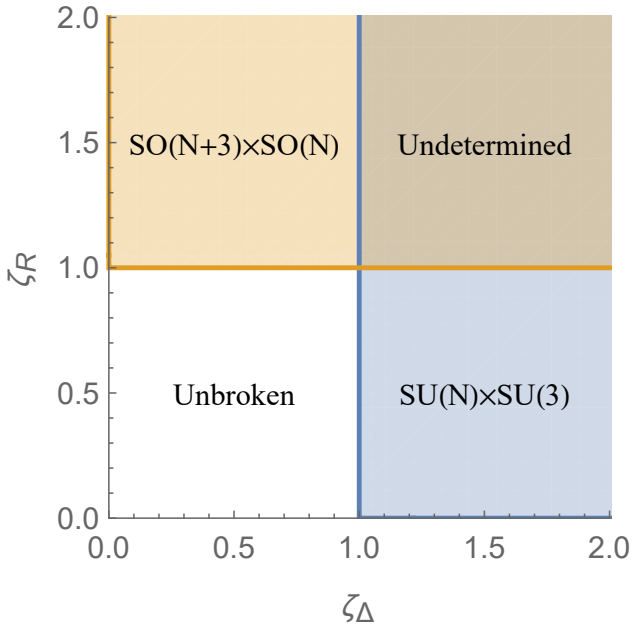

Figure 5.2: The enlarged color phase diagram, where $\zeta_\Delta = \kappa_\Delta \Lambda_{\rm UV}^2/(4\pi^2)$ and $\zeta_R = \kappa_R \Lambda_{\rm UV}^2/(4\pi^2)$ are dimensionless four-fermion couplings of Δ and R respectively.

When ζ_Δ and ζ_R are both greater than one, both auxiliary fields Δ, R can have nontrivial VEVs of order $\Lambda_{\rm UV}$. In this case the approximation $\zeta_\Delta \approx \zeta_{\widetilde{\Delta}}$ and $\zeta_R \approx \zeta_{R'}$ is too crude to capture the symmetry breaking pattern of the model. It requires a more in-depth analysis beyond the scope of this thesis, and thus this parameter regime is labelled as undetermined in Figure Figure 5.2. Nevertheless for the rest of this thesis, we will assume $\zeta_{\Delta,\widetilde{\Delta}} > 1$, while $\zeta_{R,R'} < 1$, such that Δ and $\widetilde{\Delta}$ are the only relevant VEVs. In the next section we show in detail how these VEVs imply the enlarged color breaking $\mathrm{SU}(N+3) \times \mathrm{SU}(N) \to \mathrm{SU}(N)_D \times \mathrm{SU}(3)_c$.

5.1.3 Enlarged Color Symmetry Breaking

To show that Δ_F^f, which transforms in the fundamental (antifundamental) representation of $\mathrm{SU}(N+3)$ ($\mathrm{SU}(N)'$), provides the desired local symmetry breaking pattern, we next consider the Δ kinetic term. This term is a proxy for the hyperfermion dynamics, which produces dynamical Nambu-Goldstone bosons that will be eaten by the spontaneously broken gauge

bosons. The covariant derivative with respect to the enlarged color group is

$$D_\mu \Delta = \partial_\mu \Delta - i T^A G^A_\mu \Delta + i \Delta T'^a G'^a_\mu \,, \tag{5.20}$$

where A, a are $\mathrm{SU}(N+3), \mathrm{SU}(N)'$ indices, G^A, G'^a are the corresponding gluons, and T^A, T'^a are the corresponding group generators, which are $(N+3)\times(N+3)$, $N\times N$ traceless, Hermitian matrices, respectively. The $\mathrm{SU}(N+3)$ generators can be grouped as $T^A = \{T^a_N, T^b, T^c_3, T_1\}$ where

$$\{T^a_N\} = \left\{ \left(\begin{array}{c|c} \mathrm{SU}(N) & \mathbf{0}_{N\times 3} \\ \hline \mathbf{0}_{3\times N} & \mathbf{0}_3 \end{array} \right) \right\}, \quad \{T^b\} = \frac{1}{2} \left\{ \left(\begin{array}{c|c} \mathbf{0}_N & [1]\,([i]) \\ \hline [1]\,([-i]) & \mathbf{0}_3 \end{array} \right) \right\},$$

$$\{T^c_3\} = \left\{ \left(\begin{array}{c|c} \mathbf{0}_N & \mathbf{0}_{N\times 3} \\ \hline \mathbf{0}_{3\times N} & \mathrm{SU}(3) \end{array} \right) \right\}, \quad T_1 = \frac{1}{\sqrt{6N(N+3)}} \left(\begin{array}{c|c} 3\,\mathbb{I}_N & \mathbf{0}_{N\times 3} \\ \hline \mathbf{0}_{3\times N} & -N\,\mathbb{I}_3 \end{array} \right), \tag{5.21}$$

with the normalization $\mathrm{Tr}\, T^A T^B = \frac{1}{2}\delta_{AB}$. Thus, $\{T^a_N\}$ consists of N^2-1 generators containing the subgroup $\mathrm{SU}(N)$; $\{T^b\}$ consists of $6N$ sparse matrices which have a single 1 or i in any of the $3N$ positions in the upper right region, and a 1 or $-i$ in the corresponding symmetric position of the lower left region; $\{T^c_3\}$ consists of eight generators containing the subgroup $\mathrm{SU}(3)$; and T_1 is the generator of the $\mathrm{U}(1)$ subgroup that commutes with all other elements of $\{T^a_N\}$ and $\{T^c_3\}$. Similarly, the $\mathrm{SU}(N+3)$ gauge bosons can also be grouped according to the generators in (5.21), namely $G^A_\mu = \{G^a_{N\mu}, G^b_\mu, G^c_{3\mu}, G_{1\mu}\}$. Assuming that

$\Delta_n \simeq F_{\rm HC} = \Lambda_{\rm HC}/(4\pi)$, when the hypercolor group confines, Δ obtains a VEV

$$\langle \Delta \rangle_F^f = F_{\rm HC} \begin{pmatrix} \mathbb{I}_N \\ \hline \mathbf{0}_{3\times N} \end{pmatrix}, \tag{5.22}$$

which generates mass terms for the spontaneously broken gauge bosons:

$$\mathrm{Tr}\, D_\mu \Delta D^\mu \Delta^\dagger = \frac{1}{2} F_{\rm HC}^2 (G^a_{N\mu} - G'^a_\mu)^2 + \frac{1}{2} F_{\rm HC}^2 (G^b_\mu)^2 + \frac{1}{2} \frac{3F_{\rm HC}^2}{(N+3)} (G_{1\mu})^2 \,. \tag{5.23}$$

The massive eigenstates are $\frac{1}{\sqrt{2}}(G^a_{N\mu} - G'^a_\mu), G^b_\mu$ and $G_{1\mu}$, while the massless gauge bosons are:

$$G^a_{D\mu} = \frac{1}{\sqrt{2}}(G^a_{N\mu} + G'^a_\mu)\,, \qquad G^c_{3\mu}\,, \tag{5.24}$$

which are respectively associated with the gauge groups $\mathrm{SU}(N)_D$ and $\mathrm{SU}(3)_c$ where $a = 1 \ldots N^2 - 1$ and $c = 1 \ldots 8$. The mass of the U(1) gauge boson, $G_{1\mu}$ is of order $1/N$, which vanishes in the large N limit.

Since a part of the enlarged color global symmetry is weakly gauged, there are $N(N+6)$ Nambu-Goldstone bosons from the spontaneous symmetry breaking, which are eaten by the massive gauge bosons, $\frac{1}{\sqrt{2}}(G^a_{N\mu} - G'^a_\mu), G^b_\mu$, and $G_{1\mu}$ (see Appendix Appendix C). This is unlike the spontaneous breaking of the SU(5) global symmetry, where the Higgs doublets remain as Nambu-Goldstone bosons. In other words, the hypercolor dynamics breaks the enlarged color group, but does not break the Standard Model electroweak gauge group.

We can now obtain the $\mathrm{SU}(N)_D$ and $\mathrm{SU}(3)_c$ coupling constants at the scale $\Lambda_{\rm HC}$ by considering the gauge kinetic term

$$\frac{1}{4g^2_{N+3}} F^{A\mu\nu} F^A_{\mu\nu} + \frac{1}{4g'^2} F'^{a\mu\nu} F'^a_{\mu\nu} = \frac{1}{4}\left(\frac{1}{g^2_{N+3}} + \frac{1}{g'^2}\right) F^{a\mu\nu}_D F^a_{D\mu\nu} + \frac{1}{4g^2_{N+3}} F^{c\,\mu\nu}_3 F^c_{3\mu\nu}\,, \tag{5.25}$$

where in the F_D term, $G^a_{D\mu}$ has been rescaled by $\sqrt{2}$. This leads to the identification

$$\frac{1}{\alpha_D(\Lambda_{\rm HC})} = \frac{1}{\alpha_{N+3}(\Lambda_{\rm HC})} + \frac{1}{\alpha'(\Lambda_{\rm HC})}\,, \tag{5.26}$$

and $\alpha_c(\Lambda_{\rm HC}) = \alpha_{N+3}(\Lambda_{\rm HC})$ where $\alpha_i = g_i^2/4\pi$. This breaking generalizes previous results for SU(3) × SU(3) [152, 153, 139]. Similarly, at the scale $\Lambda_{\rm HC}$ the corresponding θ terms of the gauge fields can be identified as

$$\theta_{N+3} F^{A\mu\nu}\widetilde{F}^A_{\mu\nu} + \theta' F'^{a\mu\nu}\widetilde{F}'^a_{\mu\nu} = (\theta_{N+3}+\theta')F_D^{a\mu\nu}\widetilde{F}^a_{D\mu\nu} + \theta_{N+3}F_3^{c\,\mu\nu}\widetilde{F}^c_{3\mu\nu}\,, \tag{5.27}$$

where $\widetilde{F}^i_{\mu\nu} = \frac{1}{2}\epsilon_{\mu\nu\rho\sigma}F^{i\rho\sigma}$ $(i = A, a, c)$ and $\epsilon_{0123} = \epsilon^{0123} = +1$. The new gauge fields of $\mathrm{SU}(N)_D$ and $\mathrm{SU}(3)_c$ then inherit θ terms:

$$\theta_D = \theta_{N+3} + \theta'\,, \qquad\qquad \theta_c = \theta_{N+3}\,. \tag{5.28}$$

There are also phases in the fermion sector that will contribute to an effective θ-term. We next discuss how the Standard Model quarks are embedded into the enlarged color sector.

5.1.4 Embedding the Standard Model Quarks

The Standard model quarks, $q, \bar{u}, \bar{d}$ are embedded into the larger representations $Q, \bar{U}, \bar{D}$ of the enlarged color group as shown in Table Table 5.3. After $\mathrm{SU}(N+3) \times \mathrm{SU}(N)'$ is spontaneously broken, the Standard Model quarks remain massless, while the $\mathrm{SU}(N)_D$ components, $\mathbf{q}, \bar{\mathbf{u}}, \bar{\mathbf{d}}$ pair up with $\bar{\mathbf{q}}', \mathbf{u}', \mathbf{d}'$ to obtain vector-like masses of order $F_{\rm HC}$. For example, consider the gauge interactions of the quark parent Q and $\bar{q}'$

$$\begin{aligned}
&Q^\dagger\bar{\sigma}_\mu\left(i\partial^\mu + G^{A\mu}T^A\right)Q + \bar{q}'^\dagger\bar{\sigma}_\mu\left(i\partial^\mu - G'^{a\mu}T'^a\right)\bar{q}' \\
&\to i\mathbf{q}^\dagger\bar{\sigma}_\mu\partial^\mu\mathbf{q} + i\bar{q}'^\dagger\bar{\sigma}_\mu\partial^\mu\bar{q}' + G_D^{a\mu}\left(\mathbf{q}^\dagger\bar{\sigma}_\mu T_D^a\mathbf{q} - \bar{q}'^\dagger\bar{\sigma}_\mu T_D^a\bar{q}'\right) \\
&\qquad + iq^\dagger\bar{\sigma}_\mu\partial^\mu q + G_3^{c\mu}q^\dagger\bar{\sigma}_\mu T_3^c q\,,
\end{aligned} \tag{5.29}$$

where T_D^a is an $\mathrm{SU}(N)_D$ generator, A, a, and c are $\mathrm{SU}(N+3)$, $\mathrm{SU}(N)'$, and $\mathrm{SU}(3)_c$ indices respectively, and $G_D^{a\mu}$ has been rescaled by $\sqrt{2}$ as in (5.25). In addition, there is a mass term generated by an effective Δ coupling:

$$y_Q \Delta_F^{\dagger f} Q^F \bar{q}'_f + \text{h.c.} \to y_Q F_{\text{HC}}\, \mathbf{q}^f \bar{\mathbf{q}}'_f + \text{h.c.}\,, \tag{5.30}$$

where y_Q is a 3×3 Yukawa coupling matrix in family space with family indices omitted. There are also similar couplings for the right-handed quarks $\bar{U}$ and $\bar{D}$, with respective Yukawa coupling matrices y_U and y_D.

A similar decomposition occurs for the hyperfermions χ, since they are charged under the enlarged color group (see Table 5.1 or Table 5.2). Let $\chi = (\boldsymbol{\chi}, \chi_c)$ and $\bar{\chi} = (\bar{\boldsymbol{\chi}}, \bar{\chi}_c)$, where the first (second) component corresponds to the subgroup generated by T_N^a (T_3^c) (see Eq. (5.21)). Given that the pairs $\boldsymbol{\chi}, \bar{\chi}'$ and $\bar{\boldsymbol{\chi}}, \chi'$ form the condensate (5.22), we obtain the Dirac mass terms

$$(\Delta^\dagger)_f{}^F \chi_F \bar{\chi}'^f + (\widetilde{\Delta}^\dagger)^f{}_F \bar{\chi}^F \chi'_f + \text{h.c.} = F_{\text{HC}} \boldsymbol{\chi}_f \bar{\chi}'^f + F_{\text{HC}} \bar{\boldsymbol{\chi}}^f \chi'_f + \text{h.c.}\,, \tag{5.31}$$

while the $\mathrm{SU}(3)_c$ states $\chi_c, \bar{\chi}_c$ remain massless. These colored hyperfermions eventually become part of cubic invariants which are identified with the top partners at low energy [147]. The top partners are part of the partial compositeness mechanism for generating the top quark mass.

More generally, partial compositeness near the hyperfermion confinement scale is responsible for generating the Standard Model flavor structure, although the specific details are model dependent. In order to simplify the analysis relevant for the strong CP problem, we will assume that the global symmetry associated with the electroweak sector is broken by the hyperfermion dynamics at a higher scale compared to the color breaking scale[1]. This means that there is an effective Yukawa coupling of the Higgs to the quark parents. After

[1] In fact this was argued to occur in the $\mathrm{SU}(4)_{\text{HC}}$ hypercolor model of Ref. [148].

color breaking, this Yukawa coupling becomes

$$y_u^{\rm SM} H Q \bar{U} + y_d^{\rm SM} H^\dagger Q \bar{D} + \text{h.c.} \\ \to \left(y_u^{\rm SM} H q \bar{u} + y_d^{\rm SM} H^\dagger q \bar{d} + \text{h.c.} \right) + \left(y_u^{\rm SM} H \mathbf{q} \bar{\mathbf{u}} + y_d^{\rm SM} H^\dagger \mathbf{q} \bar{\mathbf{d}} + \text{h.c.} \right) , \quad (5.32)$$

where H is an $\mathrm{SU}(2)_L$ doublet with $Y = \frac{1}{2}$, and $y_{u,d}^{\rm SM}$ are the Standard Model 3×3 Yukawa coupling matrices with family indices omitted. Since q, $\bar{u}$ and $\bar{d}$ do not receive any mass contribution from Δ in Eq. (5.30), their masses are solely obtained from the Higgs VEV. On the other hand, $\mathbf{q}, \bar{\mathbf{u}}$ and $\bar{\mathbf{d}}$ already obtain Dirac masses of order $F_{\rm HC}$, which are much larger than the contribution they receive from the Higgs Yukawa coupling.

	$\mathrm{SU}(N+3)$	$\mathrm{SU}(N)'$		$\mathrm{SU}(3)_c$	$\mathrm{SU}(N)_D$	$\mathrm{SU}(2)_L$	$\mathrm{U}(1)_Y$
Q	$\square$	$\mathbf{1}$	q	$\square$	$\mathbf{1}$	$\square$	$\frac{1}{6}$
			$\mathbf{q}$	$\mathbf{1}$	$\square$	$\square$	$\frac{1}{6}$
$\bar{U}$	$\overline{\square}$	$\mathbf{1}$	$\bar{u}$	$\overline{\square}$	$\mathbf{1}$	$\mathbf{1}$	$-\frac{2}{3}$
			$\bar{\mathbf{u}}$	$\mathbf{1}$	$\overline{\square}$	$\mathbf{1}$	$-\frac{2}{3}$
$\bar{D}$	$\overline{\square}$	$\mathbf{1}$	$\bar{d}$	$\overline{\square}$	$\mathbf{1}$	$\mathbf{1}$	$\frac{1}{3}$
			$\bar{\mathbf{d}}$	$\mathbf{1}$	$\overline{\square}$	$\mathbf{1}$	$\frac{1}{3}$
$\bar{q}'$	$\mathbf{1}$	$\overline{\square}$	$\bar{\mathbf{q}}'$	$\mathbf{1}$	$\overline{\square}$	$\square$	$-\frac{1}{6}$
u'	$\mathbf{1}$	$\square$	$\mathbf{u}'$	$\mathbf{1}$	$\square$	$\mathbf{1}$	$\frac{2}{3}$
d'	$\mathbf{1}$	$\square$	$\mathbf{d}'$	$\mathbf{1}$	$\square$	$\mathbf{1}$	$-\frac{1}{3}$
ξ	$\mathbf{Ad}$	$\mathbf{1}$	ψ'_c	$\square$	$\overline{\square}$	$\mathbf{1}$	0
			$\bar{\psi}'_c$	$\overline{\square}$	$\square$	$\mathbf{1}$	0
			λ_c	$\mathbf{Ad}$	$\mathbf{1}$	$\mathbf{1}$	0
			λ_D	$\mathbf{1}$	$\mathbf{Ad}$	$\mathbf{1}$	0
			ν'	$\mathbf{1}$	$\mathbf{1}$	$\mathbf{1}$	0
ψ'	$\mathbf{1}$	$\square$	ψ'	$\mathbf{1}$	$\square$	$\mathbf{1}$	0
$\bar{\psi}'$	$\mathbf{1}$	$\overline{\square}$	$\bar{\psi}'$	$\mathbf{1}$	$\overline{\square}$	$\mathbf{1}$	0

Table 5.3: The Weyl fermion content of the model, including the Standard Model quarks $(q, \bar{u}, \bar{d})$, charged under the various gauge groups. All listed fermions are singlets of either hypercolor gauge groups. The Weyl fermion, ξ is listed as an adjoint of $\mathrm{SU}(N+3)$, but as discussed in the text, can also be in a pseudoreal representation of $\mathrm{SU}(N{+}3)$ for $N = 3, 7, \ldots$.

Since the $\mathrm{SU}(N)'$ quarks, $\bar{q}', u', d'$ have conjugate Standard Model quantum numbers they can also couple to the Standard Model Higgs field, above the color breaking scale. The

effective Higgs couplings are:

$$\Delta\mathcal{L}' = y'_u \widetilde{H}^\dagger \bar{q}' u' + y'_d \widetilde{H} \bar{q}' d' + \text{h.c.} \to y'_u \widetilde{H}^\dagger \bar{\mathbf{q}}' \mathbf{u}' + y'_d \widetilde{H} \bar{\mathbf{q}}' \mathbf{d}' + \text{h.c.}\,, \tag{5.33}$$

where $\widetilde{H} \equiv i\sigma_2 H$ and $y'_{u,d}$ are 3×3 Yukawa coupling matrices in family space with family indices omitted. When the Higgs field obtains a VEV, the Yukawa masses generated in (5.33) are negligible compared to the vector-like masses obtained from (5.30). Since the Higgs is composite and the primed fermions are elementary, the Yukawa couplings are naturally suppressed. Later they will play an important role in the small instanton contribution to the axion mass.

Furthermore, after enlarged color and electroweak symmetry is spontaneously broken, the fermion mass term can be organized as follows

$$\mathcal{L}_{\text{Yukawa}} = \frac{v}{\sqrt{2}} \begin{pmatrix} \bar{u} & \bar{d} \end{pmatrix} Y^{\text{SM}} \begin{pmatrix} u \\ d \end{pmatrix} + F_{\text{HC}} \begin{pmatrix} \bar{\mathbf{u}}' & \bar{\mathbf{u}} & \bar{\mathbf{d}}' & \bar{\mathbf{d}} \end{pmatrix} Y^D \begin{pmatrix} \mathbf{u} \\ \mathbf{u}' \\ \mathbf{d} \\ \mathbf{d}' \end{pmatrix} + \text{h.c.}\,, \tag{5.34}$$

where $\langle H \rangle = \frac{1}{\sqrt{2}} \left(\begin{smallmatrix} 0 \\ v \end{smallmatrix}\right)$. For convenience, we have written out the $\text{SU}(2)_L$ doublet components as $q = \left(\begin{smallmatrix} u \\ d \end{smallmatrix}\right)$, $\mathbf{q} = \left(\begin{smallmatrix} \mathbf{u} \\ \mathbf{d} \end{smallmatrix}\right)$ and $\bar{\mathbf{q}}' = \left(\begin{smallmatrix} \bar{\mathbf{u}}' \\ \bar{\mathbf{d}}' \end{smallmatrix}\right)$. The Yukawa coupling matrices are given by

$$Y^{\text{SM}} = \begin{pmatrix} y_u^{SM} & 0 \\ 0 & y_d^{SM} \end{pmatrix}, \qquad Y^D = \begin{pmatrix} y_Q & 0 & 0 & \frac{v}{\sqrt{2}F_{\text{HC}}}\, y'_d \\ \frac{v}{\sqrt{2}F_{\text{HC}}}\, y_u^{\text{SM}} & y_U & 0 & 0 \\ 0 & \frac{v}{\sqrt{2}F_{\text{HC}}}\, y'_u & y_Q & 0 \\ 0 & 0 & \frac{v}{\sqrt{2}F_{\text{HC}}}\, y_d^{\text{SM}} & y_D \end{pmatrix}. \tag{5.35}$$

The first matrix, Y^{SM} in Eq. (5.35) contains the usual Standard Model quark Yukawa

couplings, and can be diagonalized through the singular value decomposition with a chiral rotation on the quarks. This procedure introduces a new phase

$$\bar{\theta}_c = \theta_c - \arg\det Y^{\rm SM} = \theta_{N+3} - \arg\det\left(y_u^{\rm SM}\, y_d^{\rm SM}\right)\,, \tag{5.36}$$

where the second relation in (5.28) has been used. Similarly, the second matrix, $Y^{\rm D}$ can also be diagonalized with a corresponding chiral rotation on the $\mathrm{SU}(N)_D$ quark fields

$$\bar{\theta}_D = \theta_D - \arg\det Y^D = \theta_{N+3} + \theta' - \arg\det Y^D\,, \tag{5.37}$$

where the first relation in (5.28) has been used. Since $v \ll F_{\rm HC}$, the phase contribution of $y_{u,d}^{\rm SM}$ and $y'_{u,d}$ to $\arg\det Y^D$ is negligible. In particular, to leading order in $v/F_{\rm HC}$, Y^D is block diagonal, similar to $Y^{\rm SM}$. In fact, it is straightforward to show that

$$\arg\det Y^D = 2\arg\det Y_Q + \arg\det Y_U + \arg\det Y_D + \mathcal{O}\left(\frac{v}{F_{\rm HC}}\right)^4. \tag{5.38}$$

The effective θ parameters (5.36) and (5.37) will later be shown to be cancelled by composite axions.

5.2 Composite Axion

5.2.1 An Invisible Axion from the Hypercolor Sector

An enlarged color group can be used to obtain a heavy axion. However, it is instructive to first consider the simpler possibility where $\mathrm{SU}(3)_c$ is not modified in the UV, and the only colored hyperfermions are $\chi_c, \bar{\chi}_c$, as in the original SU(4)/Sp(4) model [146] or the hypercolor models with colored fermions given in [148]. If ψ and $\chi_c, \bar{\chi}_c$ are massless, then there are two anomalous global symmetries $\mathrm{U}(1)_\psi, \mathrm{U}(1)_\chi$, with respect to the hypercolor dynamics. The pseudo Nambu-Goldstone bosons[2] associated with these symmetries, σ_ψ and σ_χ, then obtain the hypercolor and QCD anomalous couplings

$$\mathcal{L} \supset \frac{1}{32\pi^2}\left(a_\psi \frac{\sigma_\psi}{F_{\mathrm{HC}}} + a_\chi \frac{\sigma_\chi}{F_{\mathrm{HC}}} - \theta_{\mathrm{HC}}\right) F^a_{\mathrm{HC}\mu\nu}\widetilde{F}^{a\mu\nu}_{\mathrm{HC}} + \frac{1}{32\pi^2}\left(b_\chi \frac{\sigma_\chi}{F_{\mathrm{HC}}} - \theta_c\right) F^c_{3\mu\nu}\widetilde{F}^{c\mu\nu}_3 \,, \tag{5.39}$$

where $a_{\psi,\chi}$ and b_χ are group theoretical factors that depend on the representations of $\psi, \chi_c, \bar{\chi}_c$, and $\theta_{\mathrm{HC}}, \theta_c$ are the hypercolor and QCD θ parameters, respectively. For simplicity, we also assume a common decay constant $F_{\mathrm{HC}} \approx \Lambda_{\mathrm{HC}}/4\pi$ for both $\sigma_{\psi,\chi}$. From Eq. (5.39), the hypercolor and QCD instantons generate mass terms

$$\mathcal{L} \supset \frac{1}{2}\Lambda^4_{\mathrm{HC}}\left(a_\psi \frac{\sigma_\psi}{F_{\mathrm{HC}}} + a_\chi \frac{\sigma_\chi}{F_{\mathrm{HC}}} - \theta_{\mathrm{HC}}\right)^2 + \frac{1}{2}\Lambda^4_c\left(b_\chi \frac{\sigma_\chi}{F_{\mathrm{HC}}} - \theta_c\right)^2 . \tag{5.40}$$

Expanding (5.40) around the CP-conserving minimum (i.e. $\sigma_{\psi,\chi} \to \langle\sigma_{\psi,\chi}\rangle + \sigma_{\psi,\chi}$), leads to the Lagrangian for the physical fluctuations

$$\mathcal{L}_{\mathrm{eff}} \supset \frac{1}{2}\Lambda^4_{\mathrm{HC}}\left(a_\psi \frac{\sigma_\psi}{F_{\mathrm{HC}}} + a_\chi \frac{\sigma_\chi}{F_{\mathrm{HC}}}\right)^2 + \frac{1}{2}\Lambda^4_c\left(b_\chi \frac{\sigma_\chi}{F_{\mathrm{HC}}} + 2\frac{\eta'_{\mathrm{QCD}}}{F_\pi}\right)^2 , \tag{5.41}$$

[2] These Nambu-Goldstone bosons are assumed to arise from hypercolor bilinear condensates. Other four-fermion condensates may also be possible as long as there remains a hypercolor anomaly-free symmetry.

where the $\eta'_{\rm QCD}$ of QCD has been included with F_π the QCD pion decay constant, and the quark mass contributions have been ignored[3]. Besides $\eta'_{\rm QCD}$, the physical eigenstates resulting from Eq. (5.41) are

$$\sigma_{\rm HC} \approx \frac{a_\psi \sigma_\psi + a_\chi \sigma_\chi}{\sqrt{a_\psi^2 + a_\chi^2}}\,, \qquad \sigma_c \approx \frac{-a_\chi \sigma_\psi + a_\psi \sigma_\chi}{\sqrt{a_\psi^2 + a_\chi^2}}\,, \tag{5.42}$$

where we neglect next-to-leading corrections of order $(\Lambda_c/\Lambda_{\rm HC})^4$, and the small mixing with $\eta'_{\rm QCD}$. Thus σ_c corresponds to a hypercolor anomaly free combination of $\mathrm{U}(1)_\psi$ and $\mathrm{U}(1)_\chi$, while $\sigma_{\rm HC}$ corresponds to the orthogonal linear combination. Since we assume no explicit mass terms, the physical masses are determined purely by instanton contributions given by

$$m_{\sigma_{\rm HC}} \approx \sqrt{a_\psi^2 + a_\chi^2}\,\frac{\Lambda_{\rm HC}^2}{F_{\rm HC}}\,, \qquad m_{\eta'_{\rm QCD}} \approx 2\frac{\Lambda_c^2}{F_\pi}\,, \qquad m_{\sigma_c} = 0\,. \tag{5.43}$$

Thus besides $\eta'_{\rm QCD}$, we obtain a heavy mass eigenstate from the hypercolor instanton contributions, while the other eigenstate is massless. If the quark contributions are included, one recovers the standard axion mass relation [72, 71]. The phenomenology of $\sigma_{\rm HC}$ and σ_c was previously studied in Refs. [154, 155, 42], where an explicit mass term was assumed for the light state that kinematically allowed decays to Standard Model gauge bosons through the WZW interaction terms. However in our case, since we forbid explicit mass terms, the $\mathrm{U}(1)_\chi$ symmetry is only explicitly broken by QCD instantons, and σ_c can therefore be a composite invisible axion that solves the strong CP problem.

This can also be understood from a UV - IR matching argument. Above the hypercolor confinement scale, the massless hyperfermions ψ, χ_c, and $\bar{\chi}_c$ render the hypercolor and QCD θ terms irrelevant. Since CP must still be preserved after confinement, the pseudoscalar singlets $\sigma_{\rm HC}, \sigma_c$ must be axions that dynamically cancel the θ terms below $\Lambda_{\rm HC}$. Indeed, the minimum of the potential in Eq. (5.40) precisely occurs at vacuum expectation values of $\sigma_{\rm HC}$ and σ_c which eliminates the CP violating terms in (5.39). Thus, hypercolor can be

[3]Note that the electroweak coset may give rise to additional singlets, as in Eq. (5.6), however these singlets do not receive mass contributions from the hypercolor instanton (similar to the $\eta_{\rm QCD}$ of QCD not receiving QCD instanton contributions).

identified with the axicolor dynamics, as in Ref. [71], except that hypercolor also produces a composite Higgs. Note also that the cancellation in Eq. (5.40) only occurs if ψ does not have an explicit mass. If the electroweak coset contains a singlet (such as in Eq. (5.6)), a mass term may be desirable to avoid phenomenological constraints, and the misalignment in (5.39) may be tolerable for sufficiently small ψ masses. Alternatively, the issue can be completely avoided if the electroweak coset does not contain a singlet, and both possibilities deserves further study.

The fact that σ_c can be identified with the QCD axion requires the decay constant, which depends on the hypercolor confinement scale, to be $F_{\rm HC} \sim 10^9 - 10^{12}$ GeV. From the perspective of the Higgs sector, this makes the theory unnatural. Nevertheless it is interesting that the composite Higgs potential at $F_{\rm HC}$ has a naturally suppressed quartic coupling, that can provide the appropriate boundary condition to radiatively generate the correct Higgs quartic coupling at low energies [149]. Although interesting, we will postpone a study of specific composite Higgs models. In any case, the composite axion σ_c behaves as the usual invisible axion at low energies, and solves the strong CP problem.

Instead to construct a heavy composite axion, we will make use of the enlarged color sector, with the diagonal color $\mathrm{SU}(N)_D$ originating from this enlarged color. Besides generating the composite Higgs sector, the hypercolor is also responsible for breaking the enlarged color group. In this case, the axion may receive sizeable contributions from $\mathrm{SU}(N)'$ instantons, and thus could be heavy. However since this $\mathrm{SU}(N)'$ color also has a θ' term, other massless fermions will need to be introduced into the UV theory in order to prevent a misalignment of the strong CP axion solution.

5.2.2 A Heavy Axion from Enlarged Color

For the enlarged color sector to be totally free of the strong CP problem in the UV, the theory must admit massless fermions charged under both $\mathrm{SU}(N+3)$ and $\mathrm{SU}(N)'$. It is possible to construct a solution with heavy axions that are identified with the pseudoscalar bound states of massless hyperfermions, χ, $\bar{\chi}$ and χ', $\bar{\chi}'$. In such a solution, one would have to include the hypercolor θ angle, such as in Eq. (5.40). Instead, for simplicity, we

will consider models with extra massless quarks that are hypercolor singlets. A theory with massless colored hyperfermions will be considered in future work.

We begin by introducing a new massless Weyl fermion, ξ charged under $\mathrm{SU}(N+3)$. For $\mathrm{SU}(N+3)$ to be anomaly free, the representation of ξ must be either real or pseudoreal[4]. If the representation is pseudoreal then the bilinear $\xi\xi$ is zero and a ξ mass term is forbidden. The pseudoreal representation is the totally antisymmetric n-index tensor of $\mathrm{SU}(2n)$ where $n = 3, 5, \ldots$ is an odd integer. Thus, $\mathrm{SU}(N+3)$ admits pseudoreal representations for $N = 2n-3 = 3, 7, 11, \ldots$ The smallest pseudoreal representation of ξ is the **20** of $\mathrm{SU}(6)$ associated with $N = 3$, which was also considered in Ref. [144]. In general, under $\mathrm{SU}(3)_c \times \mathrm{SU}(N)_D$ the pseudoreal representation $\mathbf{A}_n$ decomposes as

$$\xi(\mathbf{A}_n) \to \psi_D\,(\mathbf{1},\,\mathbf{n_1}) + \bar{\psi}_D\,(\mathbf{1},\,\bar{\mathbf{n}}_\mathbf{1}) + \psi'_c\,(\mathbf{3},\bar{\mathbf{n}}_\mathbf{2}) + \bar{\psi}'_c\,(\bar{\mathbf{3}},\mathbf{n_2})\,, \tag{5.44}$$

where $\dim\xi = \binom{2n}{n}$, $n_1 = \binom{2n-3}{n}$ and $n_2 = \binom{2n-3}{n-1}$. In particular, ξ gives rise to massless $\mathrm{SU}(N)_D$ fermions as well as massless bifundamental fermions charged under $\mathrm{SU}(3)_c$ and $\mathrm{SU}(N)_D$. The diagonal color group $\mathrm{SU}(N)_D$ actually plays the role of axicolor [72, 71]. When $\mathrm{SU}(N)_D$ confines, these fermions can form axicolor bound states, $\psi_D\bar{\psi}_D$ and $\psi'_c\bar{\psi}'_c$, with a linear combination giving rise to a composite axion that will later be shown to be relevant for the strong CP problem.

For $\mathrm{SU}(2n)$ where n is an even integer, the totally antisymmetric representation, $\mathbf{A}_n$, is real instead of pseudoreal. After the enlarged color group is broken, ξ has a similar breaking pattern to Eq. (5.44). For $N > 4$ however, there is a smaller real representation, namely the adjoint representation admitted by all values of N. Upon the breaking of the enlarged color symmetry, the adjoint state ξ becomes

$$\xi(\mathbf{Ad}) \to \lambda_D\,(\mathbf{1},\mathbf{Ad}) + \lambda_c\,(\mathbf{8},\mathbf{1}) + \psi'_c\,(\mathbf{3},\overline{\mathbf{N}}) + \bar{\psi}'_c\,(\overline{\mathbf{3}},\mathbf{N}) + \nu'(\mathbf{1},\mathbf{1})\,. \tag{5.45}$$

The difference between $\xi(\mathbf{Ad})$ and $\xi(\mathbf{A}_n)$ in Eq. (5.44) is the appearance of the adjoint states

[4]The Witten anomaly [156, 157] for an odd number of Weyl fermions in the pseudoreal representation only occurs for SU(2).

λ_D, λ_c and a sterile neutrino ν'. Furthermore, the colored $\psi'_c, \bar{\psi}'$ are in the fundamental representation of $\mathrm{SU}(N)_D$, instead of being in a larger representation.

If ξ is in a real representation, it is possible for ξ to obtain a Majorana mass. This mass is a free parameter of the theory, and will be set to zero. As a result, there is a global $\mathrm{U}(1)_\xi$ symmetry. There is the issue of quantum gravitational corrections breaking the $\mathrm{U}(1)_\xi$ global symmetry. However, we will assume that the global symmetry can be gauged, embedded into a larger gauge group structure, or the mass term forbidden with a discrete symmetry, such as $\mathbb{Z}_N$ ($N \geq 3$), and we will not present the details of this additional structure.

Given the two possibilities (5.44) and (5.45) for a massless ξ, we will choose the adjoint representation to present details of the axion mechanism, since the choice of N is less constrained, and also because the resulting structure is generally simpler. For larger values of n, the dimension of $\xi(\mathbf{Ad})$ is $4n^2-1$, while the dimension of $\xi(\mathbf{A}_n)$ grows exponentially with n. Nonetheless, the axion mechanism for both representations is the same, and the results for $N = 3, 7, \ldots$ can be interpreted for a pseudoreal representation. When the diagonal color group $\mathrm{SU}(N)_D$ confines at some scale Λ_D, the two states $\psi'_c\,(\mathbf{3}, \overline{\mathbf{N}})$ and $\bar{\psi}'_c\,(\overline{\mathbf{3}}, \mathbf{N})$ form a bound state. At this energy scale ($\gtrsim 10$ TeV), the QCD coupling is weak and QCD color can be treated as flavor with respect to $\mathrm{SU}(N)_D$. Just like the QCD chiral symmetry, the global symmetry for diagonal color is then $\mathrm{U}(3)_L \times \mathrm{U}(3)_R$, giving rise to a singlet meson η'_c, similar to the η'_{QCD} of QCD. Since the η'_c constituents $\psi'_c, \bar{\psi}'_c$ are massless, η'_c can be relevant as a dynamical axion. Furthermore, the condensate $\langle \psi'_c \bar{\psi}'_c \rangle$ spontaneously breaks the $\mathrm{U}(1)_\xi$ symmetry. While the $\mathrm{SU}(N)_D$ fermions in (5.45) confine at the Λ_D scale, the λ_c, ν' fermions can obtain a mass via a four-fermion interaction between $\psi'_c \bar{\psi}'_c$ and λ_c or ν'. For instance, the adjoint λ_c can obtain mass of order Λ_D^3/M_c^2, where M_c is related to the mass of some heavy, colored bosons, such as the massive gauge bosons in Eq. (5.23). Similarly, the sterile neutrino ν' can obtain a mass of order $\Lambda_D^3/\Lambda_{\mathrm{UV}}^2$, where $\Lambda_{\mathrm{UV}} \gg \Lambda_D$. These states could lead to experimental signatures (see Section 5.3.1).

As mentioned in Section 5.2.1, besides the QCD chiral anomaly, η'_c also couples to the chiral anomaly of $\mathrm{SU}(N)_D$, which may inherit another θ term from $\mathrm{SU}(N)'$. Since the confinement scale Λ_D of $\mathrm{SU}(N)_D$ is at least a few orders of magnitude higher than Λ_c of

QCD, the η_c' axion will align with $\mathrm{SU}(N)_D$ and fail to solve the QCD strong CP problem. To avoid this problem, following [144], we include extra massless Weyl fermions ψ' and $\bar{\psi}'$ (i.e. with zero bare mass), which transform in the fundamental and antifundamental representation of $\mathrm{SU}(N)'$, respectively. When the enlarged color group is broken, these fermions transform as a corresponding fundamental (antifundamental) under $\mathrm{SU}(N)_D$:

$$\begin{aligned}&\psi'^{\dagger}\bar{\sigma}^{\mu}(i\partial_{\mu}-G'^{a}_{\mu}T'^{a})\psi'+\bar{\psi}'^{\dagger}\bar{\sigma}^{\mu}(i\partial_{\mu}+G'^{a}_{\mu}T'^{a})\bar{\psi}'\\&\rightarrow\; i\psi'^{\dagger}\bar{\sigma}_{\mu}\partial^{\mu}\psi'+i\bar{\psi}'^{\dagger}\bar{\sigma}_{\mu}\partial^{\mu}\bar{\psi}'-G_D^{a\mu}\left(\psi'^{\dagger}\bar{\sigma}_{\mu}T_D^{a}\psi'-\bar{\psi}'^{\dagger}\bar{\sigma}_{\mu}T_D^{a}\bar{\psi}'\right)+\dots\,,\end{aligned}\tag{5.46}$$

where G_D has again been rescaled as in (5.25) and the terms coupling to the massive enlarged color gauge bosons have been omitted.

The extra massless $\psi', \bar{\psi}'$ fermions extend the $\mathrm{SU}(N)_D$ global symmetry to $\mathrm{U}(4)_L \times \mathrm{U}(4)_R = \mathrm{SU}(4)_L \times \mathrm{SU}(4)_R \times \mathrm{U}(1)_V \times \mathrm{U}(1)_A$. When $\psi'\bar{\psi}'$ and $\psi_c'\bar{\psi}_c'$ form condensates near the $\mathrm{SU}(N)_D$ confinement scale, they spontaneously break the chiral symmetry to $\mathrm{SU}(4)_V \times \mathrm{U}(1)_V$, and give rise to sixteen Nambu-Goldstone bosons:

$$\mathbf{16} = \mathbf{8}_c + \mathbf{3}_c + \bar{\mathbf{3}}_c + \mathbf{1}_c + \mathbf{1}_c\,,\tag{5.47}$$

labelled by their respective QCD representations. The colored NGBs obtain radiatively-induced masses from QCD gluon loops of order the symmetry breaking scale [71]. The two singlets in (5.47) correspond to the $\mathrm{U}(1)_A$ generator $T_{16} = \mathrm{diag}(1,1,1,1)/(2\sqrt{2})$ with current j_{16}, and one of the broken $\mathrm{SU}(4)_A$ generators, $T_{15} = \mathrm{diag}(1,1,1,-3)/(2\sqrt{6})$ with current j_{15}. The $\mathrm{U}(1)_A$ symmetry is broken by the $\mathrm{SU}(N)_D$ instantons and is thus anomalous. The divergence of the j_{16} current would be proportional to $F_D^a \widetilde{F}_D^a$, but since $\mathrm{SU}(3)_c$ weakly gauges part of the global symmetry, the $\mathrm{U}(1)_A$ chiral transformation also induces an anomalous QCD contribution. The corresponding singlet state associated with T_{16} is similar to the η'_{QCD} of QCD, and since $\Lambda_D \gg \Lambda_{\mathrm{QCD}}$ will obtain a mass of order Λ_D. The second current, j_{15} is not broken by the $\mathrm{SU}(N)_D$ instantons, but is also broken by the QCD instantons. With respect to $\mathrm{SU}(N)_D$, the corresponding singlet state is similar to the η_{QCD} in QCD,

and would be massless. However, the QCD instantons will generate a mass and thus allow this composite pseudoscalar state to be identified with the invisible axion [72, 71].

It is convenient to work in a different basis of axial vector currents that separates ψ'_c and ψ' by defining

$$j'^{\mu}_{cA} = \sqrt{\frac{3}{2}}\left(\sqrt{3}j^{\mu}_{16} + j^{\mu}_{15}\right) = \bar{\psi}'^{\dagger}_c \bar{\sigma}^{\mu}\bar{\psi}'_c + \psi'^{\dagger}_c \bar{\sigma}^{\mu}\psi'_c \equiv F_D\, \partial^{\mu}\eta'_c\,, \tag{5.48}$$

$$j'^{\mu}_{A} = \frac{1}{\sqrt{2}}\left(j^{\mu}_{16} - \sqrt{3}j^{\mu}_{15}\right) = \bar{\psi}'^{\dagger} \bar{\sigma}^{\mu}\bar{\psi}' + \psi'^{\dagger} \bar{\sigma}^{\mu}\psi' \equiv F_D\, \partial^{\mu}\eta'_D\,, \tag{5.49}$$

where F_D is the axion decay constant. If ψ'_c and ψ' were the only massless $\mathrm{SU}(N)_D$ fermions above the axicolor confinement scale that render all θ angles in the theory unobservable, then below the confinement scale appropriate linear combinations of η'_c and η'_D can be identified with axions which keep the θ angles unobservable.

However in the enlarged color model, unlike [72, 71], the massless bifundamental fermions, $\psi'_c, \bar{\psi}'_c$ originate from the ξ fermion, which also contains other massless fermions. The anomalous current must therefore include the rotations of these extra fermions, besides the $\mathrm{U}(1)_A$ chiral rotation of $\psi'_c, \bar{\psi}'_c$ and $\psi', \bar{\psi}'$. The correct anomalous current which couples to the axion and generalizes Eq. (5.48), can be obtained by matching the anomaly above and below the enlarged color breaking scale, Λ_{HC}. Above Λ_{HC}, there is an anomalous $\mathrm{U}(1)_\xi$ symmetry, broken by $\mathrm{SU}(N+3)$ instantons

$$\partial^{\mu}\left(\xi^{\dagger}\bar{\sigma}_{\mu}\xi\right) = -\frac{1}{16\pi^2}T(\xi)\, F_{N+3}\widetilde{F}_{N+3} = -\frac{1}{16\pi^2}(N+3)F_{N+3}\widetilde{F}_{N+3}\,, \tag{5.50}$$

where $T(\xi) = N+3$ for the adjoint representation of the Weyl fermion ξ. Below Λ_{HC}, where the enlarged color is broken, ξ decomposes to $\lambda_D, \lambda_c, \psi'_c$ and $\bar{\psi}'_c$ as in (5.45). These states inherit the same charges under $\mathrm{U}(1)_\xi$, which leads to the anomalous current

$$j^{\mu}_{\xi} = \lambda^{\dagger}_D \bar{\sigma}^{\mu}\lambda_D + \lambda^{\dagger}_c \bar{\sigma}^{\mu}\lambda_c + \bar{\psi}'^{\dagger}_c \bar{\sigma}^{\mu}\bar{\psi}'_c + \psi'^{\dagger}_c \bar{\sigma}^{\mu}\psi'_c \equiv F_D\, \partial^{\mu}\eta'_c\,. \tag{5.51}$$

It is straightforward to check that the divergence of this current matches with the total

divergence above the $\Lambda_{\rm HC}$ scale in Eq. (5.50), namely

$$\partial_\mu j^\mu_\xi = -\frac{1}{16\pi^2}(N+3)F_D\widetilde{F}_D - \frac{1}{16\pi^2}(N+3)F_c\widetilde{F}_c\,. \tag{5.52}$$

Note that this matching condition must be satisfied regardless of the enlarged color representation of ξ. For example, when ξ is in the pseudoreal representation, j^μ_ξ must include the transformations of not only $\psi'_c, \bar{\psi}'_c$, but also $\psi_D, \bar{\psi}_D$, as given in Eq. (5.44). The **20** dimensional representation of SU(6) is special, since $\psi_D, \bar{\psi}_D$ are singlets. Again the representation of ξ does not matter, because regardless of how ξ decomposes under the broken enlarged color group, these new states still contribute to j^μ_ξ in order to match the anomaly. Nonetheless, the ξ adjoint fermion requires some caution, since ξ decomposes to adjoint fermions λ_c, λ_D, under $\mathrm{SU}(3)_c \times \mathrm{SU}(N)_D$. These adjoints may in turn form condensates, similar to the gluino condensate in the $N = 1$ super Yang-Mills theory. In this case, these condensates are θ dependent [158], and thus the θ parameter is also unphysical. In our model, we will show that λ_c will receive a dynamical mass above the TeV scale, and thus a λ_c condensate will not be formed. In such cases it has been shown that there is an anomaly-free divergence with a massless Nambu-Goldstone boson [159, 160, 161].

Next, we include the other anomalous current (5.49) arising from the massless $\mathrm{SU}(N)'$ fermions with corresponding divergence

$$\partial_\mu j'^\mu_A = -\frac{1}{16\pi^2}F^a_D\widetilde{F}^a_D\,. \tag{5.53}$$

From Eq. (5.52) and (5.53), it is now possible to form an $\mathrm{SU}(N)_D$ anomaly free current

$$\partial_\mu\left(j^\mu_\xi - (N+3)j'^\mu_A\right) = -\frac{1}{16\pi^2}(N+3)F_c\widetilde{F}_c\,, \tag{5.54}$$

which generalizes the j^μ_{15} current corresponding to the case where $\psi'_c, \bar{\psi}'_c$ are not embedded into the ξ fermion. The current given in (5.54) is only broken by QCD instantons, and shows that there still is a pseudo Nambu-Goldstone boson in the spectrum, which can be identified with the composite invisible axion.

The effective Lagrangian terms are of the form $\eta'_c \partial_\mu j^\mu_\xi$ and $\eta'_D \partial_\mu j'^\mu_A$, which gives

$$\mathcal{L}_{\text{eff}} = -\frac{1}{32\pi^2}\left(2(N+3)\frac{\eta'_c}{F_D} + 2\frac{\eta'_D}{F_D} - \bar{\theta}_D\right) F^a_D \widetilde{F}^a_D - \frac{1}{32\pi^2}\left(2(N+3)\frac{\eta'_c}{F_D} - \bar{\theta}_c\right) F^c_3 \widetilde{F}^c_3 \,, \tag{5.55}$$

where we have used the relations (5.36), and (5.37) for the effective θ terms with Yukawa phases. To the extent that N is large, the effective potential for these pseudoscalars can be written as [69]

$$\mathcal{L}_{\text{eff}} = \frac{1}{2}\Lambda^4_D \left(2(N+3)\frac{\eta'_c}{F_D} + 2\frac{\eta'_D}{F_D} - \bar{\theta}_D\right)^2 + \frac{1}{2}\Lambda^4_c \left(2(N+3)\frac{\eta'_c}{F_D} - \bar{\theta}_c\right)^2 . \tag{5.56}$$

Since all the constituent fermions are massless, the axion mass squared in (5.56) is determined by the topological susceptibility from the pure Yang-Mills gauge theory [65]. Note that if $\eta'_D = 0$, the η'_c axion cannot solve the strong CP problem because its minimum would be dominated by the first term in (5.56). This is why the second axion, η'_D (with corresponding fermions $\psi', \bar{\psi}'$) is needed [72, 71, 144]. It may appear that including the η'_{QCD} contribution at the QCD confinement scale in (5.56), could play the role of η'_c. However, the shift of η'_{QCD} to the new minimum causes $\bar{\theta}_c$ to appear in the quark masses as a phase and thus the strong CP problem would not be solved[5].

Expanding (5.56) around the CP-conserving minimum (i.e. $\eta'_{c,D} \to \langle \eta'_{c,D} \rangle + \eta'_{c,D}$), leads to the Lagrangian for the physical fluctuations

$$\mathcal{L}_{\text{eff}} \supset \frac{1}{2}\Lambda^4_D \left(2(N+3)\frac{\eta'_c}{F_D} + 2\frac{\eta'_D}{F_D}\right)^2 + \frac{1}{2}\Lambda^4_c \left(2(N+3)\frac{\eta'_c}{F_D} + 2\frac{\eta'_{\text{QCD}}}{F_\pi}\right)^2 . \tag{5.57}$$

After diagonalizing the corresponding mass matrix one obtains a massless axion, together with a heavy, dark axion with mass of order Λ_D. The massless eigenstate is identified with the usual QCD axion after including corrections from the Standard Model quark masses. These will arise by adding the contribution from η'_{QCD} to $F^c_3 \widetilde{F}^c_3$ in Eq. (5.55), which leads to

[5] Of course, this would be a solution to the strong CP problem if, for instance, the up quark were massless.

the mixing term between $\eta'_{\rm QCD}$ and η'_c in Eq. (5.57). A nonzero axion mass is then obtained from the quark mass contribution to the $\eta'_{\rm QCD}$ mass squared. While this correction to the $\eta'_{\rm QCD}$ mass is negligible, the axion mass is now proportional to the quark mass, and as expected vanishes in the chiral limit. This reproduces the composite axion model of Ref. [72, 71] with axicolor identified with the $\mathrm{SU}(N)_D$ gauge group. However, since the QCD gauge group and $\mathrm{SU}(N)_D$ are combined into a larger group structure, there are additional contributions which can increase the QCD axion mass and these will be considered next.

5.2.3 Effect of Small Instantons

It has long been known that if QCD is modified at high energies to become strong then small (UV) instantons can give rise to sizeable contributions to the axion mass [136, 137, 138]. In our particular setup, where QCD is embedded into the enlarged color group $\mathrm{SU}(N+3) \times \mathrm{SU}(N)'$, it is possible for the $\mathrm{SU}(N)'$ instantons at a sufficiently large breaking scale ($\Lambda_{\rm HC}$) to induce a large axion mass [144]. There are also $\mathrm{SU}(N+3)$ instantons, but the small $\mathrm{SU}(N)'$ instantons can dominate provided that $\alpha'(\Lambda_{\rm HC}) \gg \alpha_{N+3}(\Lambda_{\rm HC})$.

Under this assumption the contribution from the small $\mathrm{SU}(N)'$ instantons induces a scale Λ_I determined by an integral over the instanton size ρ. Since the $\mathrm{SU}(N)'$ gauge symmetry is spontaneously broken at the scale $\Lambda_{\rm HC}$ only instantons of size $\rho \leq 1/\Lambda_{\rm HC}$ are important [62]. The leading order contribution, which follows the minimal recipe [162], ignoring higher order terms suppressed by group theoretical factors, is given by[6]

$$\Lambda_I^4 \approx \int_{1/M_{\rm P}}^{1/\Lambda_{\rm HC}} \frac{\mathrm{d}\rho}{\rho^5} D[\,\alpha'(1/\rho)\,] \left(-\frac{4\pi^2}{N}\rho^3 \langle \psi'\bar{\psi}'\rangle\right) \prod_{i=1}^{n_\chi} \left(-\frac{4\pi^2}{N}\rho^3 \langle \chi'_i\bar{\chi}'_i\rangle\right) \frac{1}{(4\pi)^6} \prod_{k=1}^{3} y'^k_u y'^k_d \,, \tag{5.58}$$

where $\alpha'(1/\rho)$ is the $\mathrm{SU}(N)'$ coupling evaluated at the scale $1/\rho$, y'^k_u, y'^k_d are the Yukawa couplings of the primed sector and the Planck scale, $M_{\rm P}$ represents the UV cutoff of the

[6] Hypercolor is treated as a flavor of $\mathrm{SU}(N)'$, or to be more exact, a subgroup of the global flavor group $\mathrm{SU}(n_\chi+1)_{\chi',\psi'} \times \mathrm{SU}(n_\chi+1)_{\bar{\chi}'^\dagger,\bar{\psi}'^\dagger}$. Since the instanton only breaks the anomalous $\mathrm{U}(1)_A$ symmetry, the effective fermion interaction must be invariant under the global flavor group, and thus is hypercolor invariant. In (5.58), this is clear as the fermion condensate product arises from the $(n_\chi+1)\times(n_\chi+1)$ determinant [62].

model, and n_χ is the number of $\chi'_i, \bar{\chi}'_i$ fermions. Note that the SU$(N)'$ fermions $\psi', \bar{\psi}', \chi'_i, \bar{\chi}'_i$ contribute to (5.58) via their respective SU$(N)_D$ and hypercolor condensates, $\langle\psi'\bar{\psi}'\rangle$ and $\langle\chi'_i\bar{\chi}'_i\rangle$, where for $\chi'_i\bar{\chi}'_i$, we have neglected the contribution from $m_{\chi'} \ll \Lambda_{\rm HC}$ [7]. This new contribution from the hypercolor condensate $\langle\chi'_i\bar{\chi}'_i\rangle \sim -\Lambda^3_{\rm HC}$, is much larger than the SU$(N)_D$ condensate $\langle\psi'\bar{\psi}'\rangle \sim -\Lambda^3_D$, which was previously considered in Ref. [144]. If $y'_{u,d}$ become sufficiently small, other diagrams involving (5.30) and (5.32) can also contribute to (5.58) [144]. However, we will assume that (5.58) is the dominant contribution.

The instanton density $D[\alpha']$ is defined to be

$$D[\alpha'(1/\rho)] = e^{-\frac{2\pi}{\alpha'(1/\rho)}} \left(\frac{2\pi}{\alpha'(1/\rho)}\right)^{2N} c_I(N, N_f)\,, \tag{5.59}$$

where

$$c_I(N, N_f) = \frac{2^{2(1-N)}}{\pi^2} \frac{e^{-c(1)+2c(\frac{1}{2})(2-N+N_f)}}{(N-1)!\,(N-2)!}\,, \tag{5.60}$$

with $c(\frac{1}{2}) = 0.145873$, $c(1) = 0.443307$ (see Ref. [62]) and $N_f = 7 + n_\chi$ is the number of SU$(N)'$ Dirac fermions above the $\Lambda_{\rm HC}$ scale for the hyperfermion representation, R_χ. The running coupling $\alpha'(\mu)$ is given by

$$\frac{2\pi}{\alpha'(\mu)} = \frac{2\pi}{\alpha'(\Lambda_{\rm HC})} + b' \ln \frac{\mu}{\Lambda_{\rm HC}}\,, \tag{5.61}$$

where the one-loop β-function coefficient $b' = (11N - 2N_f)/3$.

While the integral in Eq. (5.58) can be easily numerically evaluated, it is possible to obtain a simple analytic expression. Assuming $\alpha'(\Lambda_{\rm HC}) \ll 2\pi$, the integral in Eq. (5.58) admits the closed form expression:

$$\Lambda_I^4 \simeq \Lambda_D^3 \Lambda_{\rm HC}\, e^{-\frac{2\pi}{\alpha'(\Lambda_{\rm HC})}} \left(\frac{2\pi}{\alpha'(\Lambda_{\rm HC})}\right)^{2N} \left(\frac{4\pi^2}{N}\right)^{n_\chi+1} \times \\ \times \frac{c_I(N, N_f)}{(3n_\chi + b' - 1)} \prod_{k=1}^{3} \frac{y'^k_u}{4\pi} \frac{y'^k_d}{4\pi} (1 + \delta_{1/M_{\rm Pl}})\,, \tag{5.62}$$

[7] Note that $\langle\chi'_i\bar{\chi}'_i\rangle$ represents the trace separated out from R' in Eq. (5.11).

where

$$\delta_{1/M_{\rm Pl}} \propto \frac{Nb'}{\pi}\,\frac{\alpha'(\Lambda_{\rm HC})}{(\ln(M_{\rm P}/\Lambda_{\rm HC}))^{2N}} - \left(\frac{\Lambda_{\rm HC}}{M_{\rm P}}\right)^{3n_\chi+b'-1}\,, \tag{5.63}$$

is the contribution from instantons of size $1/M_{\rm Pl}$. Since $\Lambda_{\rm HC} \ll M_{\rm Pl}$, these contributions are negligible and the integral (5.58) is dominated by instantons of size $1/\Lambda_{\rm HC}$. The approximate expression (5.62) then shows that the instanton contribution can be sizeable provided $\alpha'(\Lambda_{\rm HC})$ is not too small, and the scales Λ_D, $\Lambda_{\rm HC}$ are as large as possible.

The η'_D is a bound state consisting of the $\psi'\bar{\psi}'$ fermions, which are charged under SU$(N)'$ above the $\Lambda_{\rm HC}$ scale. Thus η'_D will receive mass contributions proportional to Λ_I^2 from the $(1/\Lambda_{\rm HC})$ small instantons[8]. Therefore, the full effective axion potential is

$$\begin{aligned}\mathcal{L}_{\rm eff} = \frac{1}{2}\,\Lambda_D^4\left(2\frac{\eta'_D}{F_D} + 2(N+3)\frac{\eta'_c}{F_D} - \bar{\theta}_D\right)^2 + \frac{1}{2}\Lambda_c^4\left(2(N+3)\frac{\eta'_c}{F_D} - \bar{\theta}_c\right)^2 + \\ + \frac{1}{2}\,\Lambda_I^4\left(2\frac{\eta'_D}{F_D} - \bar{\theta}'\right)^2\,,\end{aligned} \tag{5.64}$$

where the $\bar{\theta}'$ contribution in the last term of (5.64) arises from including $e^{i\bar{\theta}'}$ in the instanton density (5.59). The shift from θ' to $\bar{\theta}'$ takes into account the rotation of SU$(N)'$ fermions that have explicit masses, $\bar{q}', u'$ and d', which must be rotated to eliminate the phases in their respective Yukawa coupling matrices $Y^{\rm SM}$ and Y^D. To relate $\bar{\theta}'$ to $\bar{\theta}_D$ and $\bar{\theta}_c$, let us assume that the massless $\psi', \bar{\psi}'$ are not present in the theory. In this case, $\bar{\theta}'$ is the only physical θ angle in the UV. Below $\Lambda_{\rm HC}$, the physical θ angle (when there are no $\psi', \bar{\psi}'$ fermions) is $\bar{\theta}_D - \bar{\theta}_c$, due to the existence of the anomalous current $\partial_\mu j'^{\mu}_{cA}$, which shifts θ_D and θ_c equally, as shown in Eq. (5.52) (a special case with only bifundamental fermions is given in [163]). Thus, one must have

$$\bar{\theta}' = \bar{\theta}_D - \bar{\theta}_c = \theta' - \arg\det Y^D + \arg\det Y^{\rm SM}\,. \tag{5.65}$$

[8] If the hyperfermions $\chi', \bar{\chi}'$ are massless, then the σ' also receives a mass contribution from Λ_I. In this case η'_D in (5.64) is replaced by a linear combination of η'_D and σ', and the orthogonal combination is massless. In our model, since $m_\chi \Lambda_{\rm HC}$ is heavier than Λ_D^2 and Λ_I^2, the dynamical axion masses are instead determined by Λ_D and Λ_I.

Note that Eq. (5.65) can be checked explicitly at leading order in $v/F_{\rm HC}$. This is done by collecting the phases in $\bar{q}', u'$ and d' used to rotate the $Y^{\rm SM}$ and Y^D phases away in Eq. (5.36), (5.37).

With massless fermions $\psi', \bar{\psi}'$, the phase $\bar{\theta}'$ becomes unphysical in the UV. Below $\Lambda_{\rm HC}$, this is matched by the shift symmetry of η'_D in Eq. (5.64) that relaxes $\bar{\theta}'$ to zero. This is evident from the axion VEVs that minimize the potential in (5.64)

$$\langle \eta'_c \rangle = \frac{1}{2(N+3)} \bar{\theta}_c F_D \,, \tag{5.66}$$

$$\langle \eta'_D \rangle = \frac{1}{2} \left(\bar{\theta}_D - \bar{\theta}_c \right) F_D = \frac{1}{2} \bar{\theta}' F_D \,, \tag{5.67}$$

which exactly cancels the θ terms in Eq. (5.55). In other words, introducing the SU$(N)'$ small instanton contribution does not disturb the original strong CP solution, while simultaneously providing a new mass contribution to the composite axions. The physical masses of the fluctuations around these minima are then determined by diagonalizing the mass matrix that is obtained from

$$\mathcal{L}_{\rm eff} \supset \frac{1}{2}\Lambda_D^4 \left(2(N+3)\frac{\eta'_c}{F_D} + 2\frac{\eta'_D}{F_D} \right)^2 + \frac{1}{2}\Lambda_c^4 \left(2(N+3)\frac{\eta'_c}{F_D} + 2\frac{\eta'_{\rm QCD}}{F_\pi} \right)^2 + \\ + \frac{1}{2}\Lambda_I^4 \left(2\frac{\eta'_D}{F_D} \right)^2 , \tag{5.68}$$

which arises by including the small instanton contributions to Eq. (5.57). Thus, depending on Λ_D and $\Lambda_{\rm HC}$, the axion and the dark axion could be at the TeV scale. To determine the range of axion masses, we next consider the possible values of the strong coupling scales, Λ_D and $\Lambda_{\rm HC}$.

5.2.4 Axion Mass Scales

The axion mass scales are determined from the hypercolor strong scale, $\Lambda_{\rm HC}$. Given the fixed particle content of the model, we can calculate the scale of the condensates $\langle \psi\psi \rangle$ and $\langle \chi\bar{\chi}' \rangle$, which correspondingly triggers the SU(5) global symmetry breaking and the enlarged color

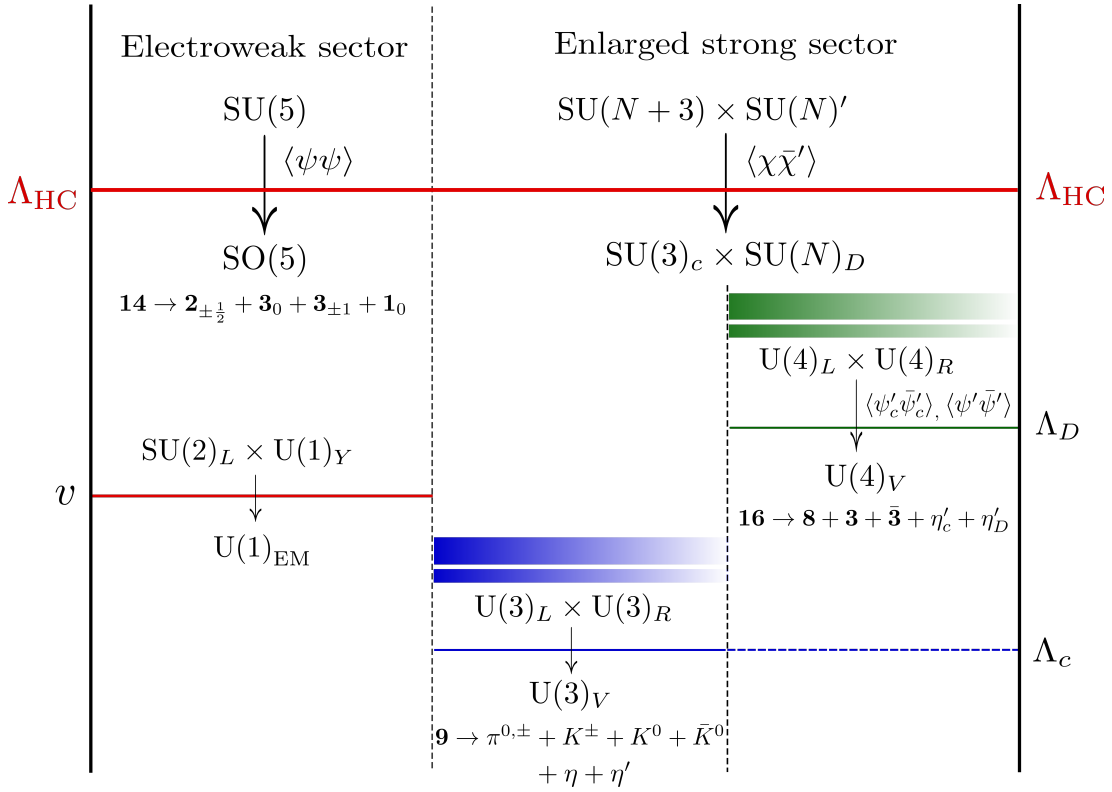

Figure 5.3: A schematic diagram showing all the relevant mass scales in the model. Both the electroweak and the enlarged strong sector contain fermions charged under the hypercolor group $\mathrm{Sp}(2N_{\mathrm{HC}})$. The green bands around Λ_D indicate bound states of the diagonal color group $\mathrm{SU}(N)_D$, while the blue bands around Λ_c represent the QCD bound states. The axions $\eta'_{c,D}$ arise from the strong dynamics at Λ_D.

symmetry breaking, respectively. The massless bound states associated with this global symmetry breaking pattern eventually determine the Higgs and axion mass scales. For example, as has been extensively studied, the Higgs is a pseudo-Nambu-Goldstone boson which eventually develops a VEV and breaks electroweak symmetry. The Standard Model fermion masses then arise from partial compositeness [145].

Instead for the colored sector, once the condensate $\langle \chi \bar{\chi}' \rangle$ breaks $\mathrm{SU}(N+3) \times \mathrm{SU}(N)' \to \mathrm{SU}(3)_c \times \mathrm{SU}(N)_D$, the massless particle content dictates the running of the $\mathrm{SU}(3)_{c,D}$ gauge couplings. This in turn determines the diagonal color confinement scale, Λ_D and the corresponding axion bound state mass scale (around $F_D \approx \Lambda_D/(4\pi)$). The instanton contribution, Λ_I to the effective potential is then determined from Λ_D, Λ_{HC} and the massless particle content using Eq. (5.58). The physical axion masses can then be obtained by diagonalizing the mass matrix obtained from Eq. (5.68).

For a given scale Λ_D, how is Λ_{HC} constrained? Assuming $\langle \chi \bar{\chi}' \rangle \approx -\Lambda_{\mathrm{HC}}^3$, the enlarged color group is broken at the hypercolor confinement scale Λ_{HC} and the gauge couplings satisfy (5.26). Below Λ_{HC}, the QCD coupling runs differently above and below Λ_D due to the different fermion content. The one loop expressions are given by

$$\frac{2\pi}{\alpha_c(\mu)} = \begin{cases} \frac{2\pi}{\alpha_c(m_t)} + b_{c1} \ln \frac{\mu}{m_t} \,, & m_t \le \mu \le \Lambda_D \,, \\ \frac{2\pi}{\alpha_c(\Lambda_{\mathrm{HC}})} + b_{c2} \ln \frac{\mu}{\Lambda_{\mathrm{HC}}} \,, & \Lambda_D \le \mu \le \Lambda_{\mathrm{HC}} \,, \end{cases} \tag{5.69}$$

where b_{c1}, b_{c2} are one loop β-function coefficients, $m_t \simeq 173$ GeV and $\alpha_c(m_t) \simeq 0.1$. The diagonal color confinement scale is approximately given by:

$$\Lambda_D \approx \Lambda_{\mathrm{HC}}\, e^{-\frac{2\pi}{b_D \alpha_D(\Lambda_{\mathrm{HC}})}} \,, \tag{5.70}$$

where b_D is the one-loop β-function coefficient.

Next we determine the β-function coefficients b_{c1}, b_{c2} and b_D. We assume that ξ transforms as an adjoint and use the fermion content listed in Table Table 5.3. Below Λ_D, only the Standard Model quarks contribute to the running and for six quark flavors this gives the usual Standard Model value $b_{c1} = 7$. However above Λ_D, there are an additional N Dirac

states, $(\psi'_c, \bar{\psi}'^{\dagger}_c)$, which transform as a fundamental under QCD, and one adjoint Majorana fermion, λ_c, which gives $b_{c2} = 5 - \frac{2}{3}N$. Similarly, the $\mathrm{SU}(N)_D$ β-function coefficient is determined from the four Dirac states, $(\psi'_c, \bar{\psi}'^{\dagger}_c)$ and $(\psi', \bar{\psi}'^{\dagger})$ transforming as a fundamental, and one adjoint Majorana fermion, λ_D, to give $b_D = 3N - \frac{8}{3}$. These β-function coefficients change if ξ transforms in a pseudoreal representation, and can be easily obtained by using the fermion content in Eq. (5.44).

Using these β-function coefficient values in ((5.69)) and ((5.70)), together with ((5.26)), leads to the relation

$$\ln \frac{\Lambda_{\mathrm{HC}}}{\Lambda_D} = \frac{1}{11N - 23}\left[6\pi\left(\frac{1}{\alpha_c(m_t)} + \frac{1}{\alpha'(\Lambda_{\mathrm{HC}})}\right) + 21 \ln \frac{\Lambda_D}{m_t}\right] . \tag{5.71}$$

Thus by specifying the diagonal color scale, Λ_D, the hypercolor confinement scale, Λ_{HC} can be determined from (5.71). Notice that as N increases, Λ_{HC} can be lower for a given value of Λ_D. Interestingly, the one loop expression (5.71) shows that in the limit $N \to \infty$, one obtains $\Lambda_{\mathrm{HC}} \to \Lambda_D$. This suggests the possibility of a natural composite Higgs together with a heavy composite axion, with the tradeoff being larger group structure. The gauge couplings and strong scales are shown in Fig. Figure 5.4 for two representative choices of the parameters.

In summary, the factors that control the axion masses are N, $\alpha'(\Lambda_{\mathrm{HC}})$, the choice of hypercolor gauge group, and the Yukawa couplings, y'. As shown in (5.71), N and $\alpha'(\Lambda_{\mathrm{HC}})$ directly control the ratio $\Lambda_{\mathrm{HC}}/\Lambda_D$. For example, when $N = 3$, Λ_{HC} may be as high as the Planck scale ($M_P = 1.22 \times 10^{19}$ GeV), and for $\alpha'(\Lambda_{\mathrm{HC}}) = 0.3\,(0.7)$, we obtain $\Lambda_D = 14.2\,(45.2)$ TeV. The choice of the hypercolor gauge group determines the number n_χ of χ' hyperfermions, which then affects the α' running. For $\mathrm{Sp}(2N_{\mathrm{HC}})$ with χ' hyperfermions in the fundamental representation, $n_\chi = 2N_{\mathrm{HC}}$. A larger fermion representation reduces the one-loop β-function coefficient, causing α' to run slower. As a result the $\mathrm{SU}(N)'$ instantons stay relevant for a larger range of energy, which in turn increases Λ_I. Nonetheless, this integral over small size instantons is highly suppressed. It turns out that for most of the allowed parameter space, $\Lambda_I \leq \Lambda_D$, with the exception of $N = 3$. However, for $N = 3$

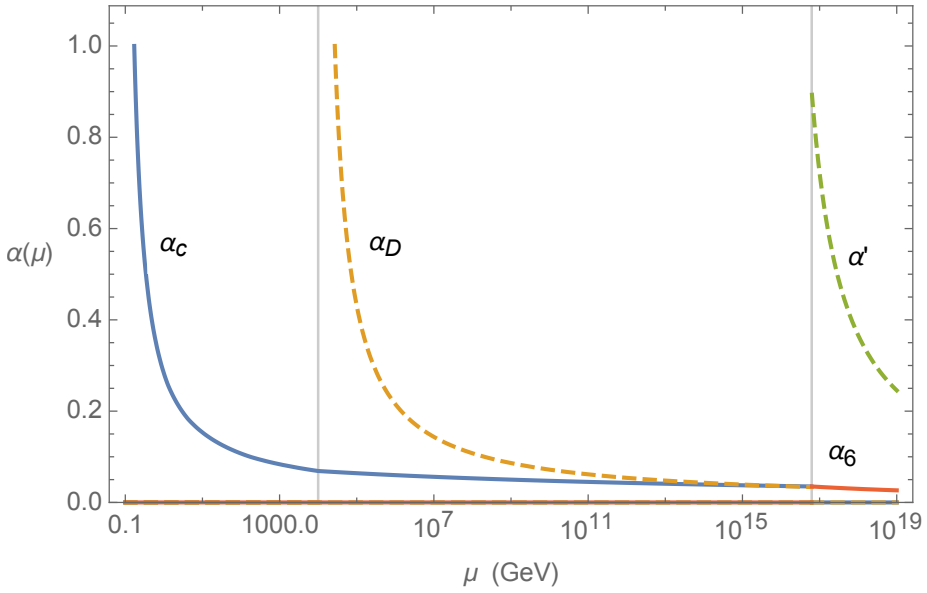

(a)

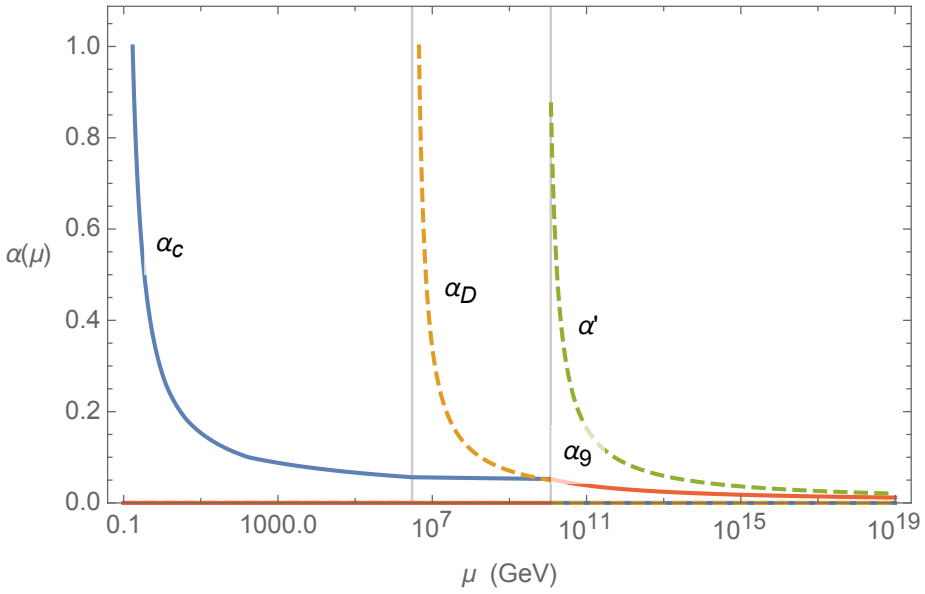

(b)

Figure 5.4: The gauge couplings of the various gauge groups as a function of the renormalization scale. In (a) we assume a hypercolor group $\mathrm{Sp}(4)_{\mathrm{HC}}$, $N = 3$, $\Lambda_{\mathrm{HC}} \simeq 6.3 \times 10^{16}$ GeV and $\alpha'(\Lambda_{\mathrm{HC}}) = 0.9$, giving rise to $\Lambda_D = 10$ TeV using ((5.71)), while in (b) we have the hypercolor group $\mathrm{SU}(4)_{\mathrm{HC}}$, $N = 6$, $\Lambda_{\mathrm{HC}} \simeq 1.2 \times 10^{10}$ GeV and $\alpha'(\Lambda_{\mathrm{HC}}) = 0.9$, giving rise to $\Lambda_D = 3000$ TeV using ((5.71)).

(with either real or pseudoreal representations), the $\mathrm{SU}(N)_D$ scale is restricted to values $\Lambda_D \lesssim 50$ TeV for $\Lambda_{\rm HC} \lesssim M_{\rm Pl}$.

The axion masses are plotted in Figure Figure 5.5 for a range of N and $\alpha'(\Lambda_{\rm HC})$ values. The lighter axion mass depends sensitively on Λ_I. The physical masses are well approximated in the limit $\Lambda_I \lesssim \Lambda_D$ by

$$m_{a_D} \approx 2(N+3)\,\frac{\Lambda_D^2}{F_D}\,, \qquad\qquad m_a \approx 2\frac{\Lambda_I^2}{F_D}\,, \tag{5.72}$$

where we have ignored the $\eta'_{\rm QCD}$ of QCD, assuming $\Lambda_I \gg \Lambda_{\rm QCD}$. The physical axion mass eigenstates are approximately

$$\begin{aligned} a &= \frac{-(N+3)\eta'_D + \eta'_c}{\sqrt{(N+3)^2+1}} \approx -\eta'_D + \frac{1}{\sqrt{(N+3)}}\eta'_c\,, \\ a_D &= \frac{\eta'_D + (N+3)\eta'_c}{\sqrt{(N+3)^2+1}} \approx \eta'_c + \frac{1}{\sqrt{(N+3)}}\eta'_D\,, \end{aligned} \tag{5.73}$$

where a can be identified with the usual QCD axion, while a_D is the $\mathrm{SU}(N)_D$ axion. Note that a aligns mostly with the $\mathrm{SU}(N)_D$ anomaly free current defined in Eq. (5.54).

We consider two limiting cases for the hypercolor confinement scale, where $\Lambda_{\rm HC}$ is as low as 10^{10} GeV, or as high as 10^{16} GeV. For the first case, assuming $\Lambda_D = 3000$ TeV, $N = 6$, $\alpha'(\Lambda_{\rm HC}) = 0.9$, $y'^i_{u,d} = 0.025$ and hypercolor group $\mathrm{SU}(4)_{\rm HC}$, one obtains $\Lambda_{\rm HC} \approx 1.2 \times 10^{10}$ GeV. This $\Lambda_{\rm HC}$ scale would be relevant for generating a composite Higgs with a vanishing quartic coupling. In this case, the field ξ can only be in the adjoint representation. The axion mass spectrum is

$$m_{a_D} \approx 6.8 \times 10^8 \text{ GeV}\ , \quad m_a \approx 2.6 \text{ TeV}\ . \tag{5.74}$$

The dark axion mass is above the Λ_D scale, while the axion mass is near the TeV scale, which could potentially be probed at the LHC. Note however that the axion mass depends on the value of the Yukawa couplings, $y'^i_{u,d}$. Smaller values of $y'^i_{u,d}$ will suppress Λ_I, leading to a lighter axion. This dependence on $y'^i_{u,d}$ also allows for TeV scale axions with other values

of N and $\Lambda_{\rm HC}$.

In the second case, we consider $\Lambda_D = 10$ TeV, $N = 3$, $\alpha'(\Lambda_{\rm HC}) = 0.9$, $y'^i_{u,d} = 0.003$ and hypercolor group $\mathrm{Sp}(4)_{\rm HC}$. For $N = 3$, the field ξ can be in either the real or pseudoreal representation. However for ξ in the real representation, we assume a dynamically generated mass for λ_c, near the Λ_D scale. This will be further discussed in Section 5.3. In either case, one obtains $\Lambda_{\rm HC} \approx 6.3 \times 10^{16}$ GeV with an axion mass spectrum

$$m_{a_D} \approx 1.5 \times 10^6 \text{ GeV} \ , \quad m_a \approx 3.1 \text{ TeV} \ . \tag{5.75}$$

In this case, the axion mass is still at the TeV scale, while the dark axion mass is now much below $\Lambda_{\rm HC}$, but still at a higher mass scale.

5.2.5 Asymptotic Freedom Condition

In order for the strong dynamics to confine, the hypercolor gauge coupling should be asymptotically free. This leads to a nontrivial condition on the hyperfermion content ψ and $\Psi_\chi = (\chi, \chi', \bar{\chi}, \bar{\chi}')$. This can be simply checked by considering the one loop β-function coefficient of the hypercolor gauge group

$$b_{\rm HC} = \frac{11}{3} C_2(\mathbf{Ad}) - \frac{2}{3}\, n_\psi\, T(R_\psi) - \frac{2}{3}\, n_{\Psi_\chi} T(R_\chi)\,, \tag{5.76}$$

where $C_2(\mathbf{Ad})$ is the quadratic Casimir invariant, $T(R_{\psi,\chi})$ is the index of the representations $R_{\psi,\chi}$, and n_{ψ,Ψ_χ} is the number of ψ, Ψ_χ Weyl hyperfermions.

Consider first the symplectic gauge group $\mathrm{Sp}(2N_{\rm HC})$ where $T(\mathbf{F}) = \frac{1}{2}$, $T(\mathbf{Ad}) = C_2(\mathbf{Ad}) = N_{HC} + 1$ and $T(\mathbf{A_2}) = N_{HC} - 1$. In principle there are two choices for the pair of representations (R_ψ, R_χ). The first case, $(\mathbf{A_2}, \mathbf{F})$, based on the SU(5)/SO(5) coset is given in Table Table 5.1, where $\mathbf{A_2}$ could also be replaced with the adjoint representation $\mathbf{Ad}$. The second possibility for (R_ψ, R_χ) is $(\mathbf{F}, \mathbf{A_2})$, which is based on the SU(4)/Sp(4) coset for the

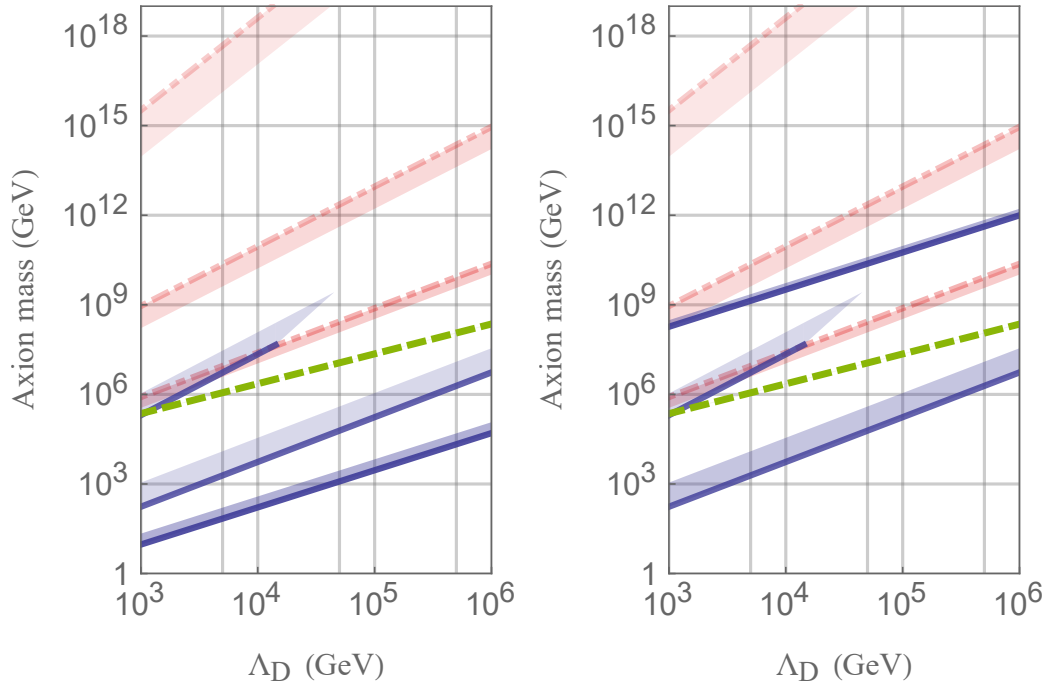

Figure 5.5: The physical axion mass m_a as a function of Λ_D, assuming $y'^i_{u,d} = 0.1$, $\alpha'(\Lambda_{\rm HC}) = 0.7$, and $N = 3, 4$ and 6 (from top to bottom in the left figure, and middle, bottom, and then top in the right figure). The bands indicate the axion mass with $\alpha'(\Lambda_{\rm HC})$ varying from 0.3 to 0.7. The physical dark axion mass m_{a_D} (dashed) assuming $\alpha'(\Lambda_{\rm HC}) = 0.7$ for $N = 6$ is also included, which is fairly insensitive to $\alpha'(\Lambda_{\rm HC})$ and N. For reference, the dot-dashed lines represents the $\Lambda_{\rm HC}$ scale determined from Eq. (5.71), for $N = 3, 4, 6$. Like the axion mass bands, the dot-dashed bands indicate varying $\alpha'(\Lambda_{\rm HC})$. Figure (a) assumes the hypercolor group $\mathrm{SU}(4)_{\rm HC}$, while figure (b) assumes the hypercolor group $\mathrm{Sp}(4)_{\rm HC}$ (for $N = 3, 4$) and $\mathrm{Sp}(20)_{\rm HC}$ (for $N = 6$). Note that for $N = 6$, the lightest axion actually becomes heavier because n_χ is larger.

Higgs sector [146]. Substituting the hyperfermion content into the expression (5.76) gives

$$b_{\rm HC} = \begin{cases} \frac{1}{3}(19 - 8N(N_{\rm HC}-1) - N_{\rm HC}) & (R_\psi, R_\chi) = (\mathbf{F}, \mathbf{A_2})\,, \\ \frac{1}{3}(15 - 4N + N_{\rm HC}) & (R_\psi, R_\chi) = (\mathbf{A_2}, \mathbf{F})\,, \end{cases} \tag{5.77}$$

where $n_\psi = 5$, $n_{\Psi_\chi} = 4N + 6$, $\dim \mathbf{F} = 2N_{\rm HC}$, and $\dim \mathbf{A_2} = (N_{\rm HC}-1)(2N_{\rm HC}+1)$.

It is also necessary to check the asymptotic freedom of the $\mathrm{SU}(N)'$ and $\mathrm{SU}(N+3)$ gauge groups, though this will be less stringent than the requirement for $b_{\rm HC}$. For $\mathrm{SU}(N)'$, this requires that the one-loop β-function coefficient b' to be positive. Using the fermion content in Table 5.1 and Table 5.3, the b' values are

$$b' = \frac{11}{3}N - \frac{14}{3} - \frac{2}{3}\,n_{\chi'}\,, \tag{5.78}$$

where $n_{\chi'} = \dim R_{\chi'}$ is the number of $\chi', \bar{\chi}'$ pairs. Similarly, the one loop β-function coefficient, b_{N+3} for $\mathrm{SU}(N+3)$ above the $\Lambda_{\rm HC}$ scale is

$$b_{N+3} = 3N + 5 - \frac{2}{3}\,n_\chi\,, \tag{5.79}$$

where $n_\chi = \dim R_\chi$ is the number of $\chi, \bar{\chi}$ pairs. Note that (5.79) assumes that ξ transforms in the adjoint representation. When $N = 3, 7, \ldots$, ξ may instead transform under the pseudoreal representations listed in Eq. (5.44). For $N = 3$ one obtains $b_6 = 16 - \frac{2}{3}\,n_\chi$, while for $N = 7$, $b_{10} = \frac{2}{3}(14 - n_\chi)$.

Using the expressions (5.77), (5.78) and (5.79), the results for requiring $b_{\rm HC}, b', b_{N+3} > 0$ are plotted in Figure 5.6 for the $\mathrm{Sp}(2N_{\rm HC})$ hypercolor group. For the case $(R_\psi, R_\chi) = (\mathbf{F}, \mathbf{A_2})$, the requirement for $\mathrm{Sp}(2N_{\rm HC})$ to be asymptotically free is $N_{\rm HC} < \frac{8N+19}{8N+1}$. For $N \geq 3$, there is no solution when $N_{\rm HC} \geq 2$ as can be seen in Figure 5.6a. The $\mathbf{A_2}$ representation for the colored hyperfermions, χ, is just too large for the theory to be asymptotically free. In the case where $(R_\psi, R_\chi) = (\mathbf{A_2}, \mathbf{F})$, the condition for asymptotic freedom is $N_{\rm HC} > 4N - 15$. The allowed region for N and $N_{\rm HC}$ is shown in figure 5.6b. In this case we see that for increasing $N_{\rm HC}$ there are values of N for which the theory is asymptotically free, and corresponds

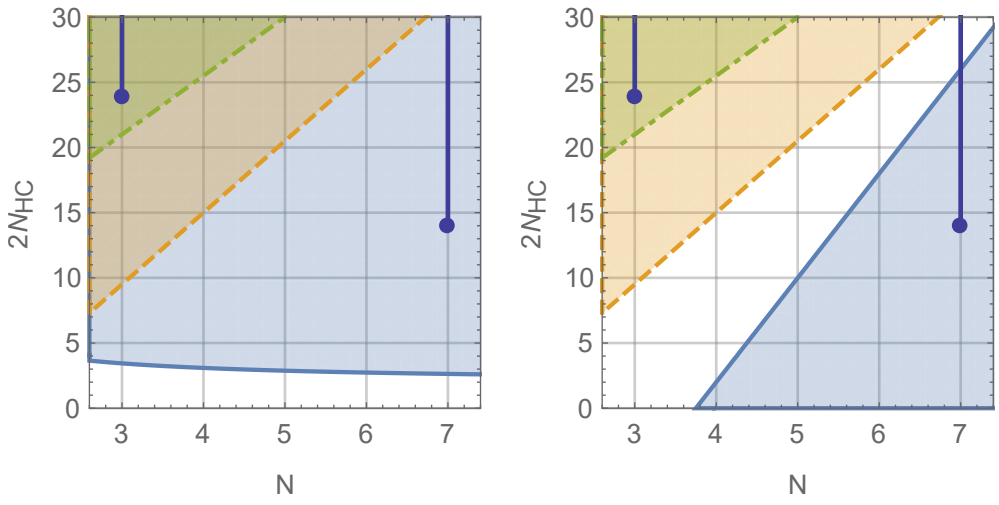

Figure 5.6: The allowed region for N and $N_{\rm HC}$ for (a) $(R_\psi, R_\chi) = (\mathbf{F}, \mathbf{A_2})$, and (b) $(R_\psi, R_\chi) = (\mathbf{A_2}, \mathbf{F})$ when the hypercolor group is $\mathrm{Sp}(2N_{\rm HC})$. The shaded regions (solid boundary) are ruled out by $b_{\rm HC} < 0$, while the orange (dashed boundary) and green (dot-dashed boundary) regions are ruled out by $b' < 0$ and $b_{N+3} < 0$, respectively. For $\mathrm{SU}(N+3)$ with $N = 3$ or 7, the fermion ξ may instead be in the pseudoreal representation, and the allowed limits are indicated by the values of $2N_{\rm HC}$ less than the dark blue dots.

to the case considered in Section 5.1.1. A slight modification of this possibility is to have $(R_\psi, R_\chi) = (\mathbf{Ad}, \mathbf{F})$. However in this case asymptotic freedom requires $N_{\rm HC} > 4N + 5$, and there is no value of $N_{\rm HC}$ that allows for an asymptotically free $\mathrm{SU}(N+3)$ and $\mathrm{SU}(N)'$ group.

When the hypercolor gauge group is $\mathrm{SU}(4)_{\rm HC}$ we have $T(\mathbf{F}) = \frac{1}{2}$, $T(\mathbf{Ad}) = 4$ and $T(\mathbf{6}) = 1$. For $(R_\psi, R_\chi) = (\mathbf{A_2}, \mathbf{F})$ the condition for $\mathrm{SU}(4)_{\rm HC}, \mathrm{SU}(N+3)$ and $\mathrm{SU}(N)'$ to be asymptotically free is $2 < N < 7$. This corresponds to the case studied in Section 5.1.1. Note that $N < 7$ is also consistent with the QCD coupling remaining asymptotically free above the Λ_D scale. Thus we see that if χ transforms in the fundamental representation $\mathbf{F}$, then the hypercolor group remains asymptotically free for a range of N. In particular, this favors the SU(5)/SO(5) composite Higgs models with either $\mathrm{Sp}(2N_{\rm HC})$ or $\mathrm{SU}(4)_{\rm HC}$ hypercolor gauge groups. Other hypercolor groups of composite Higgs models classified in Ref. [147], may also exist for small ψ, χ representations.

Finally, we should point out that the asymptotic freedom condition on $\mathrm{SU}(N+3)$ and $\mathrm{SU}(N)'$ is not strictly necessary since these gauge couplings could grow towards the UV. In this case the small instanton contribution in (5.58) would be UV dominated, and need to be recalculated. Consequently, as seen in figure 5.6b, this would then allow the values $5 \leq N_{\mathrm{HC}} \leq 12$ in the $N = 3$ pseudoreal case, while the axion mass scales for $N_{\mathrm{HC}} \leq 4$ arising from small instantons can be obtained from (5.58) and give similar results to those in Section 5.2.4.

5.3 Phenomenology

5.3.1 Axions and SU$(N)_D$ Bound States

The possible lightest states in the model are the dynamical axions with masses determined by Λ_I, the adjoint fermion λ_c, and the QCD-like bound states in the dark sector associated with the confinement scale Λ_D of the SU$(N)_D$ strong dynamics. The hypercolor confinement scale is just too large to be phenomenologically relevant for current experiments, although it provides motivation for why the Higgs coupling vanishes at $\Lambda_{\rm HC} \sim 10^{10}$ GeV. Nevertheless, as some of the hypercolor Nambu-Goldstone boson masses are dependent on the hyperfermion masses $m_{\chi,\chi'}$, these states could theoretically be anywhere between Λ_D and $\Lambda_{\rm HC}$. Though these states are still likely heavier than the SU$(N)_D$ lightest bound states, some of the hypercolor Nambu-Goldstone bosons may still affect the ratio $\Lambda_D/\Lambda_{\rm HC}$ because they are charged under QCD and SU$(N)_D$.

An example of such a light state is the adjoint fermion λ_c, which only exists in models with ξ in the adjoint representation of SU$(N+3)$. Below $\Lambda_{\rm HC}$, the broken SU$(N+3)$ gauge bosons can give rise to a four-fermion interaction $(\lambda_c\lambda_c)(\psi_c'^\dagger\bar{\psi}_c'^\dagger) + \text{h.c.}$ between the ξ components. At the scale Λ_D, the $\langle\psi_c'\bar{\psi}_c'\rangle$ condensate then spontaneously breaks the U$(1)_\xi$ symmetry, and generates[9] a λ_c mass $\sim \Lambda_D^3/F_{\rm HC}^2$, where the broken gauge boson masses depend on $F_{\rm HC}$ with $F_{\rm HC} \sim \Delta_n \lesssim \Lambda_{\rm HC}$. This λ_c mass estimate favors models with a large $\Lambda_D/\Lambda_{\rm HC}$ ratio, i.e. with higher values of N. Thus provided the ratio $\Lambda_D/\Lambda_{\rm HC}$ is not too small, it is possible to dynamically generate a TeV scale mass for λ_c. For example, a TeV scale λ_c mass can be obtained for the particular $\Lambda_D, \Lambda_{\rm HC}$ values considered in Eq. (5.74), provided $\Delta_n \simeq 0.01\,\Lambda_{\rm HC}$ (see also Figure Figure 5.1). The $\Lambda_D/\Lambda_{\rm HC}$ ratio can be further increased by including light hypercolor bound states which affect the running of the QCD and SU$(N)_D$ couplings[10]. Alternatively, larger contributions to the λ_c mass may arise from

[9] A similar mechanism in the technicolor context for quarks in the fundamental representation was considered in Ref. [164]. The mass may be further enhanced by a factor of $(\Lambda_{\rm HC}/\Lambda_D)^\gamma$, where γ is the anomalous dimension of the $\psi_c'\bar{\psi}_c'$ operator [136].

[10] For example, a bifundamental $(\mathbf{3}, \overline{\mathbf{N}})$ complex scalar, changes $b_{c2} \to b_{c2} - \frac{1}{6}N$ and $b_D \to b_D - \frac{1}{2}$, and for $N \leq 6$ both QCD and SU$(N)_D$ couplings remain asymptotically free for Λ_D scalar masses. Furthermore, we have checked that the gauge couplings can remain perturbative below $\Lambda_{\rm HC}$ for other colored light scalars that may be experimentally accessible. Nonetheless, a sizeable UV value of the QCD coupling can realize

a nonperturbatively generated four-fermion coupling or low-lying hypercolor scalar bound states. In any case, the adjoint λ_c remains a promising signal at the LHC, as it resembles a gluino in supersymmetric models. The λ_c decay signal is model dependent, but it is reasonable to expect decays to three jets, via off-shell colored scalars. A recent LHC analysis in this channel gives a gluino mass lower bound of 1.5 TeV [165]. There is also a singlet fermion component ν' of $\xi(\mathbf{Ad})$ which can similarly obtain a mass from higher-dimension terms. It will behave as a sterile neutrino and could be interesting phenomenologically.

If $\Lambda_I > \Lambda_D$, then both axions are several times heavier than the $\mathrm{SU}(N)_D$ scale, which would be the lowest new scale in the model. As a result, the next most promising signals are those arising from the $\mathrm{SU}(N)_D$ bound states, such as dark pions and glueballs. The novel signals in this case consist of the dark pion octet and triplets in Eq.(5.47), containing the same constituents as the axions. With the current LHC limit on exotic pions at 1345 GeV, this translates into the lower bound $\Lambda_D \geq 7$ TeV [166] which puts the lighter axion mass, in this case m_{a_D}, at $8\pi(N+3)\Lambda_D \approx 1000$ TeV, far above the current LHC range.

The more interesting case is when $\Lambda_I < \Lambda_D$, where one of the axion masses, m_a can be as low as 1 TeV (see Fig. Figure 5.5). This heavy axion can potentially be probed in collider experiments. At a collider, the lighter axion can be produced through the digluon channel. The production rate and the signal decay width are dictated by the effective couplings to the QCD and hypercharge anomalies

$$\mathcal{L}_a = -\frac{\alpha_c}{4\pi}\frac{N+3}{\sqrt{(N+3)^2+1}}\frac{a}{F_D}F^c_{3\mu\nu}\widetilde{F}^{c\mu\nu}_3 - \frac{\alpha_Y}{2\pi}\frac{[Y^2_{\psi'_c}-(N+3)Y^2_{\psi'}]}{\sqrt{(N+3)^2+1}}\frac{a}{F_D}B_{\mu\nu}\widetilde{B}^{\mu\nu}\,, \quad (5.80)$$

where Y_{ψ',ψ'_c} are the hypercharges of ψ' and ψ'_c, respectively and $B^{\mu\nu}$ is the $U(1)_Y$ field strength tensor. The axion production rate is then dependent on the digluon decay rate

$$\Gamma(a \to gg) = \frac{\alpha_c^2}{8\pi^3}\frac{(N+3)^2}{(N+3)^2+1}\frac{m_a^3}{F_D^2}\,, \quad (5.81)$$

which is inversely proportional to F_D. Thus the signal can be abundantly produced provided

the scenario in Ref. [138].

F_D is near the TeV scale. Once produced, the axion can decay through the digluon, diphoton, as well as into Z bosons. The corresponding decay rates are [143]

$$\Gamma(a \to \gamma\gamma) = \frac{\alpha_{\rm EM}^2}{2\pi^3} \frac{[Y_{\psi_c'}^2 - (N+3)Y_{\psi'}^2]^2}{(N+3)^2+1} \frac{m_a^3}{F_D^2}\,, \tag{5.82}$$

$$\Gamma(a \to Z\gamma) = 2\tan^2\theta_W\, \Gamma(a \to \gamma\gamma)\,, \tag{5.83}$$

$$\Gamma(a \to ZZ) = \tan^4\theta_W\, \Gamma(a \to \gamma\gamma)\,, \tag{5.84}$$

where $\alpha_{\rm EM}$ denotes the fine-structure constant and θ_W is the weak-mixing angle. In this model, just like typical hadronic axions, there is no coupling to leptons and the W bosons. However, new decay channels may arise since there is strong mixing between η_c' and η_D', allowing for a to decay into $\mathrm{SU}(N)_D$ lighter states, such as dark pions and dark glueballs, assuming these states are kinematically accessible. Specifically, the phenomenological details are dependent on the mass hierarchy of the axion and the lightest states of the dark sector. This is very similar to the hidden valley scenario in twin Higgs models [167], except that instead of the Higgs boson probing the hidden color sector, that role is now played by the heavy axions. Nonetheless, if the axion mass is close to Λ_D, then these decay widths may be suppressed, and thus the main decay channels are still the digluons and diphotons.

Depending on the free parameters $m_{\chi,\chi'}$, there may still be a light axion in the model such as σ and σ'. For instance, in the limit that $m_{\chi,\chi'}$ vanishes, one can form a combination σ_c that couples to an anomaly-free current under $\mathrm{SU}(N)_D$, and thus receives mass contributions only from QCD instantons. This σ_c would behave like a standard invisible axion with a decay constant of order $\Lambda_{\rm HC}$, which can be probed in standard invisible axion experiments. The σ_c coupling to the gluons is suppressed by $\Lambda_D^2/\Lambda_{\rm HC}^2$, and therefore its most significant coupling is to photons given by

$$\mathcal{L} = -n_\chi Y_\chi^2 \frac{\sigma_c}{F_{\rm HC}} B_{\mu\nu}\widetilde{B}^{\mu\nu}\,, \tag{5.85}$$

where Y_χ is the χ hypercharge. Given that Y_χ is model dependent and not specified, this coupling could be zero leading to a sterile axion-like particle.

5.3.2 Cosmology

The implications and constraints from cosmology are highly dependent on the early history of the universe. It can be shown that there remains a conserved baryon number, and thus the lightest baryon bound state could be stable. If the reheat temperature is above either of the confinement scales then heavy stable particles from the hypercolor or $\mathrm{SU}(N)_D$ sectors may be thermally produced. In the hypercolor case with ψ in the real or pseudoreal representation, it is possible to form a baryon combination $(\psi\psi\psi)$, which could also interact with other baryons, such as the top partner bound state $(\chi\psi\bar{\chi})$. This could cause the bound states to become unstable but a definitive answer would require a detailed study of the hyperbaryon spectrum. Nonetheless, it is reasonable to expect that a coupling between these bound states and the Standard Model can be generated when the electroweak symmetry is broken. Thus decays to Standard Model particles would prevent these states from dominating the mass density of the universe. Similarly for the axibaryons, as pointed out in Ref. [144], the enlarged color force between $\mathrm{SU}(N)_D$ and QCD can mediate axibaryon decays. Another issue, shared by the original composite axion models, is domain walls. To avoid these as well as potential stable, heavy baryons, we assume that any domain wall in the model is formed above the inflation scale. Again the details are model dependent, but it would be interesting to study how inflation models could be incorporated into our framework.

Finally, our model has the advantage of admitting several candidates for dark matter. These candidates consist of a light axion-like particle that does not directly couple to QCD, but has a large decay constant determined by the hypercolor scale. Another candidate is the dark photon of the diagonal color that can arise from a possible gauging of the $\mathrm{U}(1)_D$ global symmetry, and although interesting, the phenomenology of this dark photon will not be explored in this thesis.

5.4 Composite Axion - Summary

The Higgs and axion could both arise from the same underlying strong dynamics. In this chapter we have given a UV description of a model that produces a composite Higgs and dynamical axions based on the $\mathrm{Sp}(2N_{\mathrm{HC}})$ and $\mathrm{SU}(4)_{\mathrm{HC}}$ hypercolor gauge groups. The matter content of the theory consists of colored and uncolored hyperfermions that form condensates at the strong coupling scale Λ_{HC}. Given the dynamics and hyperfermion matter content, all other scales in the model can be determined from the single scale, Λ_{HC}.

For the hypercolor group to be asymptotically free, and therefore confine, requires the colored hyperfermions to be in the fundamental representation of the hypercolor gauge group. A particular choice satisfying this condition is a minimal modification of the SU(5)/SO(5) composite Higgs model, in which extra colored hyperfermions are added to the theory in order to incorporate an enlarged color sector $\mathrm{SU}(N+3) \times \mathrm{SU}(N)'$. The hyperfermion condensates then break the enlarged color group to $\mathrm{SU}(3)_c \times \mathrm{SU}(N)_D$. The enlarged color sector also contains massless fermions which are hypercolor singlets and render the θ angles of the enlarged color group unobservable. When the diagonal color group $\mathrm{SU}(N)_D$ confines at lower energies it produces dynamical axions which preserve the CP symmetry. Together these massless fermions and axions can eliminate all sources of strong CP violation. A more minimal version of the model is also possible, where QCD is not modified in the UV and the hypercolor dynamics produces an invisible axion, in addition to a heavy axion at the hypercolor confinement scale.

The enlarged color group allows for extra axion mass contributions that arise from small instantons associated with the $\mathrm{SU}(N)'$ gauge group. This leads to TeV scale axions for both the real and pseudoreal representations of the massless enlarged-color fermions, that can be detected at collider experiments via their decays into photons and Z bosons. This possibility exists for both high ($\simeq 10^{15}$ GeV) and low ($\simeq 1000$ TeV) values of the hypercolor confinement scale. Other axion decay channels into $\mathrm{SU}(N)_D$ pions or glueballs may be possible. A dynamical axion arising from the hypercolor dynamics has suppressed couplings to gluons, and instead could couple to photons provided the hyperfermions are charged

under $U(1)_Y$. However, besides the TeV scale axions, in the case of a massless fermion in the adjoint representation, there is also a QCD colored octet fermion in the low energy spectrum. This fermion can receive a dynamically generated TeV scale mass, which can then decay into three jets, providing a smoking gun signal of this scenario. In addition there are several dark matter candidates including the hypercolor axion, as well as a possible dark photon.

Chapter 6

Conclusion and Epilog

After the discovery of the Higgs boson, we are at the transition of a new era in Physics. As collider experiments reach their limit at the energy frontier, there has been no sign of BSM physics. As an effective theory, the Standard Model could be extrapolated all the way to the Planck scale. The *Great Desert* between the TeV scale and the Planck scale has, on occasion, been mentioned as the death of physics[1]. This sentiment is akin to the frog's world view in the old gospel. Not being able to jump up the well where he lives, he is blissfully ignorant of the beautiful world out there to discover. But different from the frog in the old tale, we know that there must be new physics around the corner; we just need the right ladder to lead us there[2]. A candidate for such a ladder is the hypothetical axion, the main topic of this thesis. The axion can simultaneously solve two of the most long-standing problems in the Standard Model: the strong CP problem and dark matter. In Chapter 4 and Chapter 5, we presented several models of the axion, ranging from 5D warped extra dimension axions to composite axions with enlarged color.

The warped extra dimension offers an attractive framework for the axion. The IR scale provides a natural scale for the axion decay constant F_a. Furthermore, by suppressing the axion on the UV brane, away from the explicit $\mathrm{U}(1)_{\mathrm{PQ}}$ violation sources, we can solve the axion quality problem. The framework also incorporates Standard Model fermions, including the quarks and charged leptons. Several recent papers [168, 169, 170] have also started to

[1] The Future of Fundamental Physics, CERN colloquium, 2021 March 25th

[2] One could argue that this is our curse, for not being able to observe new physics, knowing they must exist.

follow this approach. In our model, the fermion mass hierarchy can then be naturally explained through $\mathcal{O}(1)$ profile parameters, as explained in Chapter 3. Depending on the Higgs profile, the DFSZ-like model predicts off-diagonal mixing of the fermions through couplings to the axion. This offers the possibility of discovering the axion through precision experiments such as flavor-violating kaon decays. An obvious extension of this model is to include the neutrino sector. This gives an interesting model where the IR brane scale can also offer an explanation of the Majorana neutrino mass scale in the seesaw mechanism and is currently in preparation [34]. Nonetheless, the current model ignores the gauge hierarchy problem and possible extensions to multi-throat models could be considered. Alternatively, our model could be generalized by considering z-dependent bulk Higgs VEVs that may lead to different predictions for the axion-fermion couplings. Finally, the 5D framework not only applies to the QCD axion, but can be used to determine the couplings for any axion-like particle. For instance, having a much lower axion decay constant could lead to more stringent constraints on a particular model. Indeed, our results provide further motivation to search for axions via their couplings to fermions.

By the AdS/CFT correspondence, the warped extra dimension holographically captures a class of 4D composite axion models with an accidental $\mathrm{U}(1)_{\mathrm{PQ}}$ symmetry. A multi-throat model corresponds to multiple strong dynamics that separately give rise to the Higgs boson and the axion. This was presented as a hypercolor gauge group $\mathrm{SU}(4)_{\mathrm{HC}}$ pr $\mathrm{Sp}(2N_{\mathrm{HC}})$ with enlarged color group $\mathrm{SU}(N+3) \times \mathrm{SU}(N)'$. The hypercolor confinement then breaks the enlarged color, resulting in the Standard Model QCD and a dark axi-color strong dynamics. The unique feature of this model is that the axion could be heavy, as high as the TeV scale, accessible at collider experiments [171]. All mass scales in the model, including the axion masses, arise from the hypercolor confinement scale which can be as low as 1000 TeV. Furthermore, the dark sector low energy spectrum provides attractive dark matter candidates.

Nonetheless, the heavy axion requires “heavy machinery", as the axion is now burdened with theta angles from the new sector. Within the Higgs sector, it is also implied that the composite Higgs sector must be tuned in order to achieve electroweak symmetry breaking,

and other experimental signatures could arise from an “unnatural" Higgs sector similar to those considered in Ref. [172]. If the hypercolor strong scale is near 10^{10-11} GeV, then the quartic coupling of the Higgs potential may be generated radiatively as considered in Ref [149]. There may also exist other hypercolor groups with different hyperfermion representations, as well as small instanton contributions arising from UV modifications of QCD that could be incorporated into a composite Higgs framework. Nevertheless, it is clear that an enlarged strong dynamics can extend the range of axion masses, and provides further motivation for experimental searches of axion-like particles. In fact after this work was completed, similar models that attempted to raise the axion mass from various sources also recently appeared in the literature [173, 174, 175].

Finally, this thesis continued existing efforts to study the AdS/CFT correspondence. Holography has been successfully applied, first in studying QCD hadron structures, then in the context of composite Higgs models. It is natural to extend holography to study composite axion models, one of the most attractive UV models of the well-anticipated axion. Currently, the axion window is rapidly shrinking through experimental efforts. From the work in this thesis, we hope to contribute toward an axion discovery. It would be just as impactful or even exceed the importance of discovering the Higgs boson.

References

[1] Richard P Feynman. *QED*. Princeton University Press, 2014.

[2] H. A. Bethe. The electromagnetic shift of energy levels. *Phys. Rev.*, 72:339–341, Aug 1947.

[3] Chen-Ning Yang and Robert L Mills. Conservation of isotopic spin and isotopic gauge invariance. *Physical review*, 96(1):191, 1954.

[4] Steven Weinberg. A model of leptons. *Physical review letters*, 19(21):1264, 1967.

[5] Sheldon L Glashow. Partial-symmetries of weak interactions. *Nuclear physics*, 22(4):579–588, 1961.

[6] François Englert and Robert Brout. Broken symmetry and the mass of gauge vector mesons. *Physical Review Letters*, 13(9):321, 1964.

[7] Peter W Higgs. Broken symmetries and the masses of gauge bosons. *Physical Review Letters*, 13(16):508, 1964.

[8] SW Herb, DC Hom, LM Lederman, JC Sens, HD Snyder, JK Yoh, JA Appel, BC Brown, CN Brown, WR Innes, et al. Observation of a dimuon resonance at 9.5 gev in 400-gev proton-nucleus collisions. *Physical Review Letters*, 39(5):252, 1977.

[9] Fumio Abe, H Akimoto, A Akopian, MG Albrow, SR Amendolia, D Amidei, J Antos, C Anway-Wiese, S Aota, G Apollinari, et al. Observation of top quark production in p p collisions with the collider detector at fermilab. *Physical review letters*, 74(14):2626, 1995.

[10] K Kodama, N Ushida, C Andreopoulos, N Saoulidou, G Tzanakos, P Yager, B Baller, D Boehnlein, Walter Freeman, B Lundberg, et al. Observation of tau neutrino interactions. *Physics Letters B*, 504(3):218–224, 2001.

[11] Serguei Chatrchyan, Vardan Khachatryan, Albert M Sirunyan, Armen Tumasyan, Wolfgang Adam, Ernest Aguilo, Thomas Bergauer, M Dragicevic, J Erö, C Fabjan, et al. Observation of a new boson at a mass of 125 gev with the cms experiment at the lhc. *Physics Letters B*, 716(1):30–61, 2012.

[12] Stephen P. Martin. A Supersymmetry primer. *Adv. Ser. Direct. High Energy Phys.*, 18:1–98, 1998.

[13] Gordon L Kane. *The supersymmetric world: The beginnings of the theory.* World Scientific, 2000.

[14] M. E. Cabrera, J. A. Casas, and R. Ruiz de Austri. Bayesian approach and Naturalness in MSSM analyses for the LHC. *JHEP*, 03:075, 2009.

[15] Sylvain Fichet. Quantified naturalness from Bayesian statistics. *Phys. Rev. D*, 86:125029, 2012.

[16] G't Hooft. Naturalness, chiral symmetry, and spontaneous chiral symmetry breaking. *Recent developments in gauge theories*, pages 135–157, 1980.

[17] Nima Arkani-Hamed and Savas Dimopoulos. Supersymmetric unification without low energy supersymmetry and signatures for fine-tuning at the lhc. *Journal of High Energy Physics*, 2005(06):073, 2005.

[18] Ivan Esteban, Maria Conceptión González-García, Michele Maltoni, Thomas Schwetz, and Albert Zhou. The fate of hints: updated global analysis of three-flavor neutrino oscillations. *Journal of High Energy Physics*, 2020(9):1–22, 2020.

[19] Carl D Anderson. The positive electron. *Physical Review*, 43(6):491, 1933.

[20] Tsung-Dao Lee and Chen-Ning Yang. Question of parity conservation in weak interactions. *Physical Review*, 104(1):254, 1956.

[21] Nicola Cabibbo. Unitary symmetry and leptonic decays. *Phys. Rev. Lett.*, 10:531–533, Jun 1963.

[22] Ziro Maki, Masami Nakagawa, and Shoichi Sakata. Remarks on the unified model of elementary particles. *Progress of Theoretical Physics*, 28(5):870–880, 1962.

[23] Bruno Pontecorvo. Inverse *beta* processes and nonconservation of lepton charge. *Zhur. Eksptl'. i Teoret. Fiz.*, 34, 1958.

[24] CA Baker, DD Doyle, P Geltenbort, K Green, MGD Van der Grinten, PG Harris, P Iaydjiev, SN Ivanov, DJR May, JM Pendlebury, et al. Improved experimental limit on the electric dipole moment of the neutron. *Physical Review Letters*, 97(13):131801, 2006.

[25] JM Pendlebury, S Afach, NJ Ayres, CA Baker, G Ban, Georg Bison, Kazimierz Bodek, Martin Burghoff, Peter Geltenbort, Katie Green, et al. Revised experimental upper limit on the electric dipole moment of the neutron. *Physical Review D*, 92(9):092003, 2015.

[26] Brent Graner, Y Chen, EG Lindahl, BR Heckel, et al. Reduced limit on the permanent electric dipole moment of hg 199. *Physical review letters*, 116(16):161601, 2016.

[27] Joshua D. Simon. The faintest dwarf galaxies. *Annual Review of Astronomy and Astrophysics*, 57(1):375–415, Aug 2019.

[28] Paolo Salucci. The distribution of dark matter in galaxies. *Astron. Astrophys. Rev.*, 27(1):2, 2019.

[29] Steven W. Allen, August E. Evrard, and Adam B. Mantz. Cosmological parameters from observations of galaxy clusters. *Annual Review of Astronomy and Astrophysics*, 49(1):409–470, Sep 2011.

[30] Juan Martin Maldacena. The Large N limit of superconformal field theories and supergravity. *Int. J. Theor. Phys.*, 38:1113–1133, 1999. [Adv. Theor. Math. Phys.2,231(1998)].

[31] Tony Gherghetta and Minh D Nguyen. A composite higgs with a heavy composite axion. *Journal of High Energy Physics*, 2020(12):1–42, 2020.

[32] Peter Cox, Tony Gherghetta, and Minh D Nguyen. A holographic perspective on the axion quality problem. *Journal of High Energy Physics*, 2020(1):1–20, 2020.

[33] Bonnefoy Quentin, Peter Cox, Dudas Emilian, Gherghetta Tony, and Minh D Nguyen. Flavoured warped axion. *Journal of High Energy Physics*, 2021(4), 2021.

[34] Peter Cox, Tony Gherghetta, and Minh D Nguyen. Neutrino masses from a holographic qcd axion. *Under prepration.*

[35] R.D. Peccei and Helen R. Quinn. CP Conservation in the Presence of Instantons. *Phys. Rev. Lett.*, 38:1440–1443, 1977.

[36] R.D. Peccei and Helen R. Quinn. Constraints Imposed by CP Conservation in the Presence of Instantons. *Phys. Rev. D*, 16:1791–1797, 1977.

[37] Steven Weinberg. A New Light Boson? *Phys. Rev. Lett.*, 40:223–226, 1978.

[38] Frank Wilczek. Problem of Strong P and T Invariance in the Presence of Instantons. *Phys. Rev. Lett.*, 40:279–282, 1978.

[39] Gerard't Hooft. Symmetry breaking through bell-jackiw anomalies. *Physical Review Letters*, 37:8–11, 1976.

[40] Ann Nelson. Naturally weak cp violation. *Physics Letters B*, 136(5-6):387–391, 1984.

[41] Stephen M Barr. Solving the strong cp problem without the peccei-quinn symmetry. *Physical Review Letters*, 53(4):329, 1984.

[42] Giacomo Cacciapaglia, Gabriele Ferretti, Thomas Flacke, and Hugo Serôdio. Light scalars in composite Higgs models. *Front. in Phys.*, 7:22, 2019.

[43] Peter Svrcek and Edward Witten. Axions In String Theory. *JHEP*, 06:051, 2006.

[44] Particle Data Group et al. Review of particle physics. *Progress of Theoretical and Experimental Physics*, 2020(8):1–2093, 2020.

[45] Arthur M Jaffe. The millennium grand challenge in mathematics. *Notices of the AMS*, 53(6):652–660, 2006.

[46] Kazuhiko Nishijima. Charge independence theory of v particles. *Progress of Theoretical Physics*, 13(3):285–304, 1955.

[47] Murray Gell-Mann. The interpretation of the new particles as displaced charge multiplets. *Il Nuovo Cimento (1955-1965)*, 4(2):848–866, 1956.

[48] Murray Gell-Mann. The eightfold way: A theory of strong interaction symmetry. Technical report, California Inst. of Tech., Pasadena. Synchrotron Lab., 1961.

[49] Yuval Ne'eman. Derivation of strong interactions from a gauge invariance. *Nuclear physics*, 26(2):222–229, 1961.

[50] Murray Gell-Mann. A schematic model of baryons and mesons. In *Murray Gell-Mann: Selected Papers*, pages 151–152. World Scientific, 2010.

[51] Oscar W Greenberg. Spin and unitary-spin independence in a paraquark model of baryons and mesons. *Physical Review Letters*, 13(20):598, 1964.

[52] Moo-Young Han and Yoichiro Nambu. Three-triplet model with double su (3) symmetry. *Physical Review*, 139(4B):B1006, 1965.

[53] Elliott D Bloom, DH Coward, H DeStaebler, J Drees, Guthrie Miller, Luke W Mo, Richard E Taylor, Martin Breidenbach, Jerome I Friedman, George C Hartmann, et al. High-energy inelastic e- p scattering at 6 and 10. *Physical Review Letters*, 23(16):930, 1969.

[54] Martin Breidenbach, Jerome I Friedman, Henry W Kendall, Elliott D Bloom, DH Coward, H DeStaebler, J Drees, Luke W Mo, and Richard E Taylor. Observed behavior of highly inelastic electron-proton scattering. *Physical Review Letters*, 23(16):935, 1969.

[55] Richard P Feynman. Very high-energy collisions of hadrons. *Physical Review Letters*, 23(24):1415, 1969.

[56] James D Bjorken. Asymptotic sum rules at infinite momentum. *Physical Review*, 179(5):1547, 1969.

[57] Harald Fritzsch, Murray Gell-Mann, and Heinrich Leutwyler. Advantages of the color octet gluon picture. *Physics Letters B*, 47(4):365–368, 1973.

[58] David J Gross and Frank Wilczek. Ultraviolet behavior of non-abelian gauge theories. *Physical Review Letters*, 30(26):1343, 1973.

[59] H David Politzer. Reliable perturbative results for strong interactions? *Physical Review Letters*, 30(26):1346, 1973.

[60] DP Barber, U Becker, H Benda, A Boehm, JG Branson, J Bron, D Buikman, J Burger, CC Chang, HS Chen, et al. Discovery of three-jet events and a test of quantum chromodynamics at petra. *Physical Review Letters*, 43(12):830, 1979.

[61] Steven Weinberg. The u (1) problem. *Physical Review D*, 11(12):3583, 1975.

[62] Gerard 't Hooft. Computation of the Quantum Effects Due to a Four-Dimensional Pseudoparticle. *Phys. Rev.*, D14:3432–3450, 1976. [Erratum: Phys. Rev.D18,2199(1978); ,70(1976)].

[63] Gerard't Hooft. How instantons solve the u (1) problem. *Physics Reports*, 142(6):357–387, 1986.

[64] George A Christos. Chiral symmetry and the u (1) problem. *Physics Reports*, 116(5):251–336, 1984.

[65] Edward Witten. Current Algebra Theorems for the U(1) Goldstone Boson. *Nucl. Phys. B*, 156:269–283, 1979.

[66] RJ Crewther, P Di Vecchia, G Veneziano, and Edward Witten. Chiral estimate of the electric dipole moment of the neutron in quantum chromodynamics. *Physics Letters B*, 88(1-2):123–127, 1979.

[67] Anson Hook. Tasi lectures on the strong cp problem and axions. *arXiv preprint arXiv:1812.02669*, 2018.

[68] RJ Crewther. Chirality selection rules and the u (1) problem. *Physics Letters B*, 70(3):349–354, 1977.

[69] P. Di Vecchia and G. Veneziano. Chiral Dynamics in the Large N Limit. *Nucl. Phys. B*, 171:253–272, 1980.

[70] Marco Gorghetto and Giovanni Villadoro. Topological susceptibility and qcd axion mass: Qed and nnlo corrections. *Journal of High Energy Physics*, 2019(3):1–22, 2019.

[71] Kiwoon Choi and Jihn E. Kim. Dynamical Axion. *Phys. Rev.*, D32:1828, 1985.

[72] Jihn E. Kim. A Composite Invisible Axion. *Phys. Rev.*, D31:1733, 1985.

[73] Jihn E. Kim. Weak Interaction Singlet and Strong CP Invariance. *Phys. Rev. Lett.*, 43:103, 1979.

[74] Mikhail A. Shifman, A. I. Vainshtein, and Valentin I. Zakharov. Can Confinement Ensure Natural CP Invariance of Strong Interactions? *Nucl. Phys.*, B166:493–506, 1980.

[75] Michael Dine, Willy Fischler, and Mark Srednicki. A Simple Solution to the Strong CP Problem with a Harmless Axion. *Phys. Lett.*, 104B:199–202, 1981.

[76] A. R. Zhitnitsky. On Possible Suppression of the Axion Hadron Interactions. (In Russian). *Sov. J. Nucl. Phys.*, 31:260, 1980. [Yad. Fiz.31,497(1980)].

[77] Anson Hook. Anomalous solutions to the strong CP problem. *Phys. Rev. Lett.*, 114(14):141801, 2015.

[78] Gunnar Nordström. On the possibility of unifying the electromagnetic and the gravitational fields. *arXiv e-prints*, page physics/0702221, February 2007.

[79] OSKAR KLEIN. The atomicity of electricity as a quantum theory law. *Nature*, 118(2971):516–516, Oct 1926.

[80] Oskar Klein. Quantentheorie und fünfdimensionale relativitätstheorie. *Zeitschrift für Physik*, 37(12):895–906, Dec 1926.

[81] C. N. Yang and R. L. Mills. Conservation of isotopic spin and isotopic gauge invariance. *Phys. Rev.*, 96:191–195, Oct 1954.

[82] N. Straumann. On Pauli's invention of nonAbelian Kaluza-Klein theory in 1953. In *9th Marcel Grossmann Meeting on Recent Developments in Theoretical and Experimental General Relativity, Gravitation and Relativistic Field Theories (MG 9)*, 7 2000.

[83] Michael B. Green and John H. Schwarz. Anomaly cancellations in supersymmetric d = 10 gauge theory and superstring theory. *Physics Letters B*, 149(1):117–122, 1984.

[84] Ignatios Antoniadis, Nima Arkani-Hamed, Savas Dimopoulos, and Gia Dvali. New dimensions at a millimeter to a fermi and superstrings at a tev. *Physics Letters B*, 436(3-4):257–263, Sep 1998.

[85] Nima Arkani–Hamed, Savas Dimopoulos, and Gia Dvali. The hierarchy problem and new dimensions at a millimeter. *Physics Letters B*, 429(3-4):263–272, Jun 1998.

[86] Nima Arkani-Hamed, Savas Dimopoulos, and Gia Dvali. Phenomenology, astrophysics, and cosmology of theories with submillimeter dimensions and tev scale quantum gravity. *Physical Review D*, 59(8), Mar 1999.

[87] Wen-Hai Tan, Shan-Qing Yang, Cheng-Gang Shao, Jia Li, An-Bin Du, Bi-Fu Zhan, Qing-Lan Wang, Peng-Shun Luo, Liang-Cheng Tu, and Jun Luo. New Test of the

Gravitational Inverse-Square Law at the Submillimeter Range with Dual Modulation and Compensation. *Phys. Rev. Lett.*, 116(13):131101, 2016.

[88] Juan Maldacena. *International Journal of Theoretical Physics*, 38(4):1113–1133, 1999.

[89] Edward Witten. Anti-de Sitter space and holography. *Adv. Theor. Math. Phys.*, 2:253–291, 1998.

[90] S. S. Gubser, Igor R. Klebanov, and Alexander M. Polyakov. Gauge theory correlators from noncritical string theory. *Phys. Lett. B*, 428:105–114, 1998.

[91] Gerard 't Hooft. Dimensional reduction in quantum gravity. *Conf. Proc. C*, 930308:284–296, 1993.

[92] Leonard Susskind. The World as a hologram. *J. Math. Phys.*, 36:6377–6396, 1995.

[93] Lisa Randall and Raman Sundrum. A Large mass hierarchy from a small extra dimension. *Phys. Rev. Lett.*, 83:3370–3373, 1999.

[94] Lisa Randall and Raman Sundrum. An Alternative to compactification. *Phys. Rev. Lett.*, 83:4690–4693, 1999.

[95] Csaba Csaki. TASI lectures on extra dimensions and branes. In *Theoretical Advanced Study Institute in Elementary Particle Physics (TASI 2002): Particle Physics and Cosmology: The Quest for Physics Beyond the Standard Model(s)*, 4 2004.

[96] M. Shifman. Large Extra Dimensions: Becoming acquainted with an alternative paradigm. *Int. J. Mod. Phys. A*, 25:199–225, 2010.

[97] Cosmin Macesanu. The Phenomenology of universal extra dimensions at hadron colliders. *Int. J. Mod. Phys. A*, 21:2259–2296, 2006.

[98] R. Rattazzi. Cargese lectures on extra-dimensions. In *Cargese School of Particle Physics and Cosmology: the Interface*, 8 2003.

[99] Joseph Polchinski. Tasi lectures on D-branes. In *Theoretical Advanced Study Institute in Elementary Particle Physics (TASI 96): Fields, Strings, and Duality*, 11 1996.

[100] Constantin P. Bachas. Lectures on D-branes. In *A Newton Institute Euroconference on Duality and Supersymmetric Theories*, 6 1998.

[101] V. A. Rubakov and M. E. Shaposhnikov. Do We Live Inside a Domain Wall? *Phys. Lett. B*, 125:136–138, 1983.

[102] G. R. Dvali and Mikhail A. Shifman. Domain walls in strongly coupled theories. *Phys. Lett. B*, 396:64–69, 1997. [Erratum: Phys.Lett.B 407, 452 (1997)].

[103] G. R. Dvali and Mikhail A. Shifman. Dynamical compactification as a mechanism of spontaneous supersymmetry breaking. *Nucl. Phys. B*, 504:127–146, 1997.

[104] Daniela Bigatti and Leonard Susskind. TASI lectures on the holographic principle. In *Theoretical Advanced Study Institute in Elementary Particle Physics (TASI 99): Strings, Branes, and Gravity*, 8 1999.

[105] Juan Martin Maldacena. TASI 2003 lectures on AdS / CFT. In *Theoretical Advanced Study Institute in Elementary Particle Physics (TASI 2003): Recent Trends in String Theory*, 9 2003.

[106] Walter D. Goldberger and Mark B. Wise. Modulus stabilization with bulk fields. *Phys. Rev. Lett.*, 83:4922–4925, 1999.

[107] Walter D. Goldberger and Mark B. Wise. Phenomenology of a stabilized modulus. *Phys. Lett. B*, 475:275–279, 2000.

[108] H. Davoudiasl, J. L. Hewett, and T. G. Rizzo. Bulk gauge fields in the Randall-Sundrum model. *Phys. Lett. B*, 473:43–49, 2000.

[109] Sanghyeon Chang, Junji Hisano, Hiroaki Nakano, Nobuchika Okada, and Masahiro Yamaguchi. Bulk standard model in the Randall-Sundrum background. *Phys. Rev. D*, 62:084025, 2000.

[110] Yuval Grossman and Matthias Neubert. Neutrino masses and mixings in nonfactorizable geometry. *Phys. Lett. B*, 474:361–371, 2000.

[111] H Davoudiasl, JL Hewett, and TG Rizzo. Bulk gauge fields in the randall–sundrum model. *Physics Letters B*, 473(1-2):43–49, 2000.

[112] Alex Pomarol. Gauge bosons in a five-dimensional theory with localized gravity. *Physics Letters B*, 486(1-2):153–157, 2000.

[113] Tony Gherghetta and Alex Pomarol. Bulk fields and supersymmetry in a slice of ads. *Nuclear Physics B*, 586(1-2):141–162, 2000.

[114] Tony Gherghetta. Les Houches lectures on warped models and holography. In *Les Houches Summer School on Theoretical Physics: Session 84: Particle Physics Beyond the Standard Model*, 1 2006.

[115] Tony Gherghetta. A Holographic View of Beyond the Standard Model Physics. In *Theoretical Advanced Study Institute in Elementary Particle Physics: Physics of the Large and the Small*, 8 2010.

[116] Keith R. Dienes, Emilian Dudas, and Tony Gherghetta. Invisible axions and large radius compactifications. *Phys. Rev.*, D62:105023, 2000.

[117] Ki-woon Choi. A QCD axion from higher dimensional gauge field. *Phys. Rev. Lett.*, 92:101602, 2004.

[118] Thomas Flacke, Ben Gripaios, John March-Russell, and David Maybury. Warped axions. *JHEP*, 01:061, 2007.

[119] Francesco Bigazzi, Alessio Caddeo, Aldo L. Cotrone, Paolo Di Vecchia, and Andrea Marzolla. The Holographic QCD Axion. *JHEP*, 12:056, 2019.

[120] Leandro Da Rold and Alex Pomarol. The Scalar and pseudoscalar sector in a five-dimensional approach to chiral symmetry breaking. *JHEP*, 01:157, 2006.

[121] Norisuke Sakai and Nobuhiro Uekusa. Selecting gauge theories on an interval by 5D gauge transformations. *Prog. Theor. Phys.*, 118:315–335, 2007.

[122] Edward Witten. Multitrace operators, boundary conditions, and AdS / CFT correspondence. 2001.

[123] Hsin-Chia Cheng and David Elazzar Kaplan. Axions and a gauged Peccei-Quinn symmetry. 2001.

[124] Nathaniel Craig, Isabel Garcia Garcia, and Dave Sutherland. Disassembling the Clockwork Mechanism. *JHEP*, 10:018, 2017.

[125] Giovanni Grilli di Cortona, Edward Hardy, Javier Pardo Vega, and Giovanni Villadoro. The QCD axion, precisely. *JHEP*, 01:034, 2016.

[126] Benjamin Lillard and Tim M. P. Tait. A Composite Axion from a Supersymmetric Product Group. *JHEP*, 11:005, 2017.

[127] Benjamin Lillard and Tim M. P. Tait. A High Quality Composite Axion. *JHEP*, 11:199, 2018.

[128] M. B. Gavela, M. Ibe, P. Quilez, and T. T. Yanagida. Automatic Peccei–Quinn symmetry. *Eur. Phys. J.*, C79(6):542, 2019.

[129] Joshua Erlich, Emanuel Katz, Dam T. Son, and Mikhail A. Stephanov. QCD and a holographic model of hadrons. *Phys. Rev. Lett.*, 95:261602, 2005.

[130] Leandro Da Rold and Alex Pomarol. Chiral symmetry breaking from five dimensional spaces. *Nucl. Phys.*, B721:79–97, 2005.

[131] Jorge Martin Camalich, Maxim Pospelov, Hoa Vuong, Robert Ziegler, and Jure Zupan. Quark Flavor Phenomenology of the QCD Axion. *Phys. Rev. D*, 102(1):015023, 2020.

[132] Lorenzo Calibbi, Diego Redigolo, Robert Ziegler, and Jure Zupan. Looking forward to Lepton-flavor-violating ALPs. 6 2020.

[133] Tony Gherghetta and Alex Pomarol. Bulk fields and supersymmetry in a slice of AdS. *Nucl. Phys.*, B586:141–162, 2000.

[134] Giacomo Cacciapaglia, Csaba Csaki, Guido Marandella, and John Terning. The Gaugephobic Higgs. *JHEP*, 02:036, 2007.

[135] Peter Cox, Tony Gherghetta, and Minh D. Nguyen. A Holographic Perspective on the Axion Quality Problem. *JHEP*, 01:188, 2020.

[136] Bob Holdom and Michael E. Peskin. Raising the Axion Mass. *Nucl. Phys.*, B208:397–412, 1982.

[137] Michael Dine and Nathan Seiberg. String Theory and the Strong CP Problem. *Nucl. Phys.*, B273:109–124, 1986.

[138] Jonathan M. Flynn and Lisa Randall. A Computation of the Small Instanton Contribution to the Axion Potential. *Nucl. Phys.*, B293:731–739, 1987.

[139] Prateek Agrawal and Kiel Howe. Factoring the Strong CP Problem. *JHEP*, 12:029, 2018.

[140] Javier Fuentes-Martín, Mario Reig, and Avelino Vicente. Strong CP problem with low-energy emergent QCD: The 4321 case. *Phys. Rev. D*, 100(11):115028, 2019.

[141] Csaba Csáki, Maximilian Ruhdorfer, and Yuri Shirman. UV Sensitivity of the Axion Mass from Instantons in Partially Broken Gauge Groups. *JHEP*, 04:031, 2020.

[142] Tony Gherghetta, Valentin V. Khoze, Alex Pomarol, and Yuri Shirman. The Axion Mass from 5D Small Instantons. *JHEP*, 03:063, 2020.

[143] Tony Gherghetta, Natsumi Nagata, and Mikhail Shifman. A Visible QCD Axion from an Enlarged Color Group. *Phys. Rev.*, D93(11):115010, 2016.

[144] M. K. Gaillard, M. B. Gavela, R. Houtz, P. Quilez, and R. Del Rey. Color unified dynamical axion. *Eur. Phys. J.*, C78(11):972, 2018.

[145] Giuliano Panico and Andrea Wulzer. *The Composite Nambu-Goldstone Higgs*, volume 913. Springer, 2016.

[146] James Barnard, Tony Gherghetta, and Tirtha Sankar Ray. UV descriptions of composite Higgs models without elementary scalars. *JHEP*, 02:002, 2014.

[147] Gabriele Ferretti and Denis Karateev. Fermionic UV completions of Composite Higgs models. *JHEP*, 03:077, 2014.

[148] Gabriele Ferretti. UV Completions of Partial Compositeness: The Case for a SU(4) Gauge Group. *JHEP*, 06:142, 2014.

[149] Michele Redi and Alessandro Strumia. Axion-Higgs Unification. *JHEP*, 11:103, 2012.

[150] J. Mrazek, A. Pomarol, R. Rattazzi, M. Redi, J. Serra, and A. Wulzer. The Other Natural Two Higgs Doublet Model. *Nucl. Phys. B*, 853:1–48, 2011.

[151] Yoichiro Nambu and G. Jona-Lasinio. Dynamical Model of Elementary Particles Based on an Analogy with Superconductivity. 1. *Phys. Rev.*, 122:345–358, 1961. [,127(1961)].

[152] Nima Arkani-Hamed, Andrew G. Cohen, and Howard Georgi. (De)constructing dimensions. *Phys. Rev. Lett.*, 86:4757–4761, 2001.

[153] Hsin-Chia Cheng, Christopher T. Hill, and Jing Wang. Dynamical Electroweak Breaking and Latticized Extra Dimensions. *Phys. Rev. D*, 64:095003, 2001.

[154] Haiying Cai, Thomas Flacke, and Mickael Lespinasse. A composite scalar hint from di-boson resonances? 12 2015.

[155] Alexander Belyaev, Giacomo Cacciapaglia, Haiying Cai, Thomas Flacke, Alberto Parolini, and Hugo Serôdio. Singlets in composite Higgs models in light of the LHC 750 GeV diphoton excess. *Phys. Rev. D*, 94(1):015004, 2016.

[156] Edward Witten. An SU(2) Anomaly. *Phys. Lett. B*, 117:324–328, 1982.

[157] Juven Wang, Xiao-Gang Wen, and Edward Witten. A New SU(2) Anomaly. *J. Math. Phys.*, 60(5):052301, 2019.

[158] M.A. Shifman and A.I. Vainshtein. On gluino condensation in supersymmetric gauge theories with su(n) and o(n) groups. *Nucl. Phys. B*, 296(2):445 – 461, 1988.

[159] Andrei V. Smilga and M.I. Vysotsky. The massless gluino and the pseudoscalar meson family. *Phys. Lett. B*, 125:227–229, 1983.

[160] Glennys R. Farrar and Steven Weinberg. Supersymmetry at Ordinary Energies. 2. R Invariance, Goldstone Bosons, and Gauge Fermion Masses. *Phys. Rev. D*, 27:2732, 1983.

[161] Glennys R. Farrar and G.T. Gabadadze. Light gluino mass and condensate from properties of eta and eta-prime. *Phys. Lett. B*, 397:104–111, 1997.

[162] Mikhail A. Shifman, A. I. Vainshtein, and Valentin I. Zakharov. Instanton Density in a Theory with Massless Quarks. *Nucl. Phys.*, B163:46–56, 1980.

[163] Avner Karasik and Zohar Komargodski. The Bi-Fundamental Gauge Theory in 3+1 Dimensions: The Vacuum Structure and a Cascade. *JHEP*, 05:144, 2019.

[164] Savas Dimopoulos and Leonard Susskind. Mass Without Scalars. *Nucl. Phys. B*, 155:237–252, 1979.

[165] Albert M Sirunyan et al. Search for pair-produced three-jet resonances in proton-proton collisions at $\sqrt{s}$ =13 TeV. *Phys. Rev. D*, 99(1):012010, 2019.

[166] Morad Aaboud et al. Search for heavy charged long-lived particles in the ATLAS detector in 36.1 fb^{-1} of proton-proton collision data at $\sqrt{s} = 13$ TeV. *Phys. Rev. D*, 99(9):092007, 2019.

[167] Nathaniel Craig, Andrey Katz, Matt Strassler, and Raman Sundrum. Naturalness in the Dark at the LHC. *JHEP*, 07:105, 2015.

[168] Yuichiro Nakai and Motoo Suzuki. Axion quality from superconformal dynamics. *Physics Letters B*, 816:136239, 2021.

[169] Masaki Yamada and Tsutomu T. Yanagida. A natural and simple uv completion of the qcd axion model. *Physics Letters B*, 816:136267, 2021.

[170] Anson Hook, Soubhik Kumar, Zhen Liu, and Raman Sundrum. High quality qcd axion and the lhc. *Phys. Rev. Lett.*, 124:221801, Jun 2020.

[171] Kevin J. Kelly, Soubhik Kumar, and Zhen Liu. Heavy axion opportunities at the dune near detector. *Phys. Rev. D*, 103:095002, May 2021.

[172] James Barnard, Tony Gherghetta, Tirtha Sankar Ray, and Andrew Spray. The Unnatural Composite Higgs. *JHEP*, 01:067, 2015.

[173] R. S. Gupta, V. V. Khoze, and M. Spannowsky. Small instantons and the strong cp problem in composite higgs models, 2020.

[174] Fuminobu Takahashi and Wen Yin. Heavy qcd axion inflation, 2021.

[175] Ryuichiro Kitano and Wen Yin. Strong cp problem and axion dark matter with small instantons, 2021.

[176] Gero von Gersdorff. Universal approximations for flavor models. *JHEP*, 07:131, 2019.

[177] S. Casagrande, F. Goertz, U. Haisch, M. Neubert, and T. Pfoh. Flavor Physics in the Randall-Sundrum Model: I. Theoretical Setup and Electroweak Precision Tests. *JHEP*, 10:094, 2008.

[178] M. Tanabashi et al. Review of Particle Physics. *Phys. Rev. D*, 98(3):030001, 2018.

[179] Ivan Esteban, M.C. Gonzalez-Garcia, Michele Maltoni, Thomas Schwetz, and Albert Zhou. The fate of hints: updated global analysis of three-flavor neutrino oscillations. *JHEP*, 09:178, 2020.

[180] Giacomo Cacciapaglia, Haiying Cai, Aldo Deandrea, Thomas Flacke, Seung J. Lee, and Alberto Parolini. Composite scalars at the LHC: the Higgs, the Sextet and the Octet. *JHEP*, 11:201, 2015.

Appendix A

Analytic Standard Model Fermion Masses and Mixings

In this Appendix, we analytically describe the masses and mixing of the zero mode fermions and our procedure for fitting the bulk mass parameters, c_i, to the measured quark and charged lepton masses and the CKM and PMNS matrices. The 4D Yukawa coupling hierarchy is generated from the overlap of the bulk fermion profiles, assuming order one or "anarchic" 5D Yukawa couplings [110, 133].

Starting with the boundary Higgs case, and taking the up-type quark sector as an example, the fermion mass matrix in the 4D effective theory is given by

$$m_u^{ij} = y_{u,ij}^{(5)} \frac{v_u}{\sqrt{2k}} f_{Q_{iL}}^0(z_{UV}) f_{U_{jR}}^0(z_{UV})\,. \tag{A.1}$$

With a bulk Higgs, this generalises to

$$m_u^{ij} = y_{u,ij}^{(5)} \frac{\sqrt{2} v_u}{\sqrt{k}} \int_{z_{UV}}^{z_{IR}} \frac{dz}{(kz)^5}\; f_{Q_{iL}}^0(z) f_{U_{jR}}^0(z)\,. \tag{A.2}$$

Evaluating the overlap integral gives

$$\int_{z_{UV}}^{z_{IR}} \frac{dz}{(kz)^5}\; f^0_{Q_{iL}}(z) f^0_{U_{jR}}(z) = \frac{\mathcal{N}_{Q_i}\mathcal{N}_{U_j}}{k(c_{Q_i}-c_{U_j})}\left((kz_{UV})^{c_{U_j}-c_{Q_i}} - (kz_{IR})^{c_{U_j}-c_{Q_i}}\right), \quad \text{(A.3)}$$

$$\approx \frac{\mathcal{N}_{Q_i}\mathcal{N}_{U_j}}{k(c_{Q_i}-c_{U_j})}(kz_{UV})^{c_{U_j}}(kz_{UV})^{-c_{Q_i}}, \quad \text{if } c_{Q_i} > c_{U_i}\,. \quad \text{(A.4)}$$

The approximation in the second line holds when $c_{Q_i} > c_{U_i}$, provided $kz_{IR} \gg 1$. This will always be the case we are interested in, since for $c_{Q_i} < c_{U_i}$ the overlap integral is suppressed by $(kz_{IR})^{-n}$, with $n \geq 1$; the elements of m_{ij} are then too small to explain the observed quark masses and CKM mixing angles. Using (A.4), the bulk Higgs case can be written in a similar form to the boundary case

$$m_u^{ij} = \tilde{y}^{(5)}_{u,\,ij}\frac{v_u}{\sqrt{2k}}\tilde{f}_{Q_i}\tilde{f}_{U_j}\,, \quad \text{(A.5)}$$

where

$$\tilde{f}_{Q_i} = \frac{\mathcal{N}_{Q_i}}{\sqrt{k}}(kz_{UV})^{-c_{Q_i}}\,, \qquad \tilde{f}_{U_j} = \frac{\mathcal{N}_{U_i}}{\sqrt{k}}(kz_{UV})^{c_{U_i}}\,, \quad \text{(A.6)}$$

and $\tilde{y}^{(5)}_{u,\,ij} = 2y^{(5)}_{u,ij}/(c_{Q_i}-c_{U_j})$. Note that the $\tilde{f}_i$ are dimensionless, and we have dropped explicit chirality indices for conciseness. There are analogous expressions for the down-type quarks and charged leptons. Below, we focus on the bulk Higgs case; the corresponding results for a boundary Higgs are obtained via the replacement $\tilde{f}_i \to f^0_i(z_{UV})$ and $\tilde{y}^{(5)} \to y^{(5)}/\sqrt{k}$.

The mass matrices are diagonalised via the singular value decomposition $A_L^{u\dagger} m_u^{ij} A_R^u = m_{u_i}$, where $A^u_{L,R}$ are unitary matrices and m_{u_i} is the diagonal matrix containing the up-type masses. To simplify the analysis, we take advantage of the fact that the quark and charged lepton masses are hierarchical and use the approximation scheme of Ref. [176] (with $n = \frac{1}{2}$) for the matrices $A_{L,R}$.

A.1 Quark sector

We begin with the quark sector, and assume the following scaling for the $\tilde{f}$:

$$\tilde{f}_{Q_1} \sim \epsilon \tilde{f}_{Q_2} \sim \epsilon^2 \tilde{f}_{Q_3}\,, \qquad \tilde{f}_{U_1} \sim \epsilon \tilde{f}_{U_2} \sim \epsilon^2 \tilde{f}_{U_3}\,, \qquad \tilde{f}_{D_1} \sim \epsilon \tilde{f}_{D_2} \sim \epsilon^2 \tilde{f}_{D_3}\,, \tag{A.7}$$

with $\epsilon \ll 1$. As will become clear from the expressions below, this scaling gives the correct structure to explain the quark masses and CKM elements. Although this additional assumption is not strictly required, it allows us to analytically solve for the $\tilde{f}$ in terms of the masses and CKM elements. This scaling behaviour was also used in Ref. [177], where they considered a single, boundary-localized Higgs doublet. To leading order in ϵ, the quark masses are given by the expressions

$$\begin{aligned}
m_u &\simeq \frac{v_u}{\sqrt{2k}} \frac{|\det \tilde{y}_u^{(5)}|}{|[\tilde{y}_u^{(5)}]_{11}|} \tilde{f}_{Q_1} \tilde{f}_{U_1}\,, & m_d &\simeq \frac{v_d}{\sqrt{2k}} \frac{|\det \tilde{y}_d^{(5)}|}{|[\tilde{y}_d^{(5)}]_{11}|} \tilde{f}_{Q_1} \tilde{f}_{D_1}\,, \\
m_c &\simeq \frac{v_u}{\sqrt{2k}} \frac{|[\tilde{y}_u^{(5)}]_{11}|}{|\tilde{y}_{u,\,33}^{(5)}|} \tilde{f}_{Q_2} \tilde{f}_{U_2}\,, & m_s &\simeq \frac{v_d}{\sqrt{2k}} \frac{|[\tilde{y}_d^{(5)}]_{11}|}{|\tilde{y}_{d,\,33}^{(5)}|} \tilde{f}_{Q_2} \tilde{f}_{D_2}\,, \\
m_t &\simeq \frac{v_u}{\sqrt{2k}} |\tilde{y}_{u,\,33}^{(5)}|\, \tilde{f}_{Q_3} \tilde{f}_{U_3}\,, & m_b &\simeq \frac{v_d}{\sqrt{2k}} |\tilde{y}_{d,\,33}^{(5)}|\, \tilde{f}_{Q_3} \tilde{f}_{D_3}\,,
\end{aligned} \tag{A.8}$$

where $[\tilde{y}^{(5)}]_{ij}$ denotes the ij minor of the matrix $\tilde{y}^{(5)}$. Using the approximation of [176], and again working to leading order in ϵ, the $A_{L,R}^{u,d}$ matrices are given by

$$A_L^q \simeq \begin{pmatrix} 1 & \frac{[\tilde{y}_q^{(5)}]_{21}}{[\tilde{y}_q^{(5)}]_{11}} \frac{\tilde{f}_{Q_1}}{\tilde{f}_{Q_2}} & \frac{\tilde{y}_{q,\,13}^{(5)}}{\tilde{y}_{q,\,33}^{(5)}} \frac{\tilde{f}_{Q_1}}{\tilde{f}_{Q_3}} \\ -\frac{[\tilde{y}_q^{(5)}]_{21}^*}{[\tilde{y}_q^{(5)}]_{11}^*} \frac{\tilde{f}_{Q_1}}{\tilde{f}_{Q_2}} & 1 & \frac{\tilde{y}_{q,\,23}^{(5)}}{\tilde{y}_{q,\,33}^{(5)}} \frac{\tilde{f}_{Q_2}}{\tilde{f}_{Q_3}} \\ \frac{[\tilde{y}_q^{(5)}]_{31}^*}{[\tilde{y}_q^{(5)}]_{11}^*} \frac{\tilde{f}_{Q_1}}{\tilde{f}_{Q_3}} & -\frac{\tilde{y}_{q,\,23}^{(5)\,*}}{\tilde{y}_{q,\,33}^{(5)\,*}} \frac{\tilde{f}_{Q_2}}{\tilde{f}_{Q_3}} & 1 \end{pmatrix}\,, \tag{A.9}$$

$$A_R^q \simeq \begin{pmatrix} 1 & \frac{[\tilde{y}_q^{(5)}]_{12}^*}{[\tilde{y}_q^{(5)}]_{11}^*} \frac{\tilde{f}_{q_1}}{\tilde{f}_{q_2}} & \frac{\tilde{y}_{q,\,31}^{(5)\,*}}{\tilde{y}_{q,\,33}^{(5)\,*}} \frac{\tilde{f}_{q_1}}{\tilde{f}_{q_3}} \\ -\frac{[\tilde{y}_q^{(5)}]_{12}}{[\tilde{y}_q^{(5)}]_{11}} \frac{\tilde{f}_{q_1}}{\tilde{f}_{q_2}} & 1 & \frac{\tilde{y}_{q,\,32}^{(5)\,*}}{\tilde{y}_{q,\,33}^{(5)\,*}} \frac{\tilde{f}_{q_2}}{\tilde{f}_{q_3}} \\ \frac{[\tilde{y}_q^{(5)}]_{13}}{[\tilde{y}_q^{(5)}]_{11}} \frac{\tilde{f}_{q_1}}{\tilde{f}_{q_3}} & -\frac{\tilde{y}_{q,\,32}^{(5)}}{\tilde{y}_{q,\,33}^{(5)}} \frac{\tilde{f}_{q_2}}{\tilde{f}_{q_3}} & 1 \end{pmatrix} \cdot \mathrm{diag}\left(e^{i\phi_1}, e^{i\phi_2}, e^{i\phi_3}\right)\,, \tag{A.10}$$

with

$$\phi_1 = \arg([\tilde{y}_u^{(5)}]_{11}) - \arg(\det \tilde{y}_u^{(5)})\,, \quad \phi_2 = \arg(\tilde{y}_{u,\,33}^{(5)}) - \arg([\tilde{y}_u^{(5)}]_{11})\,, \quad \phi_3 = -\arg(\tilde{y}_{u,\,33}^{(5)})\,. \tag{A.11}$$

Notice that A_L^q, and hence the CKM matrix, depends only on ratios of the $\tilde{f}_{Q_i}$ and not on the $\tilde{f}_{u_i}$ or $\tilde{f}_{d_i}$.

From these expressions one can constrain the 5D Yukawa coupling matrices through the CKM matrix. The Wolfenstein parameters $\bar{\rho}, \bar{\eta}$ are independent of the $\tilde{f}_{Q_i}$ (and hence the quark bulk mass parameters) and are given by

$$\bar{\rho} - i\bar{\eta} = \frac{\tilde{y}_{d,\,33}^{(5)}[\tilde{y}_u^{(5)}]_{31} - \tilde{y}_{d,\,23}^{(5)}[\tilde{y}_u^{(5)}]_{21} + \tilde{y}_{d,\,13}^{(5)}[\tilde{y}_u^{(5)}]_{11}}{\tilde{y}_{d,\,33}^{(5)}[\tilde{y}_u^{(5)}]_{11}\left(\frac{\tilde{y}_{d,\,23}^{(5)}}{\tilde{y}_{d,\,33}^{(5)}} - \frac{\tilde{y}_{u,\,23}^{(5)}}{\tilde{y}_{u,\,33}^{(5)}}\right)\left(\frac{[\tilde{y}_d^{(5)}]_{21}}{[\tilde{y}_d^{(5)}]_{11}} - \frac{[\tilde{y}_u^{(5)}]_{21}}{[\tilde{y}_u^{(5)}]_{11}}\right)}\,. \tag{A.12}$$

We randomly scan over 5×10^6 samples of 5D Yukawa coupling matrices $\tilde{y}_u^{(5)}, \tilde{y}_d^{(5)}$ with complex entries of norm between 0 and 3. This results in approximately 1300 matrix pairs that satisfy (A.12) within $2\,\sigma$ of the experimental values [178],

$$\bar{\rho} = 0.122 \pm 0.018\,, \qquad \bar{\eta} = 0.355 \pm 0.012\,. \tag{A.13}$$

Histograms of the resulting Yukawas, $\tilde{y}_{u,\,ij}^{(5)}$, are shown in Figure A.1, where approximately uniform distributions can be seen. This is consistent with the assumption that the quark mass hierarchy results from the fermion profiles, rather than the 5D Yukawa couplings. There are similar, although slightly skewed, distributions for $\tilde{y}_d^{(5)}$. Ratios of the $\tilde{f}_{Q_i}$ are constrained through the remaining CKM parameters, $\lambda = 0.22453 \pm 0.00044$ and $A = 0.836 \pm 0.015$, using the expressions

$$\lambda = \frac{\tilde{f}_{Q_1}}{\tilde{f}_{Q_2}}\left|\frac{[\tilde{y}_d^{(5)}]_{21}}{[\tilde{y}_d^{(5)}]_{11}} - \frac{[\tilde{y}_u^{(5)}]_{21}}{[\tilde{y}_u^{(5)}]_{11}}\right|\,, \quad A = \frac{1}{\lambda^2}\frac{\tilde{f}_{Q_2}}{\tilde{f}_{Q_3}}\left|\frac{\tilde{y}_{d,\,23}^{(5)}}{\tilde{y}_{d,\,33}^{(5)}} - \frac{\tilde{y}_{u,\,23}^{(5)}}{\tilde{y}_{u,\,33}^{(5)}}\right|\,. \tag{A.14}$$

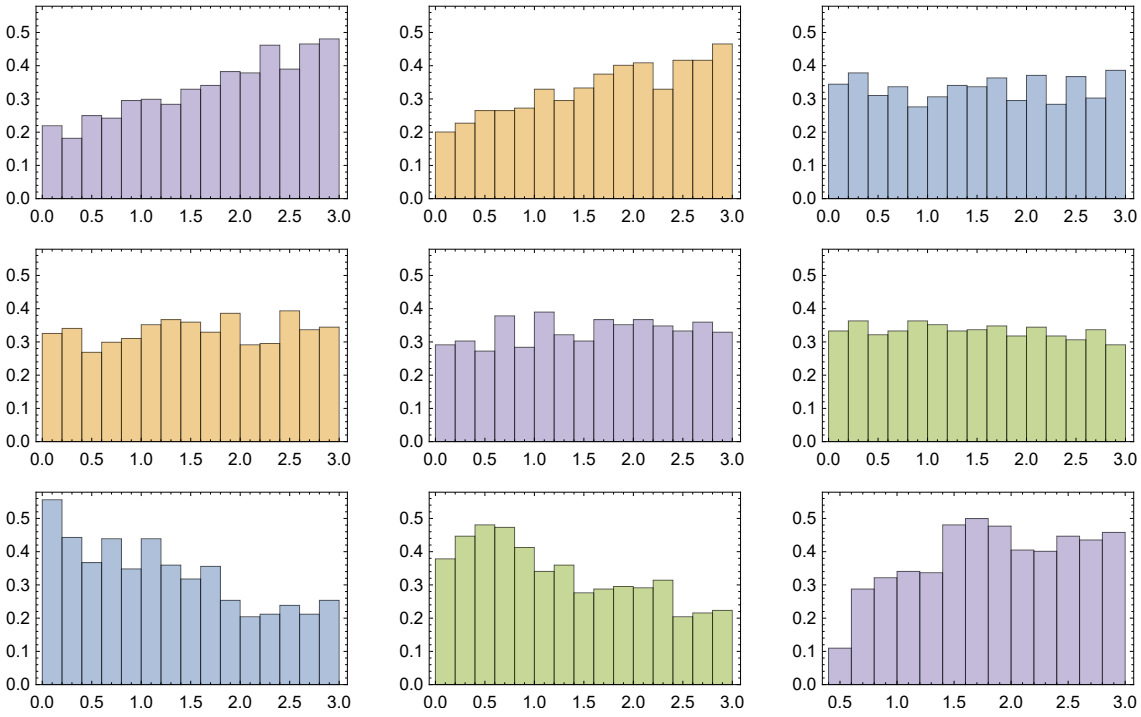

Figure A.1: Probability histograms for the absolute values of the randomly generated $\tilde{y}^{(5)}_{u,ij}$ matrix elements that satisfy (A.12).

Together, (A.8), (A.14) fix all ratios of the $\tilde{f}_{Q_i}$, $\tilde{f}_{u_i}$ and $\tilde{f}_{d_i}$. The mixing matrices in (A.10) are then fully determined. For each pair of $\tilde{y}_u^{(5)}, \tilde{y}_d^{(5)}$ that satisfies (A.12) we generate a sample of $A_{L,R}^{u,d}$ matrices. Note that the mixing matrices in (A.10) are only approximately unitary; we discard individual matrices that are not unitary to within 20% accuracy[1]. The resulting distributions for the absolute values of the elements of the $A_{L,R}^u$ and $A_{L,R}^d$ matrices are plotted in Figure A.2 and Figure A.3, respectively. The matrices are approximately symmetric, thus only the upper off-diagonal entries are shown.

Finally, to obtain the axion-fermion couplings from (4.106) we need to calculate the overlap integrals of the fermion and axion profiles. Recall that the fermion profiles are related to the $\tilde{f}$ via (A.6). Since the quark masses and CKM parameters fix only ratios of the $\tilde{f}$, there remains one free parameter which we take to be the combination $c_{Q_3} + c_{U_3}$. Due to the relation $y_{u,ij}^{(5)} = (c_{Q_i} - c_{u_j})\, \tilde{y}_{u,ij}^{(5)}/2$ (and similarly for $y_d^{(5)}$), the bulk mass parameters cannot be too large if the original 5D Yukawa couplings, $y_u^{(5)}$, are to remain perturbative. We find that the largest parameters are c_{Q_3} and c_{U_3} and for $-5 < c_{Q_3} + c_{U_3} < 5$, these always lie in the range $(0.2, 5.3)$, with the remaining bulk mass parameters between $(-0.1, 3.2)$. The final results for the axion-quark couplings are shown as a function of $c_{Q_3} + c_{U_3}$ in Figure 4.9 and Figure 4.10, where the curves and coloured bands denote the mean and standard deviation of $\log_{10} F^V$ over our sample of $(\tilde{y}_u^{(5)}, \tilde{y}_d^{(5)})$.

[1] We use the L_1 norm $||A^\dagger A - \mathbb{I}_{3\times 3}|| \leq 0.2$, where the L_1 norm is the sum of the absolute values of the matrix elements.

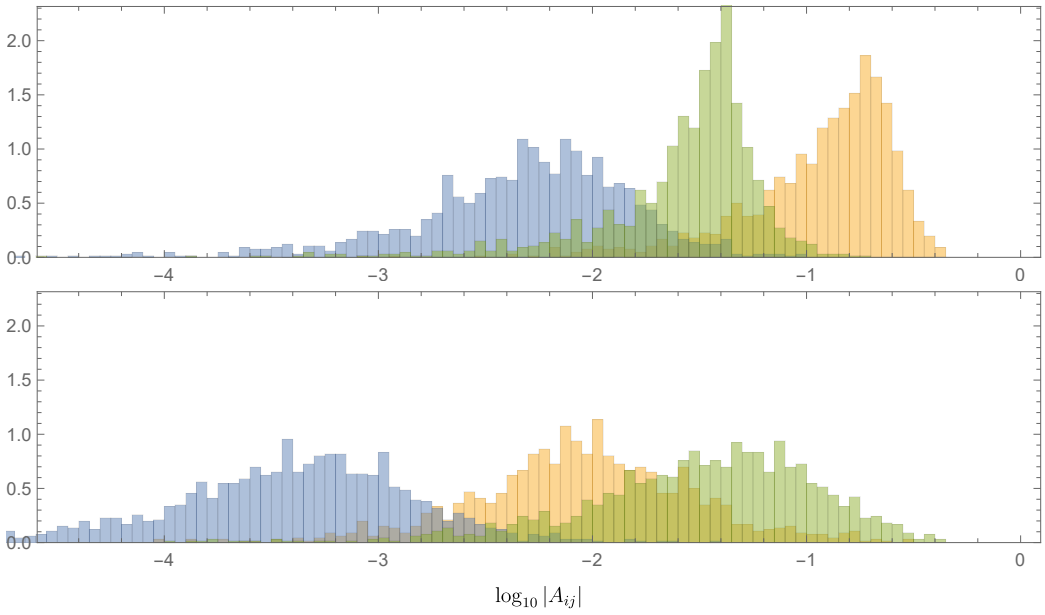

Figure A.2: Histograms for the probability distribution of the logarithm (of the absolute value) of the A_L^u (upper) and A_R^u (lower) matrix element from left to right: 12 (blue), 23 (green), 13 (orange) in the upper figure and 12 (blue), 13 (orange), 23 (green) in the lower figure.

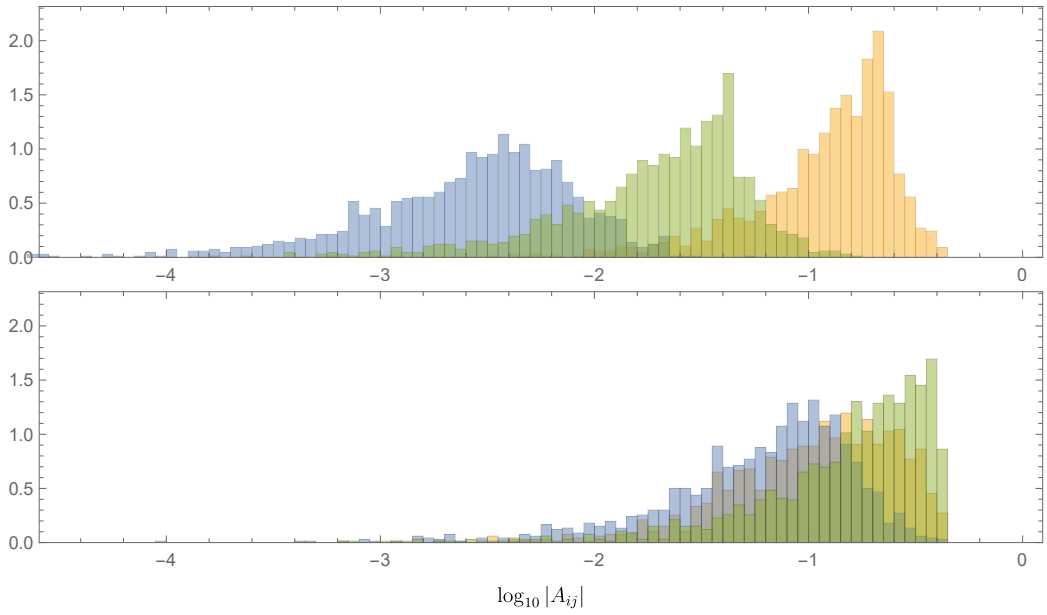

Figure A.3: Histograms for the probability distribution of the logarithm (of the absolute value) of the A_L^d (upper) and A_R^d (lower) matrix elements from left to right: 12 (blue), 23 (green), 13 (orange) in the upper figure and 12 (blue), 13 (orange), 23 (green) in the lower figure.

A.2 Lepton sector

We can perform a similar analysis for the lepton sector. However, this depends on the precise mechanism for neutrino masses, which can be either Dirac or Majorana and may or may not be hierarchical. For simplicity, we assume that the PMNS matrix is generated in the charged lepton sector. This could follow from a flavour-diagonal Weinberg operator (for instance, by localizing a right-handed neutrino sector on the UV boundary). We leave a more detailed analysis of the neutrino sector possibilities and discussion of axion-neutrino couplings for future work.

An important difference from the quark sector is that the mixing angles in the PMNS matrix are relatively large. As a consequence, an analogous assumption to (A.7) does not work for the charged leptons. Instead, we assume the following scaling

$$\tilde{f}_{E_1} \sim \epsilon \tilde{f}_{E_2} \sim \epsilon^2 \tilde{f}_{E_3} \,, \tag{A.15}$$

with $\tilde{f}_{L_i} \sim \epsilon^0$. To leading order in ϵ, the charged lepton masses are then given by

$$\begin{aligned} m_e &\simeq \frac{v_d}{\sqrt{2k}} \frac{|\det \tilde{y}_e^{(5)}|}{N_1} \frac{\tilde{f}_{L_2}}{\tilde{f}_{L_3}} \tilde{f}_{L_1} \tilde{f}_{E_1} \,, \\ m_\mu &\simeq \frac{v_d}{\sqrt{2k}} \frac{N_1}{N_3} \tilde{f}_{L_3} \tilde{f}_{E_2} \,, \\ m_\tau &\simeq \frac{v_d}{\sqrt{2k}} N_3 \tilde{f}_{L_3} \tilde{f}_{E_3} \,, \end{aligned} \tag{A.16}$$

with

$$N_1 = \sqrt{|[\tilde{y}_e^{(5)}]_{11}|^2 \frac{\tilde{f}_{L_2}^2}{\tilde{f}_{L_3}^2} + |[\tilde{y}_e^{(5)}]_{21}|^2 \frac{\tilde{f}_{L_1}^2}{\tilde{f}_{L_3}^2} + |[\tilde{y}_e^{(5)}]_{31}|^2 \frac{\tilde{f}_{L_1}^2 \tilde{f}_{L_2}^2}{\tilde{f}_{L_3}^4}} \,, \tag{A.17}$$

$$N_3 = \sqrt{|\tilde{y}_{e,\,13}^{(5)}|^2 \frac{\tilde{f}_{L_1}^2}{\tilde{f}_{L_3}^2} + |\tilde{y}_{e,\,23}^{(5)}|^2 \frac{\tilde{f}_{L_2}^2}{\tilde{f}_{L_3}^2} + |\tilde{y}_{e,\,33}^{(5)}|^2} \,. \tag{A.18}$$

The assumption (A.15) therefore allows us to trivially solve for the $\tilde{f}_{E_i}$, once the $\tilde{f}_{L_i}$ have been obtained from a fit to the PMNS matrix. Again using (A.15) and working to leading

order in ϵ, the mixing matrix A_R^e takes a comparable form to the quark sector:

$$A_R^e \simeq \begin{pmatrix} 1 & \frac{[\tilde{y}_e^{(5)}]_{12}^*}{[\tilde{y}_e^{(5)}]_{11}^*}\frac{\tilde{f}_{E_1}}{\tilde{f}_{E_2}} & \frac{\tilde{y}_{e,\,31}^{(5)\,*}}{\tilde{y}_{e,\,33}^{(5)\,*}}\frac{\tilde{f}_{E_1}}{\tilde{f}_{E_3}} \\ -\frac{[\tilde{y}_e^{(5)}]_{12}}{[\tilde{y}_e^{(5)}]_{11}}\frac{\tilde{f}_{E_1}}{\tilde{f}_{E_2}} & 1 & \frac{\tilde{y}_{e,\,32}^{(5)\,*}}{\tilde{y}_{q,\,33}^{(5)\,*}}\frac{\tilde{f}_{E_2}}{\tilde{f}_{E_3}} \\ \frac{[\tilde{y}_e^{(5)}]_{13}}{[\tilde{y}_q^{(5)}]_{11}}\frac{\tilde{f}_{E_1}}{\tilde{f}_{E_3}} & -\frac{\tilde{y}_{e,\,32}^{(5)}}{\tilde{y}_{q,\,33}^{(5)}}\frac{\tilde{f}_{E_2}}{\tilde{f}_{E_3}} & 1 \end{pmatrix} \cdot \mathrm{diag}\left(e^{-i\arg\det\tilde{y}_e^{(5)}}, 1, 1\right) . \tag{A.19}$$

The expression for A_L^e is significantly more complicated due to the absence of any assumption on the $\tilde{f}_{L_i}$, and is given (to all orders in ϵ) by

Given our assumption regarding the neutrino sector, A_L^e is directly related to the PMNS matrix: $U_{PMNS} = (A_L^e)^\dagger A_L^\nu = (A_L^e)^\dagger$, since A_L^ν is the identity matrix. The mixing angles and Dirac phase of the PMNS matrix are then simply

$$\tan\theta_{12} = \left|\frac{[\tilde{y}_e^{(5)}]_{21}}{[\tilde{y}_e^{(5)}]_{11}}\right| \frac{\tilde{f}_{L_1}}{\tilde{f}_{L_2}} , \tag{A.20}$$

$$\tan\theta_{23} = \frac{1}{N_1|\tilde{y}_{e,\,33}^{(5)}|}\left|[\tilde{y}_e^{(5)}]_{11}^*\tilde{y}_{e,\,23}^{(5)}\frac{\tilde{f}_{L_2}^2}{\tilde{f}_{L_3}^2} + [\tilde{y}_e^{(5)}]_{21}^*\tilde{y}_{e,\,13}^{(5)}\frac{\tilde{f}_{L_1}^2}{\tilde{f}_{L_3}^2}\right| , \tag{A.21}$$

$$\sin\theta_{13}\, e^{-i\delta_{CP}} = \frac{[\tilde{y}_e^{(5)}]_{31}}{N_1}\frac{\tilde{f}_{L_1}\tilde{f}_{L_2}}{\tilde{f}_{L_3}^2} . \tag{A.22}$$

We use the results from the fit to the oscillation data in [179], with normal ordering: $\theta_{12}/^o = 33.44^{+0.78}_{-0.75}$, $\theta_{23}/^o = 49.0^{+1.1}_{-1.4}$, $\theta_{13}/^o = 8.57^{+0.13}_{-0.12}$ and $\delta_{CP}/^o = 195^{+51}_{-25}$.

We randomly scan over approximately 2×10^5 possible 5D Yukawa coupling matrices $\tilde{y}_e^{(5)}$, with complex entries of norm between 0 and 3. Equations (A.20) and (A.22) are then used to solve for the ratios $\tilde{f}_{L_1}/\tilde{f}_{L_3}$ and $\tilde{f}_{L_2}/\tilde{f}_{L_3}$. These ratios are substituted into equation (A.21), which is required to satisfy the experimental value at $2\,\sigma$. This process yields about 2400 viable matrices $\tilde{y}_e^{(5)}$. After imposing the relations (A.16) for the charged lepton masses, all ratios of the $\tilde{f}_{L_i}$ and $\tilde{f}_{E_i}$ are fixed. The matrix A_R^e is then also determined, and distributions of the absolute values of the elements are plotted in Figure A.4. A_R^e is approximately symmetric, and hence only the upper off-diagonal elements are shown.

Finally, the axion-fermion couplings are calculated as a function of the remaining free

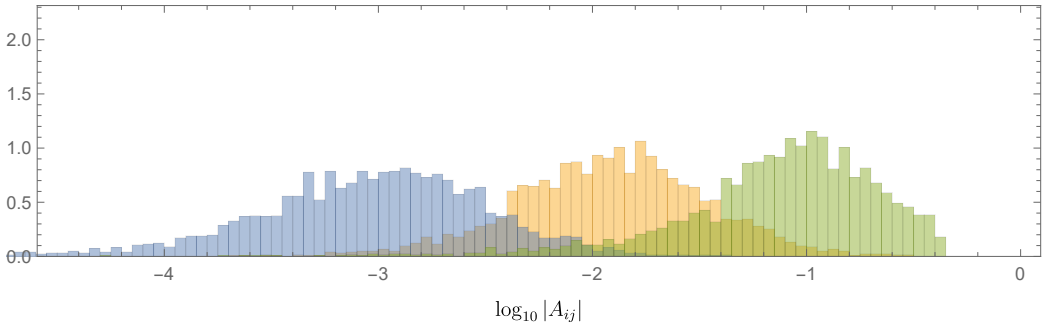

Figure A.4: Histograms for the probability distribution of the logarithm (of the absolute value) of the A^e_R matrix elements from left to right: 12 (blue), 13 (orange), 23 (green). A^e_L is directly correlated with the PMNS matrix and thus is not plotted.

parameter, which we take to be the combination $c_{L_3} + c_{E_3}$. The results are shown in Figure 4.9 and Figure 4.10, where the curves and coloured bands denote the mean and standard deviation of $\log_{10} F^V$ over our sample of $\tilde{y}_e^{(5)}$.

Appendix B

Exact 1-Loop Effective Potential for the Top Partner Hyperfermion

In this Appendix, we derive the gap equation for R, R', Δ and $\widetilde{\Delta}$, with the Yukawa Lagrangian

$$\begin{aligned}\mathcal{L}_\chi = &-\Big[(R^T)^F{}_G(\chi_F\bar{\chi}^G) + (R'^T)^f{}_g(\chi'_f\bar{\chi}'^g) + \Delta^{\dagger F}_f(\chi_F\bar{\chi}'^f) + \widetilde{\Delta}^{\dagger f}{}_F(\bar{\chi}^F\chi'_f) + \text{h.c.}\Big] \\ &- \frac{2N_{\text{HC}}}{\kappa_R}R_F{}^G R_G{}^F - \frac{2N_{\text{HC}}}{\kappa_{R'}}R'_f{}^g R'_g{}^f - \frac{2N_{\text{HC}}}{\kappa_\Delta}\Delta^F{}_f\Delta^{\dagger f}{}_F - \frac{2N_{\text{HC}}}{\kappa_{\widetilde{\Delta}}}\widetilde{\Delta}^f_F\widetilde{\Delta}^{\dagger F}_f\,, \end{aligned} \tag{B.1}$$

by integrating out the hyperfermions. First we wish to derive the exact one-loop effective potential

$$V_{\text{eff}} = \sum_\phi \frac{2N_{\text{HC}}}{\kappa_\phi}\,\text{Tr}\,(\phi\phi^\dagger) - \frac{1}{2}\sum_\phi \int \frac{d^4k_E}{(2\pi)^4}\,\text{Tr}\,\log\left(1+\frac{\phi\phi^\dagger}{k_E^2}\right) + V_{\text{mix}}\,, \tag{B.2}$$

where $\phi = R, R', \Delta, \widetilde{\Delta}$. The trace runs over both the enlarged color indices, F, f, and the hypercolor indices, which are suppressed. The integrals are performed over Euclidean four momentum, k_E with a UV cutoff Λ_{UV}, similar to the case for M^{ab}. The first two terms are the standard Coleman-Weinberg potential for ϕ, and thus we will focus on deriving the last term V_{mix} that mixes different fields.

First we choose a convention for the enlarged color indices. The fields Δ and $\widetilde{\Delta}$ can be treated as matrices with the first index associated with the fundamental in SU$(N+3)$ and the second index with the fundamental in SU$(N)'$. Similarly, R is a $(N+3)\times(N+3)$

traceless matrix, while R' is a $N \times N$ traceless matrix. For all of these auxiliary fields, the upper indices are fundamental, while the lower indices are anti-fundamental. Thus repeated indices between different fields can be summed only if they have opposite representations. The interacting vertices are

$$\chi^{\dagger F} R_F^{\ G} \bar{\chi}_G^{\dagger}\,, \qquad \chi'^{\dagger f} R'_f{}^{g} \bar{\chi}'^{\dagger}_g\,, \qquad \chi^{\dagger F} \Delta_F^{\ f} \bar{\chi}'^{\dagger}_f\,, \qquad \bar{\chi}^{\dagger}_F \widetilde{\Delta}^F{}_f \chi'^{\dagger f}\,. \tag{B.3}$$

Note that Eq. (B.1) and (B.3) include some assumptions about the scalar fields. The fields R, R' can be chosen to be real, since if R is complex we can simply redefine $(R + R^{\dagger})_F^{\ G}$ as the new $R_F^{\ G}$. This follows from the fact that $R^{\dagger}(R'^{\dagger})$ has the same index structure as $R(R')$, since both are in the adjoint representation of $\mathrm{SU}(N+3)(\mathrm{SU}(N)')$. Similarly, $\Delta_F^{\ f}$ is in the same representation as $\widetilde{\Delta}^{*f}_F$, and thus $\widetilde{\Delta}^{*f}_F$ share the same coupling to χ, χ' with $\Delta_F^{\ f}$. These couplings are not present in Eq. (B.1), (B.3) since we can redefine $(\Delta + \widetilde{\Delta}^*)_F^{\ f}$ as $\Delta_F^{\ f}$. Ignoring the momenta and the integral over momentum space, the lowest order Feynman diagrams give

$$\mathrm{Tr}\left[\Delta R' \Delta^{\dagger} R + \widetilde{\Delta} R'^{T} \widetilde{\Delta}^{\dagger} R^{T} + \mathrm{h.c.}\right]. \tag{B.4}$$

Higher order diagrams can be obtained from (B.4) by including more fields. For instance, from the first term in Eq. (B.4), one can add any number of pairs $\Delta^{\dagger}\Delta$ between the original Δ and R'. The sum of all such diagrams is

$$\mathrm{Tr}\left[\Delta\left(\mathbb{I} + \frac{\Delta^{\dagger}\Delta}{k_E^2} + \frac{(\Delta^{\dagger}\Delta)^2}{k_E^4} + \cdots\right) R' \Delta^{\dagger} R\right] \equiv \mathrm{Tr}\left[\{\Delta\} R' \Delta^{\dagger} R\right], \tag{B.5}$$

where in the second term, we have introduced the notation $\{\Delta\}$ for the infinite sum of Δ. Since the cyclic symmetry between the $(\Delta^{\dagger}\Delta)$ vertex pairs is broken by the presence of other fields in the sequence, there is no symmetry factor accompanying each new diagram. The sum of these diagrams is thus $\{\Delta\}$ instead of $\Delta \log(1 + |\Delta|^2/k_E^2)$, which would be the case if the other fields were not present. One can now include diagrams that repeat other fields,

and the sum of all these diagrams is

$$\mathrm{Tr}\left[\{\Delta\}\{R'\}\{\Delta^\dagger\}\{R\}\right]. \tag{B.6}$$

Of course for the original sequence in Eq. (B.4), instead of contracting the last R with the first Δ to form the loop, one can include a new Δ in the sequence, which must also include $R', \Delta^\dagger$ and R at least once as dictated by gauge invariance. This is equivalent to repeating the sequence in Eq. (B.6) any amount of times. The sum of these sequences is

$$V_{\mathrm{mix}} \supset \int \frac{d^4k_E}{(2\pi)^4}\,\mathrm{Tr}\left[\log\left(1+\frac{\{\Delta\}\{R'\}\{\Delta^\dagger\}\{R\}}{k_E^4}\right)+\mathrm{h.c.}\right], \tag{B.7}$$

where the log term now takes into account the cyclic symmetry. This would be the full one-loop effective potential if R, R' are complex. Instead, there are additional terms such as

$$\mathrm{Tr}\left[\Delta R'^2\widetilde{\Delta}R^2\right], \tag{B.8}$$

which have not been taken into account in Eq. (B.6) since it contains only odd powers of R and R' (inside the logarithmic sum). These terms can easily be included by adding a new term $\mathrm{Tr}\left[\{\Delta\}R'\{R'\}\{\Delta^\dagger\}R\{R\}\right]$, which is further suppressed by $1/\Lambda_{\mathrm{UV}}^2$. Since we are only interested in the leading order, these terms will be ignored when we derive the gap equation. Again, note that the effective potential in (B.7) should only be used as a book keeping device to list out the diagrams. To obtain the exact one loop effective potential, one needs to perform a nontrivial summation of higher order diagrams.

The integral over the lowest order (B.4), however, contains an infrared divergence, while there is no closed-form expression for the integral over (B.6) and in (B.7). When deriving the gap equation for a particular field ϕ, a simple trick to avoid the infrared divergence is to retain the corresponding sum $\{\phi\}$, while dropping higher order terms for the other fields. For instance, choosing Δ and keeping only $\{\Delta\}$ in (B.6), the approximation for the mixing

term is:

$$V_{\text{mix}} \supset \int \frac{d^4k_E}{(2\pi)^4} \frac{1}{k_E^4} \,\text{Tr}\left(\frac{\Delta}{1+\frac{\Delta^\dagger\Delta}{k_E^2}} \widetilde{\Phi}^\dagger \widetilde{\Delta} \Phi^\dagger + \text{h.c.} \right) . \tag{B.9}$$

The integral can now be performed, giving the effective potential in Eq. (5.13).

Appendix C

Hypercolor Nambu-Goldstone Boson Spectrum

For the sake of completeness, we discuss the hypercolor Nambu-Goldstone bosons resulting from the enlarged color breaking. In the symplectic hypercolor case, the mass matrix in the $(\boldsymbol{\chi}, \chi_c, \chi', \bar{\boldsymbol{\chi}}, \bar{\chi}_c, \bar{\chi}')$ hyperfermion basis is

$$\left(\begin{array}{cc|cc} & & & \Delta_n \mathbb{I}_N \\ & \mathbf{0}_{(2N+3)} & & m_\chi \mathbb{I}_3 \\ & & \widetilde{\Delta}_n \mathbb{I}_N & \\ \hline & -\Delta_n \mathbb{I}_N & & \\ & -m_\chi \mathbb{I}_3 & & \mathbf{0}_{(2N+3)} \\ -\widetilde{\Delta}_n \mathbb{I}_N & & & \end{array}\right) . \tag{C.1}$$

Similar to the analysis in Section Section 5.1, the fermion condensates $\langle \chi \bar{\chi} \rangle, \langle \chi' \bar{\chi}' \rangle$ arising from the trace $\chi_F \bar{\chi}^F, \chi'_f, \bar{\chi}'^f$ are excluded. It is straightforward to see that including these terms simply shifts m_χ and rotates $\Delta, \widetilde{\Delta}$ among each other, and thus have no effect on the resulting Nambu-Goldstone boson structure. We have also excluded the subleading term $m_\chi \boldsymbol{\chi} \bar{\boldsymbol{\chi}}$ since we have taken $m_\chi \ll \Delta_n$. However, m_χ is the leading mass contribution to χ_c,

and thus has been retained in (C.1). The VEV (C.1) breaks the global symmetry

$$G_{\mathrm{Sp}} = \mathrm{U}(4N+6) \to \mathrm{Sp}(4N+6)\,. \tag{C.2}$$

If the hyperfermion representation is real instead of pseudoreal, then the unbroken symmetry is $\mathrm{SO}(4N+6)$. The pure QCD case, where $N = 0$, was considered in [180]. For SU(4) hypercolor, the same mass matrix can be expressed in a simpler form

$$\begin{pmatrix} \bar{\chi}' & \bar{\chi}_c & \bar{\boldsymbol{\chi}} \end{pmatrix} \begin{pmatrix} \Delta_n \mathbb{I}_N & & \\ & m_\chi \mathbb{I}_3 & \\ & & \widetilde{\Delta}_n \mathbb{I}_N \end{pmatrix} \begin{pmatrix} \boldsymbol{\chi} \\ \chi_c \\ \chi' \end{pmatrix}. \tag{C.3}$$

This leads to the global symmetry breaking pattern

$$G_{\mathrm{SU}} = \mathrm{U}(2N+3)_L \times \mathrm{U}(2N+3)_R \to \mathrm{U}(2N+3)_V\,. \tag{C.4}$$

For either hypercolor group choices, the global symmetry of the color sector has greatly increased, resulting in multiple extra U(1) group factors upon symmetry breaking. It is important to check the breaking pattern and identify the anomalous symmetries, since they might contribute to the θ-terms of the strong sectors and spoil the strong CP solution. We start with the simpler case G_{SU}, and later give the details for G_{Sp}.

Just like the quark masses responsible for breaking the global chiral symmetry, the mass term m_χ, Δ_n and $\widetilde{\Delta}_n$ breaks G_{SU} to the diagonal subgroup. However, unlike in QCD, Δ and $\widetilde{\Delta}$ are not bare masses, but rather dynamically generated by four-fermion couplings. Similar to the pion octet in QCD, the Nambu-Goldstone boson spectrum in this case fits into an adjoint multiplet of $\mathrm{SU}(2N+3)_V$. To label these states, we proceed to gauge the unbroken $\mathrm{U}(2N+3)_V$ by $\mathrm{SU}(3)_c \times \mathrm{U}(1)_X$ and $\mathrm{SU}(N)_D$, where $\mathrm{U}(1)_X$ is the global symmetry that will mix with another unbroken U(1) from the global symmetry of $\psi\psi$ to form the hypercharge $\mathrm{U}(1)_Y$. The unbroken subgroup contains $\mathrm{U}(3) \times \mathrm{U}(N)_\Delta \times \mathrm{U}(N)_{\widetilde{\Delta}}$,

corresponding to the vectorlike transformations of $\chi_c\bar{\chi}_c$, $\boldsymbol{\chi}\bar{\chi}'$, and $\chi'\bar{\boldsymbol{\chi}}$. The U(1) parts in these groups are respectively (up to normalization)

$$\mathrm{U}(1)^V_{\Delta}: \quad \mathrm{diag}(\mathbb{I}_N, \mathbf{0}_3, \mathbf{0}_N, \mathbf{0}_N, \mathbf{0}_3, -\mathbb{I}_N)\,, \tag{C.5}$$

$$\mathrm{U}(1)^V_{\chi_c}: \quad \mathrm{diag}(\mathbf{0}_N, \mathbb{I}_3, \mathbf{0}_N, \mathbf{0}_N, -\mathbb{I}_3, \mathbf{0}_N)\,, \tag{C.6}$$

$$\mathrm{U}(1)^V_{\widetilde{\Delta}}: \quad \mathrm{diag}(\mathbf{0}_N, \mathbf{0}_3, \mathbb{I}_N, -\mathbb{I}_N, \mathbf{0}_3, \mathbf{0}_N)\,, \tag{C.7}$$

where these vector generators have been written in the hyperfermion basis of (C.1) to make the connection to the Sp case clearer. Thus the SU(3) and the $\mathrm{U}(1)^V_{\chi_c}$ symmetry in (C.6) can be identified with $\mathrm{SU}(3)_c$ and $\mathrm{U}(1)_X$. We gauge both $\mathrm{SU}(N)_{\Delta}$ and $\mathrm{SU}(N)_{\widetilde{\Delta}}$ with the same $\mathrm{SU}(N)_D$, meaning we only gauge part of the global symmetry corresponding to identical $\mathrm{SU}(N)_{\Delta}$, $\mathrm{SU}(N)_{\widetilde{\Delta}}$ transformations. Note that the diagonal color admits a $\mathrm{U}(1)_D$, similar to the $\mathrm{U}(1)_X$ of the $\mathrm{SU}(3)_c$. If $m_{\chi}\boldsymbol{\chi}\bar{\boldsymbol{\chi}}$ is taken into account, the other two $\mathrm{U}(1)^V_{\Delta,\widetilde{\Delta}}$ symmetries in (C.5) and (C.7) are explicitly broken, leaving only the linear combination $\mathrm{U}(1)_D \equiv \mathrm{U}(1)^V_{\Delta} \times \mathrm{U}(1)^V_{\widetilde{\Delta}}$. The spectrum labeled under $\mathrm{SU}(3)_c \times \mathrm{SU}(N)_D \times \mathrm{U}(1)_X \times \mathrm{U}(1)_D$ is thus

$$(\mathbf{8},\mathbf{1})_{(0,0)} + 2(\mathbf{3},\overline{\mathbf{N}})_{(x,-z)} + 2(\overline{\mathbf{3}},\mathbf{N})_{(-x,z)} + 4(\mathbf{1},\mathbf{Ad})_{(0,0)} + 5(\mathbf{1},\mathbf{1})_{(0,0)}\,. \tag{C.8}$$

Some of these fields are eaten by the broken $\mathrm{SU}(N+3) \times \mathrm{SU}(N)'$ gauge bosons. Specifically, one of the adjoint states $(\mathbf{1},\mathbf{Ad})$, corresponding to $\boldsymbol{\chi}\bar{\chi}'$ with N^2-1 degrees of freedom (d.o.f), is eaten by $\frac{1}{\sqrt{2}}(G_N - G')^a_{\mu}$. The complex bifundamental $\chi_c\bar{\chi}'$ with $2\times 3N$ d.o.f is eaten by G^b_{μ}, and one of the real singlets corresponding to $\mathrm{Tr}\,\boldsymbol{\chi}\bar{\chi}'$ is eaten by $G_{1\mu}$. In total, there are $N(N+6)$ Nambu-Goldstone bosons eaten.

It is nontrivial to derive the mass of these states, since there are multiple sources that can contribute, depending on which Nambu-Goldstone boson is considered. For instance, the charged states in (C.8) receive two sources of mass from $m_{\chi}, \Delta, \widetilde{\Delta}$ (similar to the pion masses being proportional to the quark masses), and from color and diagonal color loop corrections (similar to photon loop corrections for the QCD pion masses). Thus, these masses should

be $\sim \Lambda_{\rm HC}$. The other four singlets in (C.8) correspond to a $\mathrm{Tr}\,\chi'\bar{\boldsymbol{\chi}}$, which is also heavy due to the contribution from $\widetilde{\Delta} \sim \Lambda_{\rm HC}$, and the remaining three Nambu-Goldstone bosons are associated with the anomalous generators

$$\mathrm{U}(1)^A_{\boldsymbol{\chi}}: \quad \mathrm{diag}(\mathbb{I}_N, \mathbf{0}_3, \mathbf{0}_N, \mathbb{I}_N, \mathbf{0}_3, \mathbf{0}_N)\,, \tag{C.9}$$

$$\mathrm{U}(1)^A_{\chi_c}: \quad \mathrm{diag}(\mathbf{0}_N, \mathbb{I}_3, \mathbf{0}_N, \mathbf{0}_N, \mathbb{I}_3, \mathbf{0}_N)\,, \tag{C.10}$$

$$\mathrm{U}(1)^A_{\chi'}: \quad \mathrm{diag}(\mathbf{0}_N, \mathbf{0}_3, \mathbb{I}_N, \mathbf{0}_N, \mathbf{0}_3, \mathbb{I}_N)\,. \tag{C.11}$$

These generators, respectively, correspond to the axial transformations of $\boldsymbol{\chi}\bar{\boldsymbol{\chi}}$, $\chi_c\bar{\chi}_c$, and $\chi'\bar{\chi}'$. Note that the product of these symmetries is the overall anomalous U(1) of the U($4N+6$). The $\mathrm{U}(1)^A_{\boldsymbol{\chi},\chi_c}$ symmetries are explicitly broken by a mass term $m_\chi\chi\bar{\chi} = m_\chi\boldsymbol{\chi}\bar{\boldsymbol{\chi}} + m_\chi\chi_c\bar{\chi}_c$, while the $\mathrm{U}(1)^A_{\chi'}$ is broken by $m_{\chi'}\chi'\bar{\chi}'$. Thus like the $\eta'_{\rm QCD}$ receiving mass from QCD instantons, these states can also receive mass from the enlarged color instantons, even though they don't contribute to the strong CP solution.

The Sp hypercolor follows a similar story. Given that $\mathrm{SU}(2N+3)_V \subset \mathrm{Sp}(4N+6) \subset \mathrm{SU}(4N+6)$, we can decompose the Nambu-Goldstone bosons from the spontaneous breaking $\mathrm{SU}(4N+6) \to \mathrm{Sp}(4N+6)$ as $\mathbf{Ad} + \mathbf{A}_2 + \overline{\mathbf{A}}_2$ under $\mathrm{SU}(2N+3)_V$. Thus the spectrum contains all of the states in the $G_{\rm SU}$ case, namely the $\mathbf{Ad}$ multiplet, together with the additional multiplets $\mathbf{A}_2$ and $\overline{\mathbf{A}}_2$ of $\mathrm{SU}(2N+3)_V$. After weakly gauging the global symmetry, $\mathrm{SU}(2N+3)_V$ with $\mathrm{SU}(3)_c \times \mathrm{SU}(N)_D$, we obtain in addition to (C.8), the spectrum

$$\begin{aligned}&(\mathbf{3},\mathbf{1})_{(2x,0)} + (\overline{\mathbf{3}},\mathbf{1})_{(-2x,0)} + 2\,(\mathbf{3},\mathbf{N})_{(x,z)} + 2\,(\overline{\mathbf{3}},\overline{\mathbf{N}})_{(-x,-z)} \\ &+ 4(1,\mathbf{A}_2)_{(0,2z)} + 4\,(1,\overline{\mathbf{A}}_2)_{(0,-2z)} + 2\,(1,\mathbf{S}_2)_{(0,2z)} + 2\,(1,\overline{\mathbf{S}}_2)_{(0,-2z)} + (\mathbf{1},\mathbf{1})_{(0,\pm 2z)}\,,\end{aligned} \tag{C.12}$$

where the subscripts refer to the $\mathrm{U}(1)_X$, $\mathrm{U}(1)_D$ charges. The two new singlets in (C.12) correspond to $\mathrm{Tr}\,\boldsymbol{\chi}\chi'$ and $\mathrm{Tr}\,\bar{\boldsymbol{\chi}}\bar{\chi}'$, which are obviously broken explicitly by $m_{\chi,\chi'}$. The detection of the states in (C.12) would be a way to distinguish the hypercolor gauge group.

In summary, the pseudo Nambu-Goldstone spectrum arising from the hypercolor top

partners obtain masses depending on Λ_{HC} and $m_{\chi,\chi'}$. It can be expected that all of these states lie between the Λ_D and Λ_{HC} scales, although the exact spectrum would require a more in-depth analysis. Interestingly, as some of the hypercolor Nambu-Goldstone boson masses are proportional to $\sqrt{m_{\chi,\chi'}\Lambda_{\mathrm{HC}}}$, these bound states could be experimentally accessible if $m_{\chi,\chi'} \ll \Lambda_{\mathrm{HC}}$. Finally, in both hypercolor cases, there are unbroken U(1) groups, which can be associated with the baryon number of the QCD and $\mathrm{SU}(N)_D$ quarks. It is possible, though unnecessary for our purposes, to define a generalized baryon number that combines the $\mathrm{U}(1)_D$ and QCD baryon numbers. Alternatively, one can gauge the $\mathrm{U}(1)_D$ symmetry to give a dark photon, which could be a potential dark matter candidate.